UNIVERSITÀ DEGLI STUDI DI PALERMO
Dottorato in Scienze Fisiche e Chimiche
Dipartimento di Fisica e Chimica – Emilio Segrè
Settore Scientifico Disciplinare FIS/03

Objective features in quantum states

IL DOTTORE
DIANA ALEXANDRIA CHISHOLM

IL COORDINATORE
MARCO CANNAS

IL TUTOR
G. MASSIMO PALMA

CICLO XXXV
ANNO CONSEGUIMENTO TITOLO - 2023

I've looked at clouds from both sides now
From up and down, and still somehow
It's cloud illusions I recall
I really don't know clouds at all

Joni Mitchell

Contents

List of publications

This is a list of works this dissertation is based upon.

The importance of using the averaged mutual information in quantum objectivity
Diana A. Chisholm, Luca Innocenti, and G. Massimo Palma.
Submitted, 2022.

Nonlocality breaks the relations between measures of quantum objectivity
Diana A. Chisholm, Luca Innocenti, and G. Massimo Palma.
Submitted, 2022.

Witnessing objectivity on a quantum computer
Diana A. Chisholm, Guillermo García-Pérez, Matteo A.C. Rossi, Sabrina Maniscalco, and G. Massimo Palma.
Quantum Science and Technology, 2022.

Stochastic collision model approach to transport phenomena in quantum networks
Diana A. Chisholm, Guillermo García-Pérez, Matteo A.C. Rossi, G. Massimo Palma, and Sabrina Maniscalco.
New Journal of Physics, 2021.

Decoherence without entanglement and quantum darwinism
Guillermo García-Pérez, Diana A. Chisholm, Matteo A.C. Rossi, G. Massimo Palma, and Sabrina Maniscalco.
Physical Review Research, 2020.

The following work is not included in this dissertation.

Quantum scrambling via accessible tripartite information
Gabriele Lo Monaco, Luca Innocenti, Dario Cilluffo, Diana A. Chisholm, Salvatore Lorenzo, and G. Massimo Palma.
Submitted, 2022.

Abstract

One of the key features of quantum mechanics is that any superposition of quantum states is in itself a legitimate quantum state. This has far reaching consequences, and is behind the stark difference in behaviour between quantum and classical systems. In particular, quantum systems are not -unlike classical ones- intrinsically objective, that is, different observers are not always able to agree on the properties of the system. Understanding the conditions for objectivity in quantum states is therefore key to address the wider issue of the quantum-to-classical transition. Here, we discuss several aspects of quantum objectivity, and in particular subtleties that arise to the definitions of objectivity whenever non-ideal scenarios are taken into account. We first explore the emergence of objectivity in novel open system dynamics. We then discuss the relations between different methods to quantify objectivity, prove their non-equivalence and the implications that this entails. Finally, we provide proof-of-principle evidence on the reproducibility of non-trivial objective states on quantum computers.

Introduction

Since its very beginning, quantum mechanics had a difficult relationship with the pre-existing classical physics. It is a self-evident fact that several of the predictions of quantum mechanics, such as the possibility for quantum systems to be in superpositions, or the fact that measurements inevitably alter the properties of a quantum system, goes against the behaviour of classical systems.

Quantum systems can be in a superposition of states, while classical systems can be in only one state at any given time. In turn, whenever quantum states are measured, the measurement outcomes are compatible with classical physics, in the sense that quantum systems are always measured in well defined states. This is possible however because the measurement of quantum systems inevitably perturbs the system, in order to destroy any superposition of states, which is yet another divergence from classical physics, where measurements do not influence the system itself.

Classical systems are however, nothing more than very large quantum systems. This has led to speculation that, despite the stark differences, classical physics should emerge from the quantum substrate. Arguably, the linking bridge between quantum and classical physics is the measurement process, which is however added *ad hoc* to the theory and itself not well understood. Therefore, trying to explain the measurement process is a promising strategy for closing the gap between the quantum world and the classical one.

Decoherence [1, 2] is often considered a promising mechanism to explain both the measurement problem and the quantum-to-classical transition [3, 4]: as quantum systems are never really isolated [1, 2], their surrounding environment "reads" the system, causing coherent superpositions to be replaced by statistical mixtures, and the corresponding loss of quantum features [4]. However, the theory of decoherence is not *per se* sufficient to directly explain some pivotal markers of classicality, such as the emergence of *objectivity* in quantum systems, that is, the mechanism allowing multiple observers to agree on some property of a quantum state.

While an intrinsic property of classical systems, "objectivity" is usually understood in the quantum domain as consensus between observers. More specifically, given a quantum system $\mathcal{S}$ interacting with an environment $\mathcal{E}$ composed of a number of constituents $\mathcal{E}_i$, we say that the system is objective when observers performing independent measurements on different $\mathcal{E}_i$ reach a consensus about some property of the system [5]. This is only possible if, due to prior interactions between system and environment, the relevant information was encoded with high *redundancy* into the environment [6, 7, 8, 9]. Research in the field of quantum objectivity concerns itself to understand under which conditions quantum states can be considered objective, and what are the typical features of such states.

Outline of the disseration—In chapter 1 we will offer an introduction to some base concepts of open quantum systems and quantum information theory. This will be helpful to introduce many of the tools that we will use throughout this dissertation.

In chapter 2 we will introduce the concept of quantum objectivity. We will give an operative definition of objectivity in the quantum scenario and outline its main features. We will then describe the two main measures of quantum objectivity used in this context, namely quantum Darwinism (QD) and spectrum broadcast structure (SBS). The first two chapters will essentially cover known material.

In chapter 3 we will introduce the stochastic collision model, a versatile model for open system dynamics. We will give a full characterization of the open system dynamics resulting from such models, including an analysis of the emergence of objectivity. We will also prove the versatility of the stochastic collision model by applying it to a network excitation transfer problem.

In chapter 4 we will expand on the concepts of redundancy and consensus, two different quantifiers of quantum objectivity. We will show that, while the two concepts are often considered as synonyms, they actually capture different features of quantum objectivity, and the relationship between them can be non-trivial in some cases. In particular, we will discuss the consequences that this has for the connection between quantum Darwinism and spectrum broadcast structure. The operative definitions given to redundancy and consensus will provide tools to analyse the meaning of quantum objectivity in several scenarios of interest.

Finally, in chapter 5 we provide experimental evidence of objective states in a superconducting quantum computer, showing that quantum computers are a promising platform for future experimental investigations of quantum objectivity.

Chapter 1

Open quantum systems and quantum information theory

Properties of a quantum system can be objective only if information about those properties is encoded into a larger system (the environment). This is only possible through a system-environment interaction. As such, the study of quantum objectivity rests on the shoulders of open quantum systems and quantum information theory.

In this chapter we will offer a basic introduction to the theories of open quantum systems and quantum information, as well as their formalism. As we will only focus on some concepts, the most useful ones in relation to this dissertation, this introduction will be far from complete. The interested reader can find more about open quantum systems in [1, 2] and about quantum information theory in [10, 11].

1.1 Unitary evolution

It is standard practice, in physics, to connect the time evolution of a system with some of its properties, by means of an equation of motion. In quantum mechanics, the equation of motion that describes the evolution of quantum states is the Schrödinger equation:

$$\frac{d}{dt}\left|\psi(t)\right\rangle = -iH\left|\psi(t)\right\rangle, \tag{1.1}$$

where H is the Hamiltonian of the system. Here, and throughout the dissertation, we will work in units of $\hbar = 1$. The formal solution to eq. (1.1) is

$$\left|\psi(t+\tau)\right\rangle = U(\tau)\left|\psi(t)\right\rangle, \tag{1.2}$$

with $U = e^{-iHt}$ the time evolution operator[1]. Since $U^\dagger U = \mathbb{1}$, the time evolution is described by a unitary operator and the inner product is preserved, in particular $\langle\psi(t)|\phi(t)\rangle = \langle\psi(t+\tau)|\phi(t+\tau)\rangle\ \forall\tau$.

The Schrödinger equation can be straightforwardly generalized to describe (closed) evolutions of density operators, resulting in what is referred to as the von Neumann equation:

$$\frac{d}{dt}\rho(t) = -i[H, \rho(t)]. \tag{1.3}$$

[1] Assuming for simplicity that the Hamiltonian H is time independent.

Box 1: Open evolutions do not preserve the purity of the reduced subsystems

Take for instance a qubit (a two level system) that is in the possession of Alice. Alice's qubit is not isolated, and it interacts with another qubit, in the possession of Bob. The two qubits are initially in the $|\psi\rangle_{\mathcal{A}} = \frac{1}{\sqrt{2}}(|0\rangle_{\mathcal{A}} + |1\rangle_{\mathcal{A}})$ and $|\psi\rangle_{\mathcal{B}} = |0\rangle_{\mathcal{B}}$ states respectively, the joint state is $|\Psi\rangle = |\psi\rangle_{\mathcal{A}} \otimes |\psi\rangle_{\mathcal{B}}$. Suppose the two qubits evolve according to the unitary transformation $U = |0\rangle\langle 0| \otimes \mathbb{1} + |1\rangle\langle 1| \otimes \sigma_x$ which, as it happens, is the quantum equivalent of the controlled NOT (CNOT) logic gate. After the evolution, the two qubits will be in an entangled state $|\Psi\rangle = \frac{1}{\sqrt{2}}(|0\rangle_{\mathcal{A}} |0\rangle_{\mathcal{B}} + |1\rangle_{\mathcal{A}} |1\rangle_{\mathcal{B}})$. If we are not interested in Bob's qubit, we can recover the state of Alice's qubit by performing the partial trace over the Bob's qubit degrees of freedom, which effectively corresponds to ignoring them. $\rho_{\mathcal{A}} = \mathrm{Tr}_{\mathcal{B}}(|\Psi\rangle\langle\Psi|) = \frac{1}{2}(|0\rangle\langle 0|_{\mathcal{A}} + |1\rangle\langle 1|_{\mathcal{A}})$, so that an initially pure state is now in a statistical mixture.
While the two qubits, shared between Alice and Bob, follow a unitary evolution, the individual qubits are described by an open evolution. While one could argue that this is always the case, and that open evolutions are always the result of ignoring the environment, in most cases of interest keeping track of the environmental degrees of freedom is both unfeasible and undesirable, which justifies an open system approach.

1.2 Open evolutions

Any isolated system evolves according to an appropriate von Neumann equation. However, when the system interacts with other systems -the environment- this is no longer true.

Suppose we have an atom interacting with the electromagnetic vacuum. The atom is initially in an excited state, that we write as $|\psi(0)\rangle = |1\rangle$. After some time it will emit a photon through spontaneous decay and jump to the ground state, so that $|\psi(\tau)\rangle = |0\rangle$. At the same time, if the atom is initially in the ground state, it will simply remain there throughout the time evolution: $|\phi(0)\rangle = |\phi(\tau)\rangle = |0\rangle$. The inner product is not conserved, indeed $\langle\psi(0)|\phi(0)\rangle = 0$, while $\langle\psi(\tau)|\phi(\tau)\rangle = 1$. Whatever dynamics describes the spontaneous decay of an atom, it is clearly not unitary. Non-unitary evolutions are often referred as "open", since they are usually the consequence of the environment not being isolated, but interacting with an environment. Furthermore, as shown in Box 1, open evolutions do not preserve the purity of the system.

Generic transformations of a quantum system, thus including open evolutions, are described by quantum channels, trace preserving completely positive maps. A channel Φ acts on a quantum state ρ, so that $\rho' = \Phi(\rho)$. Channels can be represented in many different ways, here we will show the Kraus representation and the Stinepring representation.

Kraus representation—It is always possible to find a set of operators $\{K_i\}$ that follow the condition $\sum_i K_i^\dagger K_i = \mathbb{1}$, for which it holds that

$$\Phi(\rho) = \sum_i K_i \rho K_i^\dagger. \tag{1.4}$$

This is referred to as the Kraus representation of the channel Φ. It should be noted that the set of Kraus operators $\{K_i\}$ is not unique, in other words, one could find a different set $\{M_i\}$ that results in the same channel.

Stinespring representation—Just as we have seen that non-unitary transformations are the result of unitary interactions between the system and the environment, we can always represent channels as a unitary transformation involving the system and an ancillary state

$$\Phi(\rho) = \mathrm{Tr}_\mathrm{a}(U\rho \otimes \rho^\mathrm{a} U^\dagger), \tag{1.5}$$

where ρ^a is an ancillary state and U a unitary operation acting on both ρ and ρ^a. Like the Kraus representation, the Stinespring representation is also not unique.

1.3 Master equations and non-Markovianity

Even for open evolutions it is usually desirable to be able to describe them using an equation of motion. While the most general equation that describes the time evolution of generic open quantum systems does not exist, it is possible to show how, provided that some conditions are met, the equation of motion can be cast in a specific form.

Given a system in the state ρ_0 at time $t = 0$, the state of the system at a generic time t is given by $\mathcal{D}_t(\rho(0))$, where the $\mathcal{D}$ channel is called the dynamical map. If it holds true that $\mathcal{D}_{t+\tau} = \mathcal{D}_t\mathcal{D}_\tau$, then the dynamical map has the semi-group property, meaning that any composition of dynamical maps is itself a legitimate dynamical map. Since $\mathcal{D}$ usually describes open, irreversible evolutions, it cannot be inverted, which is why the *semi* prefix is used. While only a restricted number of dynamical maps have the semi-group property, they correspond to a wide array of relevant physical scenarios.

The semi-group property implies that it is sufficient to know the state of the system at a given time to be able to predict its whole future, a concept that is often expressed by saying that the time evolution depends only on the present, and is not influenced by the past of the system. This property strongly resembles the Markovian assumption [12] for classical stochastic processes, which is why the semi-group property is often considered to be the analogous of the Markovian condition for quantum systems [13, 14, 15].

Provided that the dynamical map has the semi-group property, we can write the master equation that describes the time evolution of the system.

$$\rho(t + dt) = \mathcal{D}_{dt}(\rho(t)). \tag{1.6}$$

Let's expand the map in linear order:

$$\mathcal{D}_{dt} = I + dt\mathcal{L}, \tag{1.7}$$

then

$$\frac{\rho(t+dt) - \rho(t)}{dt} = \mathcal{L}(\rho(t)). \tag{1.8}$$

This finite difference equation is the master equation that describes the process.

We recovered the master equation based on an important assumption: we required the semi-group property for the dynamical map, which in turn ensured that the process is Markovian. It should be noted however, that there is not a universally agreed upon definition of quantum Markovian processes, and the aforementioned semi-group property is often considered to be an over-stringent requirement [16]. While discussing the different measures and interpretations of non-Markovianity is outside of the scope of this dissertation, we will point out that the distinguishability between two different states can never increase under quantum channels [17]. The degree of dintinguishability between two different quantum states can be put in terms of the trace distance $D(\rho_1, \rho_2) = \frac{1}{2}\,\mathrm{Tr}|\rho_1\text{-}\rho_2|$, and we have that $D\left(\Phi(\rho_1), \Phi(\rho_2)\right) \leq D(\rho_1, \rho_2)$ for every channel Φ. If the dynamical map has the semi-group property, then we can always represent it as a collection of channels, and it holds true that $\sigma(t, \rho_{1,2}) = \frac{d}{dt}D(\rho_1(t), \rho_2(2)) \leq 0\ \forall t$, i.e. the distinguishability between quantum states monotonically decreases in time. If the semi-group property is not satisfied, then it is not always possible to represent the dynamical map as a collection of channels, meaning that the trace distance does not have to decrease monotonically. The fact that σ is larger than zero at any time can be seen as a hallmark of non-Markovianity, employed in the BLP measure [18]

$$\mathcal{N}\left(\Phi\right) = \max_{\rho_{1,2}(0)} \int_{\sigma>0} dt\sigma(t, \rho_{1,2}(0)), \tag{1.9}$$

that quantifies the degree of non-Markovianity of a quantum process. It should be noted however that this is not a measure of whether a dynamical map has the semi-group property or not, as $\mathcal{N}\left(\Phi\right)$ can be zero (and the process Markovian), even if Φ does not have the semi-group property.

1.4 Collision models

A useful tool to address open quantum systems that has received growing interest in recent years is the one of collision models (CM) [19, 20, 21, 22]. In collision models, the system interacts with the environment through a series of repeated interactions with ancillary systems. While this approach may seem an idealization of more realistic scenarios, it proves to be advantageous in the derivation of master equations equivalent to microscopic derivations, and is able to provide useful physical insights in several scenarios [23, 24, 25]. In the following we will illustrate the simplest (and archetypal) collision model.

Suppose we start with the system initially in the ρ_0 state, and N ancillae all in the same state ν. System and ancillae start in a product state

$$\rho_{\text{tot}}(0) = \rho_0 \otimes \nu^{\otimes N}. \tag{1.10}$$

The system interacts with the first ancilla by means of a unitary evolution U_I, after the first interaction system and ancilla will be in the $U_I(\rho_0 \otimes \nu)U_I^\dagger$ state. We assume that the ancilla will never interact with the system again. This way, we can safely recover the state of the system after the first collision, ρ_1, by tracing out the ancillary degrees of freedom, so that $\rho_1 = \text{Tr}_\nu[U_I(\rho_0 \otimes \nu)U_I^\dagger]$. This is effectively a Stinespring representation of a quantum channel, so that $\rho_1 = \Phi(\rho_0)$. This represents the first time step in the system dynamics. The system then interacts with the second ancilla in an similar way, and so on. Since the ancillae are all in the same initial state, and interact with the system with the same unitaries, each collision corresponds to the same Φ channel. Each collision represents a time step in the discrete-time evolution of the system, and at the generic n-th time step, the dynamical map will be Φ^n.

The dynamical map clearly has the semi-group property, in the sense that $\Phi^n = \Phi^m\Phi^{n-m}$. This ensures that the time evolution of the system is Markovian and, as a direct consequence, it is described by a discrete-time master equation, similar to the one in eq. (1.8). Collision models can be modified in many ways depending on the dynamics one may wish to describe [26, 27]. In particular, non-Markovian evolutions are usually described by using three different approaches: allowing for the ancillae to be initially correlated [28], letting the ancillae interact more than once with the system [29], or having ancilla-ancilla interactions [30].

1.5 Measurement theory: PVM and POVM

The most commonly found type of measurement is the projective valued measurement (PVM). PVMs are defined as a set $\{P_i\}$ of orthonormal operators such that

$$P_i P_j = P_i \delta_{ij}. \tag{1.11}$$

and

$$\sum_i P_i = \mathbb{1}. \tag{1.12}$$

After a measurement, the outcome i is obtained with probability $p_i = \text{Tr}(P_i\rho)$, and the system is projected in the $P_i\rho P_i/p_i$ state. The fact that $\sum_i P_i = \mathbb{1}$ can be interpreted as the fact that we must find the system is *some* state after a measurement, so that the sum of all probabilities is one.

$$\sum_i p_i = \sum_i \text{Tr}(P_i\rho) = \text{Tr}(\rho \sum_i P_i) = \text{Tr}(\rho) = 1. \tag{1.13}$$

An interesting property of PVMs is that they are repeatable, in other words, after performing a PVM and obtaining a measurement outcome, performing the same PVM once again yields the same measurement outcome and leaves the state unaltered. This is not a universal property of measurements, but rather a specific one of PVMs

A generalised class of measurements are the positive operator valued measurements (POVMs). A POVM is defined by a set of positive operators $\{\Pi_i\}$ that sum up to identity

$$\sum_i \Pi_i = \mathbb{1}, \tag{1.14}$$

and the outcome i is obtained with probability $p_i = \mathrm{Tr}(\Pi_i \rho)$. Notice that, unlike PVMs, the operators of a POVM need not be orthonormal, so that PVMs are a specific case of POVMs. At the same time, the POVM itself does not tell us the post-measurement state. In order to know it, we would have to find a set of operators E_{ij} such that $\Pi_i = \sum_j E_{ij}^\dagger E_{ij}$, the post-measurement state would then be $\frac{1}{p_i}\sum_j E_{ij}\rho E_{ij}^\dagger$. Since the choice of $\{E_{ij}\}$ is not unique, the POVM itself is not enough to know the post measurement state. Moreover, repeatedly performing a POVM many times does not necessarily yield the same result each time.

1.6 Information entropy

Given a (discrete for simplicity) stochastic variable X with an associated probability distribution $p(x)$, the information entropy —or Shannon entropy— is defined as $H(X) = -\sum_x p(x)\log p(x)$, and it describes the degree of ignorance associated with the stochastic variable. For quantum systems, the analogous version is the von Neumann entropy

$$S(\rho) = -\mathrm{Tr}(\rho \log(\rho)). \tag{1.15}$$

By writing the state in its eigenvector basis, $\rho = -\sum_i \lambda_i |\psi_i\rangle\langle\psi_i|$, the von Neumann entropy reads

$$S(\rho) = \sum_i \lambda_i \log(\lambda_i). \tag{1.16}$$

It is therefore possible to interpret the von Neumann entropy as the degree of uncertainty about in which of the $\{|\psi_i\rangle\}$ states the system is in. If instead we perform a measurement operation, we recover a probability distribution $p_i = \mathrm{Tr}(\Pi_i\rho)$, where Π is a generic POVM. From this probability distribution it is possible to compute the associated Shannon entropy $H_{\{\Pi\}}(\rho)$. Said entropy is of course highly dependent on the chosen POVM, and it is always satisfied that $H_{\{\Pi\}}(\rho) \geq S(\rho)$ [31].

1.7 Measuring correlations

In a classical system, the mutual information between two random variables is defined as

$$I(X:Y) = H(X) + H(Y) - H(XY). \tag{1.17}$$

It quantifies how much knowledge we recover on X by measuring Y, and vice versa. As a matter of fact, $I(X:Y) \leq \min\{H(X), H(Y)\}$ which simply implies that the knowledge we recover on one of the two variables by measuring the other cannot be higher than the initial degree of uncertainty.

Given a bipartite quantum state $\rho_{\mathcal{AB}}$, the quantum mutual information (QMI) between $\mathcal{A}$ and $\mathcal{B}$ is defined as

$$I(\mathcal{A}:\mathcal{B}) = S(\rho_{\mathcal{A}}) + S(\rho_{\mathcal{B}}) - S(\rho_{\mathcal{AB}}), \tag{1.18}$$

as a direct generalization of the mutual information for classical systems, using the von Neumann entropy instead of the Shannon entropy. The QMI can be higher than the individual entropies of $\rho_{\mathcal{A}}$ and $\rho_{\mathcal{B}}$. In particular, if $\rho_{\mathcal{AB}}$ is a pure state, $S(\rho_{\mathcal{AB}}) = 0$ and $S(\rho_{\mathcal{A}}) = S(\rho_{\mathcal{B}})$, while we have full knowledge on the global state, we are ignorant about the individual ones, and $I(\mathcal{A}:\mathcal{B}) = 2S(\rho_{\mathcal{A}})$. The fact that in some cases $I(\mathcal{A}:\mathcal{B}) \geq \max\{S(\mathcal{A}), S(\mathcal{B})\}$ already suggests that the QMI does not have the same operative interpretation as with the classical setting.

If we perform measurement operations on both subsystems, however, we recover a classical probability distribution, from which we can compute a classical mutual information, recovering the operative interpretation. Given the state $\rho_{\mathcal{AB}}$ we can perform two measurement operations $\Pi^{\mathcal{A}}$ and $\Pi^{\mathcal{B}}$ on the respective subsystems, the joint probability distribution for the outcomes of the two measurements reads $p_{ij} = \mathrm{Tr}(\Pi_i^{\mathcal{A}}\Pi_j^{\mathcal{B}}\rho_{\mathcal{AB}})$, and the marginal probabilities are $p_{i(j)} = \sum_{j(i)} p_{ij}$. This is a classical probability distribution, from which we recover a classical mutual information, that is however dependant on the chosen measurement operators. We are often interested in recovering the maximum obtainable mutual information (which we will refer to as the *accessible* mutual information I_{acc}), so we maximise over all possible POVMs and write

$$I_{\mathrm{acc}}(\mathcal{A}:\mathcal{B}) = \max_{\Pi^{\mathcal{A}}\Pi^{\mathcal{B}}} \left(H_{\Pi^{\mathcal{A}}}(\rho_{\mathcal{A}}) + H_{\Pi^{\mathcal{B}}}(\rho_{\mathcal{B}}) - H_{\Pi^{\mathcal{A}}\Pi^{\mathcal{B}}}(\rho)\right). \tag{1.19}$$

It always holds that $I_{\mathrm{acc}}(\mathcal{A}:\mathcal{B}) \leq I(\mathcal{A}:\mathcal{B})$. Even though the accessible information is a quantity of great interest, the fact that it requires the simultaneous optimization over all possible POVMs on two subsystems makes its computation unfeasible in most cases.

Another useful quantifier of correlations is represented by the Holevo χ (also known as Holevo quantity) [32]. Suppose Alice has a classic register of states $\{\rho_i\}$, and decides to send the state ρ_i with the corresponding probability p_i to Bob, who then performs a POVM on the received state. The POVM yields outcome j provided the input state was ρ_i with a corresponding probability $p_{j|i}$. The result is a joint probability distribution $p_{ij} = p_i p_{j|i}$ of the classical register and the outcomes of Bob's POVM, resulting in a (classical) corresponding mutual information. Such mutual information is upper bounded by the Holevo χ, defined as

$$\chi\{\rho_i\} = S\left(\sum_i p_i\rho_i\right) - \sum_i p_i S(\rho_i). \tag{1.20}$$

Suppose now that we have a bipartite quantum state $\rho^{\mathcal{AB}}$ shared between Alice and Bob. Alice decides to perform a projective measurement P on her subsystem, she obtains the outcome i with probability $p_i = \mathrm{Tr}(P_i\rho^{\mathcal{AB}}P_i)$ in which case Bob's subsystem is in the $\rho_i^{\mathcal{B}} = \frac{1}{p_i}P_i^{\mathcal{A}}\rho^{\mathcal{AB}}P_i^{\mathcal{A}}$ state. This scenario is analogous to the previous one, only that the classical register is now replaced by the outcomes of the projective measurement. Also in this case the mutual information between Alice's outcomes and Bob's outcomes is bounded by the Holevo χ. After Alice's measurement, the joint state will be the following

$$\sum_i p_i \left|i\right\rangle\!\left\langle i\right| \otimes \rho_i^{\mathcal{B}}. \tag{1.21}$$

With $\left|i\right\rangle$ eigenstates of P_i. If we want to compute the QMI of this state, we have that $S(\mathcal{A}) = -\sum_i p_i \log(p_i)$, $S(\mathcal{B}) = S\left(\sum_i p_i\rho_i^{\mathcal{B}}\right)$ and $S(\mathcal{AB}) = -\sum_i p_i \log(p_i) + \sum_i p_i S(\rho_i^{\mathcal{B}})$, so that the resulting QMI is exactly the same as the Holevo χ. This is true whenever we have states of the form of eq. (1.21). The measurement performed by Alice is a local operation, and the QMI between $\mathcal{A}$ and $\mathcal{B}$ can never increase under local operations. This implies that the Holevo χ can never be higher than the QMI.

By maximising over all the possible projective measurements performed by Alice, we obtain an upper bound for the accessible information between Alice and Bob. The Holevo χ is itself bounded by the QMI, so that the following relations always hold

$$I_{\mathrm{acc}}(\mathcal{A}:\mathcal{B}) \leq \max_{P^{\mathcal{A}}} \chi_{P^{\mathcal{A}}}(\mathcal{A}:\mathcal{B}) \leq I(\mathcal{A}:\mathcal{B}). \tag{1.22}$$

The advantage of the Holevo χ is that we only need to maximise over all possible PVMs on Alice's system, instead of maximising simultaneously over two different POVMs.

The numerical difference between the maximised Holevo χ and the QMI is called discord [33, 34], defined as

$$D(\mathcal{A}:\mathcal{B}) = I(\mathcal{A}:\mathcal{B}) - \max_{P^{\mathcal{A}}} \chi_{P^{\mathcal{A}}}(\mathcal{A}:\mathcal{B}), \tag{1.23}$$

and it represents correlations that cannot be accessed by performing local operations on the two subsystems. Notice how the Holevo χ as it appears in eq. (1.23) bounds the accessible information between $\mathcal{A}$ and $\mathcal{B}$, after a projective measurement has been performed on $\mathcal{A}$. When instead measurements are performed on $\mathcal{B}$, the corresponding Holevo χ will not in general be the same quantity. Henceforth, discord is an asymmetric quantity: $D(\mathcal{A}:\mathcal{B}) \neq D(\mathcal{B}:\mathcal{A})$.

To finish this chapter, we point out that there are some states, called classical-quantum (CQ) and classical-classical (CC), with some interesting properties regarding their correlations. A state is referred to as CQ if it can be written as $\rho = \sum_i p_i |i\rangle\langle i| \otimes \rho_i^{\mathcal{B}}$, CC if it can be written as $\rho = \sum_{ij} p_{ij} |i\rangle\langle i| \otimes |j\rangle\langle j|$, with $\{|i\rangle\}$ and $\{|j\rangle\}$ two orthonormal sets. We have already seen that, if a state is CQ, the Holevo χ is the same as the QMI. If a state is CC, the accessible information, the maximised Holevo χ and the QMI all reduce to the same quantity [35]. Both CQ and CC states are therefore zero-discord, and their correlations can be accessed locally.

Chapter 2

Quantum objectivity

While it may be common to have an intuitive understanding of what it means for something to be objective, it is not trivial to offer a rigorous and unambiguous definition of objectivity. To avoid the difficulties of dealing with a proper definition of objectivity, we will adopt the convention of defining objectivity in terms of consensus between observers. Within this convention, if different individuals can simultaneously agree on a statement, then that is an objective statement [5, 36]. Quantum objectivity tries to understand when, in the quantum settings, we can say that a particular system has objective features.

Objectivity is a typical property of classical systems, and for this reason understanding quantum objectivity is considered as a fundamental step in understanding the quantum-to-classical transition [37, 38, 39, 40], the process through which quantum systems lose their quantum features and become classical, as well as objective.

In this chapter we will offer an introduction to the subject of quantum objectivity. We will begin in section 2.1 by introducing the notion of decoherence [1, 2, 41], while strictly speaking uncorrelated with quantum objectivity, decoherence, can be considered as a precursor of some of its key concepts, and it has been for a long time a much studied tool in the wider context of the quantum-to-classical transition. In section 2.2 we will delve into the definition of state objectivity in the quantum context, and we will describe the framework of quantum Darwinism [42, 43], that can be used to measure the degree of objectivity of a quantum state. In section 2.3 we will reason in terms of accessible information to discuss some issues that may arise in the framework of quantum Darwinism, we will then introduce an alternative framework, spectrum broadcast structure [44], that allows to solve said issues. We will finally discuss the relations between these two measures of quantum objectivity. Throughout this dissertation, we will refer to objectivity in quantum systems as “quantum objectivity”, this should not be interpreted as a quantum version of objectivity, as opposed to a classical one, but simply highlights that the system with objective features is of a quantum nature.

Box 1: Proper and improper mixtures

We toss a coin, and if the result is heads the system is prepared in the state $|\phi\rangle$, if the result is tails it is prepared in the state $|\psi\rangle$. We don't get to see the result of the coin toss. The system is in a well defined state, but we are fully ignorant about it. The best thing we can do is to describe it as a statistical mixture between $|\phi\rangle$ and $|\psi\rangle$. This is an example of a proper mixture.
Suppose instead that we have a pure system in a superposition between two states, $|\phi\rangle$ and $|\psi\rangle$. The system interacts with an environment and becomes entangled with it, by performing the partial trace over the environment we recover the local state that is once again in a statistical mixture between $|\phi\rangle$ and $|\psi\rangle$ (see Box 1 of chapter 1). This is an example of an improper mixture.
In a proper mixture the system is in a well defined state, but we are forced to describe it as a mixed state because we don't know in which, among the many possible states, is the system. On the other hand, in an improper mixture the system is entangled with an environment, the system is not in a well defined state and our need to describe it as a mixed state does not arise from ignorance on our part.
In the two cases here considered the same final state is produced by means of two very different processes. It is however not possible, by performing measurements on the system, to understand whether we are dealing with a proper or an improper mixture. The impossibility to distinguish between proper and improper mixtures means that, from the operational point of view, there is no distinction between them.

2.1 Decoherence

The emergence of classicality is arguably one of the oldest foundational open questions in quantum mechanics, and the quantum-to-classical transition is still the subject of active research.

Decoherence [1, 2, 41] is often considered a promising mechanism to explain such a transition [3, 4]: as quantum systems are never really isolated [1, 2], their surrounding environment "reads" the system, causing coherent superpositions to be replaced by statistical mixtures, and the corresponding loss of quantum features [4, 45].

Decoherence is usually due to the system interacting with an environment that acquires information about the system in a specific basis, as a consequence of which the system entangles with the environment. The system-environment interaction is usually through Hamiltonians of the type $H_I = A_{\mathcal{S}} \otimes B_{\mathcal{E}}$, where $A_{\mathcal{S}}$ is an operator that acts on the system and $B_{\mathcal{E}}$ an operator that acts on the environment. In this case, should we write the density operator of the system in the basis of the eigenstates of $A_{\mathcal{S}}$, provided that the Hamiltonian of the system $H_{\mathcal{S}}$ commutes with $A_{\mathcal{S}}$, the off-diagonal elements would decay as time progresses, while the diagonal elements would remain unaltered. At the end of a successful decoherence process, the system will be in a statistical mixture of the various eigenstates of $A_{\mathcal{S}}$, and by measuring the whole environment we would be able to infer in which among those is the system. Since the interaction with the environment is unavoidable, and control of the whole environment is usually impossible, decoherence is seen as an irreversible loss of quantum information.

Decoherence consists of the environment acquiring information about the system. This can be interpreted as the environment performing an act of measurement on the system, and subsequently ignoring the outcome. This is because, while the environment effectively contains information about the system, that information is not being accessed. Performing a PVM measurement P on the system ρ, given the outcome i, the post measurement state is $\frac{1}{p_i}P_i\rho P_i$, however, if we do not read the outcome, the resulting state is $\sum_i P_i\rho P_i$. If ρ is written in the basis of the $\{P_i\}$ states, we can see that performing a PVM and ignoring the outcomes results in setting the off diagonal elements to zero, and leaving the diagonal elements unaltered.

The distinction between a measurement process and decoherence is fully analogous to the distinction between proper and improper mixtures (see Box 1). A system that undergoes decoherence entangles with its environment, and while the system and environment together are in a well defined state, the system alone must be described as a statistical mixture of states, making it an improper mixture. On the other hand, if a measurement is performed on a system, and the measurement outcome is ignored, the system is in a proper mixture. While the system is in a well defined state, ignorance about it forces us to describe it as a mixture of states.

There is then no distinction, at the operative level, between a full decoherence process and a measurement process, in the sense that both have the same effects on the system. In a similar manner, a partial decoherence can be seen as a PVM mixed with the identity channel.

The states that the environment "reads" also take the name of pointer states [46]. Being eigenstates of $A_{\mathcal{S}}$, the pointer states are impervious to the effects of decoherence, and can effectively be regarded as classical states as far as the environmental interaction is concerned.

2.2 Objective states

However successful at tackling some aspects of classicality, the theory of decoherence is not "per se" sufficient to directly explain some other pivotal markers of classicality, such as the emergence of objectivity in quantum systems. Understood as consensus between observers, objectivity is an intrinsic property of classical systems, but not of quantum system.

The reason why objectivity is not an intrinsic property of quantum system is that, while a classical system can usually be measured simultaneously by more than one observer and as many times as needed, once a quantum system has been measured it is permanently altered, so that any subsequent measure is actually measuring a different state. It is also a well known fact that unknown quantum states cannot be cloned [47, 48], meaning that an easy strategy to circumvent the fragility of quantum states (creating multiple copies of the same state) is not a viable option. However, information about a given state in one specific basis can be copied without limitations, meaning that, while the full information about the system is not obtainable, limited information (the diagonal elements of the density operator in a given basis) can in principle be simultaneously accessed many observers, who would then be able to share their acquired information and reach a consensus.

While a quantum state can never be considered objective in itself, objectivity may emerge from the quantum state being part of a larger context [49]. Objectivity then becomes a property of the system, dependent on the joint properties of the system and its context, in other words, the environment that caused the decoherence process in the first place. While decoherence is only concerned with studying the dynamical properties of the open system alone, it now becomes necessary take into account the environment as well, and to study the resulting system-environment state.

Given a quantum system $\mathcal{S}$ interacting with an environment $\mathcal{E}$ composed of a number of constituents $\mathcal{E}_i$, we say that the system is objective when observers performing independent measurements on different portions of $\mathcal{E}$ reach a consensus about some property of the system [5, 36]. This is only possible if, due to prior interactions between system and environment, the relevant information was encoded with a high level of redundancy into the environment.

The first framework we will consider is quantum Darwinism (QD) [42, 43]. In quantum Darwinism, given a system-environment state $\rho_{\mathcal{S}\mathcal{E}}$, the objectivity of the system is checked by computing the quantum mutual information between system and environmental fraction, $I(\mathcal{S}:\mathcal{E}_f) = S(\rho_{\mathcal{S}}) + S(\rho_{\mathcal{E}_f}) - S(\rho_{\mathcal{S}\mathcal{E}_f})$ where $\mathcal{E}_f$ is a fraction of the environment such that $\dim(\mathcal{E}_f) = f \dim(\mathcal{E})$ and $f \in (0,1)$. If $I(\mathcal{S}:\mathcal{E}_f) = S(\rho_{\mathcal{S}})$ for a small values of f, then we can divide the environment in roughly $1/f$ fractions, and be confident that an equal amount of observers can make measurements on their respective fractions and recover information about the system. More specifically, it is required that $I(\mathcal{S}:\mathcal{E}_f) = S(\rho_{\mathcal{S}})$ for all $f_0 \leq f \leq 1 - f_0$, and the number of observers that can reach a consensus is precisely $1/f_0$.

In the topical literature, $1/f_0$ is referred to as the "redundancy" of the information encoding. In chapter 4 however, we will show that there is a fundamental difference between the notion of how many times information about the system is encoded into the environment, and how many observers can independently agree on properties of the system. This will lead us to provide operatively clear definitions of "consensus" and "redundancy". Our definition of redundancy will therefore depart from how it is commonly intended in the literature, while consensus will become a technical term with a precise definition, while it currently is a non-technical term, essentially used as synonym of redundancy.

The redundancy of information is made manifest by the behaviour of $I(\mathcal{S}:\mathcal{E}_f)$ as a function of the environmental fraction size f. In objective states, this plot presents a characteristic plateau, once the QMI reaches the value of $S(\rho_{\mathcal{S}})$, it does not increase by increasing the size of the environmental fraction, if not when the whole environment is taken into account ($\rho_{\mathcal{SE}}$ is pure, so that $I(\mathcal{S}:\mathcal{E}) = 2S(\rho_{\mathcal{S}})$). The plateau is a manifestation of the redundancy of the encoded information. If we have access to two environmental fractions, each containing full information about the system, our understanding of the system should not increase, hence the plateau.

The global state $\rho_{\mathcal{SE}}$ is usually assumed to be pure, this assumption is by no means necessary and can be easily relaxed [50]. Should $\rho_{\mathcal{SE}}$ be mixed however, we can always introduce and additional environment $\mathcal{F}$ such that the global state $\rho_{\mathcal{SEF}}$ is pure. This means that considering only pure $\rho_{\mathcal{SE}}$ states by no means incurs in a loss of generality.

Let us remark that $\mathcal{I}(\mathcal{S}:\mathcal{E}_f)$ is the mutual information between the system and a specific environmental fraction of size f, and may depend on the chosen fraction [51, 52]; in order to evaluate QD we must in general perform the average of the mutual information with all possible environmental fractions of the same size [53], we will refer to this quantity as $\tilde{I}(\mathcal{S}:\mathcal{E}_f)$. Provided that $\rho_{\mathcal{SE}}$ is a pure state, it always holds that $I(\mathcal{S}:\mathcal{E}_f) + I(\mathcal{S}:\mathcal{E}\backslash\mathcal{E}_f) = 2S(\rho_{\mathcal{S}})$, where $\mathcal{E}\backslash\mathcal{E}_f$ consists in all the environment apart from $\mathcal{E}_f$.

$$\tilde{I}(\mathcal{S}:\mathcal{E}_f) + \tilde{I}(\mathcal{S}:\mathcal{E}_{1-f}) = \binom{N}{fN} \sum_{\{\mathcal{E}_f\}} I(\mathcal{S}:\mathcal{E}_f) + I(\mathcal{S}:\mathcal{E}\backslash\mathcal{E}_f) = 2S(\rho_{\mathcal{S}}). \tag{2.1}$$

This means that the average mutual information is antisymmetric with respect to the point $f = 1/2$, and that $\tilde{I}(\mathcal{S}:\mathcal{E}_{1/2}) = S(\rho_{\mathcal{S}})$

It should be noted that objective states are a minority among all possible states, in the sense that a generic state randomly extracted from the Hilbert space will most likely not have objective features. At the same time, system-environment states that are the result of a decoherence process will usually be objective [54].

Finally, having introduced the environment as a the repository of information about the system, we can redefine the pointer states as the states the environment holds most information about. In other words, observers measuring their environmental fractions will be able to infer in which among the pointer states is the system.

2.3 Accessible information

Quantum Darwinism defines objectivity in terms of QMI between system and environmental fractions. However, what is really required for quantum objectivity is for observers to be able to recover information about the system by measuring said environmental fractions. This property is quantified by the accessible information, that as we know is strictly less than the QMI. This implies that the use of QMI is actually imprecise, since it could prove to be misleading: if a system-environment state satisfies the conditions of QD, the system would be interpreted as objective, even when observers would actually not be able to reach a consensus about properties of the system. Since the Holevo χ offers a more precise way to bound the accessible information, it has been proposed that quantum objectivity should be measured my means of the Holevo χ, and not QMI. This approach takes the name of strong quantum Darwinism (SQD) [55].

An alternative framework used to measure objectivity is that of spectrum broadcast structure (SBS) [44]. According to SBS, the state of a system is considered to be objective if the system-environment state can be cast in the following form

$$\rho_{\text{SBS}} = \sum_i p_i \left|i\right\rangle\!\left\langle i\right| \otimes R_i^{(1)} \otimes R_i^{(2)} \otimes \cdots \otimes R_i^{(N)}, \tag{2.2}$$

with the extra condition that

$$R_i^{(j)} R_{i'}^{(j)} = \delta_{ii'} \left(R_i^{(j)}\right)^2 \forall i, i', j. \tag{2.3}$$

The $|i\rangle$ states are an orthonormal basis for the system, and the various $R_i^{(j)}$ states are the states of the environmental fractions $\mathcal{E}_j$, conditioned by the fact that the state of the system is $|i\rangle$.

Provided that each observer has access to an environmental fraction $\mathcal{E}_j$, if one of them measures their fraction to be in the state $R_i^{(j)}$, they will infer that the system is in the state $|i\rangle\!\langle i|$, additionally, eq. (2.3) ensures that, for each fragment $\mathcal{E}_j$ the possible $R_i^{(j)}$ can all be distinguished from one another without mistakes. From the structure of the state in eq. (2.2) it can be seen that if one observer determines that the system is in the $|i\rangle\!\langle i|$ state, all other observers will independently reach the same conclusion, and thus consensus among them is ensured. Since there are N such environmental fractions, then N is the number of observers that can simultaneously agree on the state of the system.

The environmental fractions $\mathcal{E}_j$ are by no means bound to be the individual constituents of the environment: each of the $\mathcal{E}_j$ fractions can be composed by several of the environmental constituents, and therefore take the name of macrofractions [56, 57]. This is analogous to the fact that in QD we do not expect that $I(\mathcal{S} : \mathcal{E}_f) = S(\rho_{\mathcal{S}})$ when $\mathcal{E}_f$ is the individual environmental constituent, and it is perfectly accepted that the individual environmental constituents may not, by themselves, contain enough information about the system. According to SBS, so long as it is possible to partition the environment into appropriate macrofractions, the state of the system is objective. Consider for example the state

$$\rho_{\mathcal{S}\mathcal{E}} = p_0 \left|0\right\rangle\!\left\langle 0\right|_{\mathcal{S}} \otimes \left|0\right\rangle\!\left\langle 0\right|^{\otimes N} + p_1 \left|1\right\rangle\!\left\langle 1\right|_{\mathcal{S}} \otimes \left|+\right\rangle\!\left\langle +\right|^{\otimes N}. \tag{2.4}$$

One may initially think that this state does not satisfy the SBS condition. This is because $|0\rangle$ and $|+\rangle$ are not distinguishable from one another, and observers accessing an environmental constituent will not be able to recover sufficient information about the system. However, it is simply required that it is possible to divide the environment into a sufficient number of macrofractions such that the condition in eq. (2.3) is

Box 2: Encoding information about qudits into qubits

For an system to be objective, the macrofractions need to have at least the same dimensionality of the system. From a QD perspective because objectivity is possible only if the entropy of the environmental fraction is the same as the entropy of the system. From an SBS perspective because the number of distinguishable states conditioned by the state of the system needs to be the same as the number of pointer states.

However, the individual environmental constituents can be of lower dimensions, even for objective states. Here we propose the example where, the system is a qutrit, and the environment is made out of qubits. The system —a qutrit— can be in one of the following states: $|0\rangle_{\mathcal{S}}$, $|1\rangle_{\mathcal{S}}$ and $|2\rangle_{\mathcal{S}}$. The global state is

$$|\psi\rangle = \frac{1}{\sqrt{3}}\left(|0\rangle_{\mathcal{S}} \otimes |0\rangle^{\otimes N} + |1\rangle_{\mathcal{S}} \otimes |+\rangle^{\otimes N} + |2\rangle_{\mathcal{S}} \otimes |1\rangle^{\otimes N}\right). \tag{2.6}$$

Its not difficult to check that the state above is objective, by reasoning in a similar fashion to how we did in eq. (2.5) we can divide the environment into fractions comprised by m qubits each. While a qubit may only be in two distinguishable states, several qubits all in product states are increasingly orthogonal even if the individual states are not, and can thus be in several (almost) distinguishable states. It is possible then to encode information about the system in (for example) qubits, regardless of the dimensionality of the system, provided that the environment is large enough.

satisfied. We can indeed rewrite the previous state as

$$\rho_{\mathcal{SE}} = p_0\, |0\rangle\!\langle 0|_{\mathcal{S}} \otimes \left(|0\rangle\!\langle 0|^{\otimes m}\right)^{\otimes N/m} + p_1\, |1\rangle\!\langle 1|_{\mathcal{S}} \otimes \left(|+\rangle\!\langle +|^{\otimes m}\right)^{\otimes N/m}. \tag{2.5}$$

The ability to distinguish between $|0\rangle^{\otimes m}$ and $|+\rangle^{\otimes m}$ scales with m, $|\,\langle 0|^{\otimes m}\,|+\rangle^{\otimes m}\,| = \left(\frac{1}{2}\right)^m$. Therefore we can arbitrarily increase the degree of distinguishability by increasing the size of the macrofractions, provided of course that the value of N allows us to do so and still remain with a significant number of macrofractions. By following an analogous reasoning, we show in Box 2 that the environmental constituents can be of a lower dimensionality than the system.

The state in eq. (2.2) is a mixed state, while in QD the global state is usually assumed to be pure. This is because a state should have SBS after we have traced out at least one macrofraction. Let us consider the following pure state

$$\rho = \sum_i \sqrt{p_i}\, |i\rangle \otimes \bigotimes_j \left|R_i^{(j)}\right\rangle, \tag{2.7}$$

with $\left\langle R_i^{(j)} \middle| R_{i'}^{(j)} \right\rangle = \delta_{ii'}$. With a slight abuse of notation, we could say that the state in eq. (2.7) also has SBS since, by tracing out one macrofraction, we recover the state in eq. (2.2). It is not required however that the $R_i^{(j)}$ states are pure, so that eq. (2.2) is more general than eq. (2.7).

The SBS framework also proves to be a tool to measure the pointer states of the system: the possible states observers may find the system to be in emerge naturally from eq. (2.2), and are precisely the set of $\{|i\rangle\}$ states [44]. Notice however that the pointer states were originally introduced in the context of pure decoherence. The frameworks in quantum objectivity are generally unconcerned with the dynamics from which the objective state arises, and the SBS state could be the result of dynamics that are not pure dephasing.

As a measure of objectivity, QD relies on entropic properties, whereas SBS relies on the geometric properties of the overall system-environment state. While the two measures may seem to take two very different approaches, they are actually strongly connected [58, 59]. There is indeed a hierarchy between the measures of objectivity, that we will present here.

SBS implies SQD and QD— Given the state in eq. (2.2), the state of system and a portion of the environment is $\rho_{\mathcal{S}\mathcal{E}_f} = \sum_i p_i |i\rangle\langle i| \otimes R_i^{(1)} \otimes R_i^{(2)} \otimes \cdots \otimes R_i^{(fN)}$. The state of the system is $\rho_{\mathcal{S}} = \sum_i p_i |i\rangle\langle i|$ and the state of the environmental fraction is $\rho_{\mathcal{E}_f} = \sum_i p_i R_i^{(1)} \otimes R_i^{(2)} \otimes \cdots \otimes R_i^{(fN)}$. The three states have the same entropy, $S(\rho_{\mathcal{S}\mathcal{E}_f}) = S(\rho_{\mathcal{E}_f}) = S(\rho_{\mathcal{S}})$, therefore $I(\mathcal{S} : \mathcal{E}_f) = S(\rho_{\mathcal{S}})\ \forall f$, moreover, since eq. (2.2) is a CQ state, it is naturally zero-discord, and the QMI coincides with the Holevo χ, which is also $S(\rho_{\mathcal{S}})$.

SQD implies bipartite SBS— One of the requirements of SQD is that there is no discord between system and environmental fractions, which is satisfied if the state is CQ. A generic CQ state has the form

$$\rho_{\mathcal{S}:\mathcal{E}_f} = \sum_i p_i |i\rangle\langle i| \otimes R_i^{(f)}. \tag{2.8}$$

Since SQD also requires that $I_{\text{acc}}(\mathcal{S} : \mathcal{E}_f) = S(\rho_{\mathcal{S}})$, for a state like the one above this is only satisfied if $R_i^{(f)} R_{i'}^{(f)} = \delta_{ii'}$. We then recover a bipartite SBS state [59].

SQD and strong independence implies SBS— We first need to introduce the concept of "strong independence" [44] between the environmental macrofractions. Strong independence states that the environmental fractions are only correlated through the system, and it can be put in terms of the multipartite mutual information conditioned by the state of the system $I(\mathcal{E}_0 \dots \mathcal{E}_N|\mathcal{S}) = \sum_j S(\rho_{\mathcal{E}_j|\mathcal{S}}) - S(\rho_{\mathcal{E}|\mathcal{S}}) = 0$. The strong independence requirement is satisfied if the states of the macrofractions, conditioned by the state of the system, are in a product states. If we impose strong independence between the environmental macrofractions in eq. (2.8), the resulting state is SBS. What we have provided here is more of an argument rather than a rigorous proof, which can be found in [55].

If a system is objective according to SBS, then it also is objective according to QD. The opposite of this statement however is not true, so that SBS is considered to be a more stringent measure of quantum objectivity.

Chapter 3

Stochastic Collision Models

In this chapter, we introduce the stochastic collision models (SCMs), a class of open system dynamics that combine quantum collision models and classical stochastic processes. After a description of the framework, we will explore some features of the stochastic collision models by applying it to some relevant scenarios. In particular, in section 3.1 we will use the SCM to study the open dynamics of a qubit in a pure dephasing regime. We will see how decoherence and non-Markovianity can both be present without system-environment entanglement, while the same is not true when it comes to quantum Darwinism, suggesting that the emergence of objectivity within a dynamical model requires for system-environment entanglement to be established, more details can be found in [60]. In section 3.2 we will further explore the versatility of the SCM by using it to model the environmental effects on a quantum network, and show how it proves to be a useful tool for studying transport phenomena in quantum networks. More details in [61].

In a SCM the ancillae collide with the system at non-deterministic times, according to a stochastic process. While this may *a priori* seem to be a minor difference with respect to deterministic-time collisions, we will show how it has important physical implications. The dynamics of the system is recovered by averaging over the stochastic realizations, and depending on the parameters of the stochastic process, it can exhibit both Markovian and non-Markovian behaviors.

As with standard CMs, system and environment are initially in a product state

$$\rho_{\text{tot}} = \rho_0 \otimes \nu^{\otimes N}. \tag{3.1}$$

Between one collision and the next the system evolves by means of a unitary channel $\rho(t+\tau) = \mathcal{F}(\tau)\rho(t) = U(\tau)\rho(t)U^\dagger(\tau)$, where $U(\tau) = e^{-i\tau H_\mathcal{S}}$ and $H_\mathcal{S}$ is the free Hamiltonian of the system.

The collision between an ancilla and the system is modeled through the unitary dynamics generated by the interaction Hamiltonian H_I during a short period of time τ_c. We assume the collision time τ_c to be much shorter than any relevant time scale in the free system dynamics, so that collisions can be regarded as an instantaneous processes, effectively resulting in the application of the unitary transformations $U_I = e^{-i\tau_c H_I}$. We assume that the ancilla does not collide again with the system, meaning that its degrees of freedom can be safely traced out after the collision. This effectively implies that, just like for CMs, the individual collisions correspond to the system evolving according to the same quantum channel Φ.

After a certain amount of time, the system will have evolved according to the following expression:

$$\rho_t = \mathcal{F}(t-t_n)\Phi \ldots \Phi\mathcal{F}(t_2-t_1)\Phi\mathcal{F}(t_1)\rho_0, \tag{3.2}$$

where the collision times t_i are such that the time interval between one collision and the next follows a given probability distribution.

It should be stressed that this is the resulting state for one single realization of the stochastic process. The ensemble dynamics is obtained by averaging over all possible realizations of the stochastic process, and it can be written in the following general form (see [62])

$$\rho(t) = p_0(t)\mathcal{F}\rho(0) + \sum_{n=1}^{\infty}\int_0^t dt_n \cdots \int_0^{t_2} dt_1 p_n(t_n,\ldots,t_1)\mathcal{F}(t-t_n)\Phi\ldots\Phi\mathcal{F}(t_2-t_1)\Phi\mathcal{F}(t_1)\rho(0). \tag{3.3}$$

where $p_n(t_n,\ldots,t_1)$ is the probability density for the realization of n collisions, so that $p_n(t) = \int_0^t dt_n \cdots \int_0^{t_2} dt_1 p_n(t_n,\ldots,t_1)$ is the probability that at time t the system went through precisely n collisions.

For simplicity, we have assumed that there is only one type of ancilla that can collide with the system, and only one underlying stochastic process that determines the collision times. It is nonetheless straightforward to relax these assumptions, and in section 3.2 we will see an example where the system evolves due to multiple stochastic collision models.

Throughout the chapter, we will focus on situations in which the ancillae are all initially in a product state and collide with the system only once. It should be noted however, that the model can accommodate the same scenarios that have been explored in the literature of collision models, such as allowing the ancillae to be initially correlated or to collide multiple times with the system.

3.1 Decoherence without entanglement and quantum Darwinism

In this section we study the open system evolution of a single qubit modelling the interaction with the environment by means of a stochastic collision model.

We first focus on the connections between the qubit decoherence and entanglement production between the qubit and the ancillae. The very idea that open system dynamics arises from the interaction between two parts of a bipartite total system naturally suggests that entanglement must be established between the two during the time evolution. This is indeed very often the case and it is therefore not surprising that environment-induced decoherence has been until now associated with the presence of entanglement between system $\mathcal{S}$ and environment $\mathcal{E}$. However, it can be shown

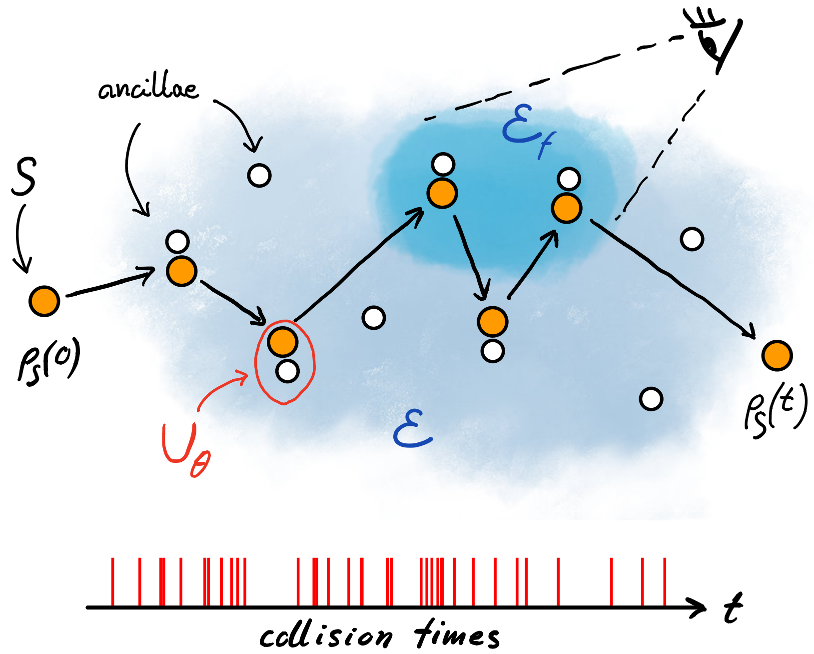

FIGURE 3.1: Sketch illustrating the model. The orange dots represent the system $\mathcal{S}$ colliding with different ancillae (white dots) at exponentially distributed random times, depicted as red vertical lines on the t-axis. During each collision, the system and the corresponding ancilla undergo a unitary transformation U_θ. The set of all ancillae defines the environment $\mathcal{E}$, whereas $\mathcal{E}_f$ represents a randomly chosen fraction f of the ancillae, to which an observer might have access in order to acquire information about the state of the system.

that, contrarily to this intuition, as long as we limit our attention to the reduced dynamics of the system $\mathcal{S}$ only, decoherence may take place without entanglement. Specifically, we identify two different microscopic descriptions of the total system, one establishing $\mathcal{S}-\mathcal{E}$ entanglement while the other one does not, leading to the same reduced dynamics for $\mathcal{S}$.

The same model shows that also information back-flow, identified as the source of memory effects, i.e., non-Markovian dynamics [18], does not require $\mathcal{S}-\mathcal{E}$ entanglement. Finally, we show that entanglement plays a pivotal role in the objectification process, since it appears to be needed for it to take place.

The environment is composed of a set of initially uncorrelated ancillae colliding with the system sequentially and only once. This interaction mechanism results on pure dephasing of the system qubit, exhibiting both Markovian and non-Markovian dynamics, depending on the relevant parameters. Our analysis reveals that, while the SCM can give rise to exactly the same qubit dephasing as the one caused by an entangling interaction, it is not capable of accounting for QD. However, the introduction of a super-environment acting as the source for the randomness in the collision times elucidates the origin of QD and the role played by entanglement in it.

Let us first describe the model under consideration, which is also depicted in fig. 3.1. The system is a single qubit with free Hamiltonian $H_\mathcal{S} = \frac{\omega}{2}\sigma_z$, where ω is the qubit frequency, subject to collisions with qubit ancillae at random times. The collision times follow a Poisson process with rate λ, meaning that the inter-collision time is exponentially distributed. The initial state of all the ancillae is $\rho_a = |0\rangle\langle 0|$, henceforth uncorrelated. When an ancilla collides with the system, it interacts with it with Hamiltonian $H_I = \frac{\eta}{2}\sigma_x^a \otimes \sigma_z^{\mathcal{S}}$, where the superscripts stand for ancilla and system, respectively. The interaction time is considered to be extremely short, so the collision can be regarded as instantaneous, and its effect amounts to a unitary transformation applied to both the system and the ancilla. Here we denote by interaction strength the limit $\theta = \lim_{t\to 0} t\eta$, where t is the duration of the collision. The resulting unitary transformation for the collision is $U_\theta = \exp\{-i\frac{\theta}{2}\sigma_x^a \otimes \sigma_z^{\mathcal{S}}\}$.

Since all the ancillae are initially uncorrelated with each other and with the system, and they collide with the system only once, we can describe the change on the system's state in terms of the collision channel

$$\Phi_c[\rho_{\mathcal{S}}] = \mathrm{Tr}_a\left[U_\theta \rho_a \otimes \rho_{\mathcal{S}} U_\theta^\dagger\right]. \tag{3.4}$$

which can be cast in Kraus form as $\Phi_c[\rho_{\mathcal{S}}] = K\rho_{\mathcal{S}}K^\dagger + K^\dagger\rho_{\mathcal{S}}K$, with

$$K = \frac{1}{\sqrt{2}}\begin{pmatrix} e^{-i\theta/2} & 0 \\ 0 & e^{i\theta/2} \end{pmatrix}. \tag{3.5}$$

As a result, the effect of the channel is a factor $\cos\theta$ multiplying the coherences of the qubit state.

3.1.1 Decoherence

The state of the system at time t is given by the convex sum of all possible stochastic realisations of the ancillary dynamics (trajectories), each of them weighted by its probability. We notice that K commutes with $H_{\mathcal{S}}$ and, therefore, with $U_t^{\mathcal{S}} = e^{-itH_{\mathcal{S}}}$. This in turn implies that, if the number of collisions at time t is k, we can simply write the state of system as $\rho_k(t) = U_t^{\mathcal{S}}\Phi_c^{(k)}\left[\rho_{\mathcal{S}}(0)\right]U_t^{\mathcal{S}\dagger}$, where the superscript (k) indicates that the channel is applied k times. According to our previous observation, the state in every trajectory is fully determined by the number of collisions, so we can write

$$\rho_{\mathcal{S}}(t) = \sum_{k=0}^{\infty} p_k(t)\rho_k(t), \tag{3.6}$$

where $p_k(t)$ is the probability for k collision events to have happened at time t. Since collisions follow a Poisson process,

$$\rho_{\mathcal{S}}(t) = e^{-\lambda t}\sum_{k=0}^{\infty}\frac{(\lambda t)^k}{k!}\rho_k(t). \tag{3.7}$$

In Box 1 we show how to obtain the integrated dynamics. Here we recover the master equation of the process, starting with the time derivative of eq. (3.7) that gives

$$\dot{\rho}_{\mathcal{S}}(t) = -\lambda\rho_{\mathcal{S}}(t) + e^{-\lambda t}\left(\sum_{k=0}^{\infty}\frac{(\lambda t)^k}{k!}\dot{\rho}_k(t) + \sum_{k=1}^{\infty}\frac{\lambda^k t^{k-1}}{(k-1)!}\rho_k(t)\right). \tag{3.8}$$

The leftmost term in the parenthesis gives the unitary evolution of the system,

$$e^{-\lambda t}\sum_{k=0}^{\infty}\frac{(\lambda t)^k}{k!}\dot{\rho}_k(t) = e^{-\lambda t}\sum_{k=0}^{\infty}\frac{(\lambda t)^k}{k!}\left(-i\left[H_{\mathcal{S}},\rho_k(t)\right]\right) = -i\left[H_{\mathcal{S}},\rho_{\mathcal{S}}(t)\right], \tag{3.9}$$

whereas the rightmost one is

$$\lambda e^{-\lambda t}\sum_{k=0}^{\infty}\frac{\lambda^k t^k}{k!}\rho_{k+1}(t) = \lambda e^{-\lambda t}\sum_{k=0}^{\infty}\frac{\lambda^k t^k}{k!}\Phi_c\left[\rho_k(t)\right] = \lambda\Phi_c\left[\rho_{\mathcal{S}}(t)\right]. \tag{3.10}$$

Finally, we can write

$$\dot{\rho}_{\mathcal{S}}(t) = -i\left[H_{\mathcal{S}},\rho_{\mathcal{S}}(t)\right] + \lambda\left(\Phi_c\left[\rho_{\mathcal{S}}(t)\right] - \rho_{\mathcal{S}}(t)\right), \tag{3.11}$$

which is in GKSL [63, 64] form, with K and $K^\dagger$ as Lindblad operators. Hence, we conclude that the system undergoes Markovian dynamics.

The master equation eq. (3.11) describes a pure dephasing dynamics with decoherence factor $c(t) = \exp[-\lambda(1-\cos\theta)t]$. We notice that $c(t)$ is invariant with respect to changes of the interaction strength θ upon a proper modification of the collision rate. In particular, the system undergoes the same temporal evolution for $\lambda\,(1-\cos\theta) = C$, where C is constant. This is an interesting observation, since the interaction strength θ defines the level of entanglement between the system and a given ancilla after a collision has taken place. For instance, for $\theta = (2m+1)\pi$, $m \in \mathbb{Z}$, $U_\theta\left|0\right\rangle_a \otimes \left|+\right\rangle_{\mathcal{S}} = e^{-i\pi/2}\left|1\right\rangle_a \otimes \left|-\right\rangle_{\mathcal{S}}$, yielding a product state, while for $\theta = (2m+1)\pi/2$, $m \in \mathbb{Z}$, the two become maximally entangled. Hence, we can conclude that, in the former case, the system undergoes pure dephasing while remaining in a separable state with respect to the environment.

The source of randomness in the collision times can be seen as originating from a quantum process where the particle is emitted, for instance, as a result of a spontaneous emission process. This would reintroduce entanglement, in this case with an effective super-environment, in the overall picture. We will analyse the consequences of such an effective description in more detail when focusing on QD. At this point, it is sufficient to stress that a quantum super-environment does not need to enter the description, since the collisions with the ancillae can be triggered by some classical and largely macroscopic stochastic process.

Box 1: Integrated dynamics

Invoking again the commutativity of the Kraus operators with the system Hamiltonian, and using eq. (3.7), the state of the system at time t can be expressed as

$$\rho_{\mathcal{S}}(t) = e^{-\lambda t} \sum_{k=0}^{\infty} \frac{(\lambda t)^k}{k!} \Phi_c^{(k)} \left[U_t^{\mathcal{S}} \rho_{\mathcal{S}}(0) U_t^{\mathcal{S}\dagger} \right]. \tag{3.12}$$

Denoting

$$\rho_{\mathcal{S}}(0) = \begin{pmatrix} \rho_{00} & \rho_{01} \\ \rho_{10} & \rho_{11} \end{pmatrix}, \tag{3.13}$$

the term $U_t^{\mathcal{S}} \rho_{\mathcal{S}}(0) U_t^{\mathcal{S}\dagger}$ becomes

$$U_t^{\mathcal{S}} \rho_{\mathcal{S}}(0) U_t^{\mathcal{S}\dagger} = \begin{pmatrix} \rho_{00} & \rho_{01} e^{-i\omega t} \\ \rho_{10} e^{i\omega t} & \rho_{11} \end{pmatrix}. \tag{3.14}$$

Therefore, using the Kraus decomposition of the collision channel, we see that

$$\Phi_c^{(k)} \left[U_t^{\mathcal{S}} \rho_{\mathcal{S}}(0) U_t^{\mathcal{S}\dagger} \right] = \begin{pmatrix} \rho_{00} & \rho_{01} e^{-i\omega t} \cos^k \theta \\ \rho_{10} e^{i\omega t} \cos^k \theta & \rho_{11} \end{pmatrix}. \tag{3.15}$$

Introducing this result into eq. (3.12), we can write

$$\rho_{\mathcal{S}}(t) = \begin{pmatrix} \rho_{00} & \rho_{01} e^{-i\omega t} \langle \cos^k \theta \rangle_t \\ \rho_{10} e^{i\omega t} \langle \cos^k \theta \rangle_t & \rho_{11} \end{pmatrix}, \tag{3.16}$$

where $\langle \cos^k \theta \rangle_t$ is a shorthand notation for

$$\langle \cos^k \theta \rangle_t = e^{-\lambda t} \sum_{k=0}^{\infty} \frac{(\lambda t)^k}{k!} \cos^k \theta = e^{-\lambda t} e^{\lambda t \cos \theta} = e^{-\lambda t (1 - \cos \theta)}, \tag{3.17}$$

and yields the coherence factor $c(t)$ in the main text. Hence, the state of the system at time t is

$$\rho_{\mathcal{S}}(t) = \begin{pmatrix} \rho_{00} & \rho_{01} e^{-t(i\omega + \lambda(1-\cos\theta))} \\ \rho_{10} e^{t(i\omega - \lambda(1-\cos\theta))} & \rho_{11} \end{pmatrix}. \tag{3.18}$$

From the latter result, we see that the system decoheres with rate $\lambda\,(1 - \cos\theta)$.

3.1.2 Non-Markovianity

The model introduced above describes the situation in which the system undergoes Markovian pure dephasing dynamics while remaining in a separable state with the environment. We now show that SCMs can induce non-Markovian behaviour as well. To this end, we modify the previous model by limiting the number of ancillae to a finite amount n. Here, every ancilla's collision time has an exponential probability density with rate λ/n, so that the probability for any ancilla to have collided at time

t is $p_t = 1 - e^{-\lambda t/n}$. The effect of the collisions is not altered. The state of the system at time t, in the case in which there are n ancillae, now reads

$$\rho_{\mathcal{S}}(t) = \sum_{\alpha_1=0}^{1} \cdots \sum_{\alpha_n=0}^{1} \Lambda(\vec{\alpha}_n) \Phi_c^{(\sum_i \alpha_i)} \left[U_t^{\mathcal{S}} \rho_{\mathcal{S}}(0) U_t^{\mathcal{S}\dagger} \right]. \tag{3.19}$$

Where we have introduced the vector $\vec{\alpha}_n = (\alpha_1, \cdots, \alpha_n)$. Each index α_i represents the state of the i-th ancilla, that is, whether it has collided or not, so the sum runs over all possible histories. The function $\Lambda(\vec{\alpha}_n)$ accounts for the probability of each trajectory, and is given by

$$\Lambda(\vec{\alpha}_n) = \prod_{i=1}^{n} \left[p_t^{\alpha_i} (1 - p_t)^{1-\alpha_i} \right], \tag{3.20}$$

Using eq. (3.15), we obtain

$$\rho_{\mathcal{S}}(t) = \begin{pmatrix} \rho_{00} & \rho_{01} e^{-i\omega t} \left\langle (\cos\theta)^{\sum_i \alpha_i} \right\rangle_t \\ \rho_{10} e^{i\omega t} \left\langle (\cos\theta)^{\sum_i \alpha_i} \right\rangle_t & \rho_{11} \end{pmatrix}, \tag{3.21}$$

where $\langle \cdot \rangle_t$ stands for the average over trajectories at time t. This quantity can be computed as

$$\begin{aligned} \left\langle (\cos\theta)^{\sum_i \alpha_i} \right\rangle_t &= \sum_{\alpha_1=0}^{1} \cdots \sum_{\alpha_n=0}^{1} \Lambda(\vec{\alpha}_n) (\cos\theta)^{\sum_i \alpha_i} \\ &= \sum_{\alpha_1=0}^{1} \cdots \sum_{\alpha_n=0}^{1} \prod_{i=1}^{n} \left[(p_t \cos\theta)^{\alpha_i} (1 - p_t)^{1-\alpha_i} \right] \\ &= (p_t \cos\theta + 1 - p_t)^n = \left[1 + (\cos\theta - 1) \left(1 - e^{-\lambda t/n} \right) \right]^n. \end{aligned} \tag{3.22}$$

The integrated dynamics reduces to that of infinitely many ancillae at short times, $\lambda t \ll n$. Coherences are multiplied by the factor

$$c_{\mathrm{NM}}(t) = \left[1 + (\cos\theta - 1) \left(1 - e^{-\lambda t/n} \right) \right]^n. \tag{3.23}$$

In this case, the entanglement-invariance in the dynamics no longer holds. Furthermore, this new phase factor $c_{\mathrm{NM}}(t)$ gives rise to non-Markovian dynamics. In the particular case in which the system and the ancilla entangle maximally after a collision ($\cos\theta = 0$), the system dephases monotonically with $c_{\mathrm{NM}}(t) = e^{-\lambda t}$, exactly like in the model with infinitely many ancillae. In the case of entanglement-free interaction ($\cos\theta = -1$), however, the off-diagonal elements of the density matrix are multiplied by the factor $c_{\mathrm{NM}}(t) = \left(2e^{-\lambda t/n} - 1 \right)^n$, which is equal to zero at $t_m = n \ln 2/\lambda$ (mixture time) and tends to $(-1)^n$ as $t \to \infty$. As a consequence, if the initial state of the system is, e.g., $\rho_{\mathcal{S}}(0) = |+\rangle\langle +|$, it becomes maximally mixed at $t = t_m$ and it gradually recovers its purity thereafter. Moreover, the system remains in a highly mixed state for longer periods as the environment size n increases (see fig. 3.2). Remarkably, this

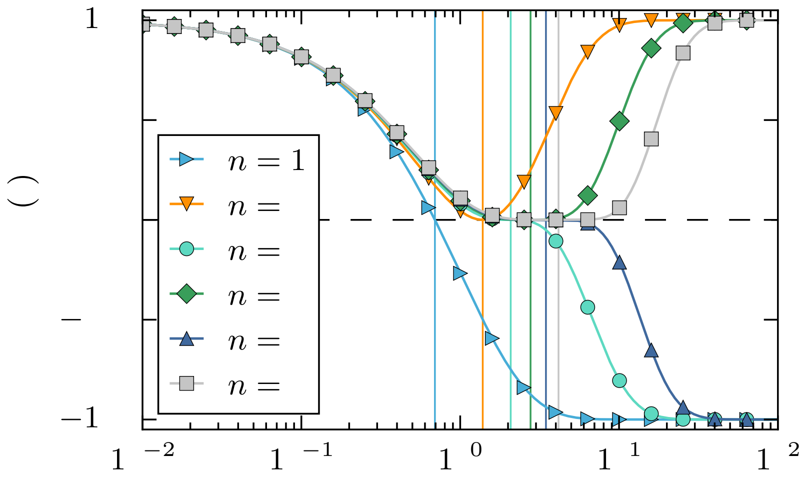

FIGURE 3.2: Coherence factor for the qubit, eq. (3.23), as a function of time for different number of ancillae with non-entangling interaction strength, $\theta = \pi$ and $\lambda = 1$. The vertical lines indicate the corresponding mixture time t_m, at which the coherence vanishes. The recoherence effect is a direct consequence of the environmental finite size. As time progresses, the probability that all ancillae collided with the system increases, reducing the information the environment holds about the system. As the number of ancillae increases, the coherence remains close to zero for longer periods of time

phenomenon of recoherence takes place despite the fact that the system never collides with the same ancilla more than once, and despite the absence of interactions [65] between ancillae.

3.1.3 Quantum Darwinism

So far we have shown that it is possible for a system to undergo exactly the same decoherence dynamics whether or not it becomes entangled with its environment, or even to exhibit non-Markovian dynamics, as a consequence of a SCM. Needless to say, this raises the question of what role does entanglement play in the quantum-to-classical transition. In what follows, we address this issue in the context of QD. As we will show, decoherence without entanglement does not allow for the encoding of information about the system's state into the environment, whereas this is possible when one considers a super-environment giving a quantum origin to the randomness in the collision times.

We focus first on the case in which the interaction is non-entangling, namely $\theta = \pi$, and the initial state of the system is $\rho_{\mathcal{S}}(0) = |+\rangle\langle+|$. By tracing out $k = (1-f)n$ ancillae from the total state of system and environment $\rho_{\mathcal{SE}}(t)$, one can calculate the reduced state when only a fraction f of the latter is considered, $\rho_{\mathcal{SE}_f}(t) = \mathrm{Tr}_k\left[\rho_{\mathcal{SE}}(t)\right]$, while further tracing out the system $\mathcal{S}$ yields the reduced state of the fraction of the environment, $\rho_{\mathcal{E}_f}(t)$. The total system-environment state at time t, $\rho_{\mathcal{SE}}(t)$, can be written as the convex sum

$$\rho_{\mathcal{SE}}(t) = \sum_{\alpha_1=0}^{1} \cdots \sum_{\alpha_n=0}^{1} \Lambda(\vec{\alpha}_n)|\vec{\alpha}_n\rangle\langle\vec{\alpha}_n| \otimes \left(\delta_{\text{even}}(\vec{\alpha}_n)|+_t\rangle\langle+_t| + \delta_{\text{odd}}(\vec{\alpha}_n)|-_t\rangle\langle-_t|\right), \tag{3.24}$$

where we have denoted $|\pm_t\rangle = U_t^{\mathcal{S}}|\pm\rangle$ and defined the functions $\delta_{\text{even}}(\vec{\alpha}_n)$ and $\delta_{\text{odd}}(\vec{\alpha}_n)$, which are equal to one if their argument represents an even (odd) number of collisions and zero otherwise. These can be written as $\delta_{\text{even}}(\vec{\alpha}_n) = \frac{1+(-1)^{\sum_i \alpha_i}}{2}$ and $\delta_{\text{odd}}(\vec{\alpha}_n) = \frac{1-(-1)^{\sum_i \alpha_i}}{2}$. Equation (3.24) explicitly shows that the state is fully separable. Now, in order to compute the mutual information, we need to characterise the reduced state of the system and a fraction f of the environment, $\rho_{\mathcal{SE}_f}(t) = \text{Tr}_k\left[\rho_{\mathcal{SE}}(t)\right]$, resulting from tracing out $k = (1-f)n$ ancillae. To do so, consider a projector $|\vec{\alpha}_{n-k}\rangle\langle\vec{\alpha}_{n-k}|$ corresponding to some state of the $n-k$ non-traced-out ancillae representing an even number of collisions. In the reduced density operator, it will appear tensored with both $|+_t\rangle\langle+_t|$ and $|-_t\rangle\langle-_t|$, since $|\vec{\alpha}_{n-k}\rangle\langle\vec{\alpha}_{n-k}| \otimes |+_t\rangle\langle+_t|$ will be the result of integrating over all the states of the k traced-out ancillae representing an even number of collisions, whereas the integration over odd collisions of the k ancillae will give $|\vec{\alpha}_{n-k}\rangle\langle\vec{\alpha}_{n-k}| \otimes |-_t\rangle\langle-_t|$. Now, their corresponding matrix elements can be readily computed, since they are simply given by the probability of $\vec{\alpha}_{n-k}$ multiplied by the sum of the probabilities of all the states of the k traced-out ancillae with either even or odd parities. Hence, we can write $\rho_{\vec{\alpha}_{n-k},+t} = \Lambda(\vec{\alpha}_{n-k})P_k^{\text{e}}(t)$ and $\rho_{\vec{\alpha}_{n-k},-t} = \Lambda(\vec{\alpha}_{n-k})\left(1-P_k^{\text{e}}(t)\right)$, where $P_k^{\text{e}}(t)$ is the probability for the k ancillae to yield an even number of collisions at time t and can be computed as

$$\begin{aligned} P_k^{\text{e}}(t) &= \sum_{\alpha_1=0}^{1} \cdots \sum_{\alpha_k=0}^{1} \Lambda(\vec{\alpha}_k)\delta_{\text{even}}(\vec{\alpha}_k) \\ &= \frac{1}{2}\left(1 + \sum_{\alpha_1=0}^{1} \cdots \sum_{\alpha_k=0}^{1} \Lambda(\vec{\alpha}_k)(-1)^{\sum_i \alpha_i}\right) \\ &= \frac{1}{2}\left[1 + \left(2e^{-\lambda t/n} - 1\right)^k\right]. \end{aligned} \tag{3.25}$$

Notice that $+_t$ and $-_t$ need to be swapped in the previous discussion if the parity of $\vec{\alpha}_{n-k}$ is odd. With this result in hand, we can now compute all reduced density matrices in diagonal form. First, by setting $k = n$, we immediately obtain the reduced state of the system as $\rho_{\mathcal{S}}(t) = P_n^{\text{e}}(t)\,|+_t\rangle\langle+_t| + (1-P_n^{\text{e}}(t))\,|-_t\rangle\langle-_t|$. The reduced state of the environment is given by $\rho_{\mathcal{E}_f}(t) = \text{Tr}_{\mathcal{S}}\left[\rho_{\mathcal{SE}_f}(t)\right] = \sum_{\alpha_1=0}^{1} \cdots \sum_{\alpha_{n-k}=0}^{1} \Lambda(\vec{\alpha}_{n-k})\,|\vec{\alpha}_{n-k}\rangle\langle\vec{\alpha}_{n-k}|$. With these results, we can immediately compute the entropies involved in the mutual

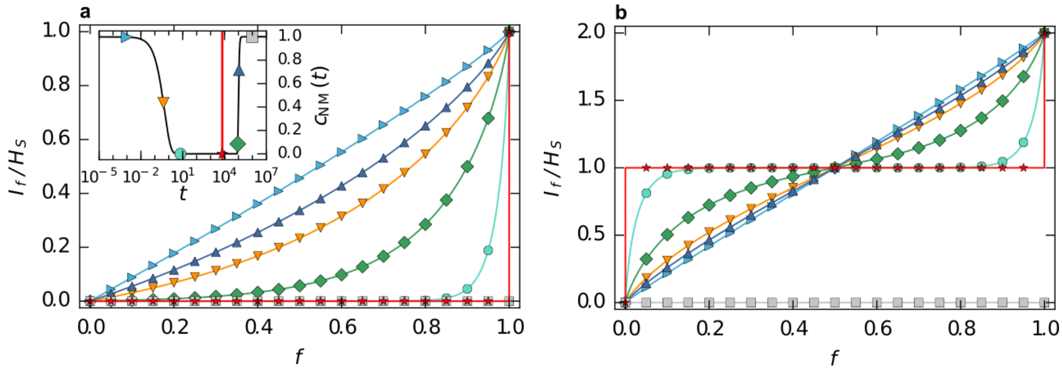

FIGURE 3.3: Mutual information over system entropy as a function of environment fraction for the two settings at different times, for $n = 10^4$ ancillae and $\lambda = 1$. To indicate the state of the system at the time to which each curve corresponds, they have been coloured matching the corresponding dot in the inset, which shows the coherence factor as in fig. 3.2. The times have been chosen to cover the different dynamical regimes undergone by the system. **a**, the origin of the randomness in the collision times is not considered. The plateau in the mutual information occurs for $I_f = 0$, meaning that the ancillae alone barely carry any information. **b**, the emitters are part of the quantum state as well. The effect of the emitters is the appearance of QD while the system is in a highly mixed state.

information. We have

$$\begin{aligned}
H_{\mathcal{S}} &= -P_n^{\mathrm{e}}(t)\log P_n^{\mathrm{e}}(t) - (1-P_n^{\mathrm{e}}(t))\log\left(1-P_n^{\mathrm{e}}(t)\right), \\
H_{\mathcal{E}_f} &= -\sum_{\alpha_1=0}^{1}\cdots\sum_{\alpha_{n-k}=0}^{1}\Lambda(\vec{\alpha}_{n-k})\log\left(\Lambda(\vec{\alpha}_{n-k})\right), \\
H_{\mathcal{S}\mathcal{E}_f} &= -\sum_{\alpha_1=0}^{1}\cdots\sum_{\alpha_{n-k}=0}^{1}\sum_{\alpha_{\mathcal{S}}=0}^{1}\Lambda(\vec{\alpha}_{n-k})\left[P_k^{\mathrm{e}}(t)^{\alpha_{\mathcal{S}}}\left(1-P_k^{\mathrm{e}}(t)\right)^{1-\alpha_{\mathcal{S}}}\right] \\
&\quad\times\log\left(\Lambda(\vec{\alpha}_{n-k})\left[P_k^{\mathrm{e}}(t)^{\alpha_{\mathcal{S}}}\left(1-P_k^{\mathrm{e}}(t)\right)^{1-\alpha_{\mathcal{S}}}\right]\right),
\end{aligned} \tag{3.26}$$

where we have included an additional index $\alpha_{\mathcal{S}}$ in the last expression to account for the state of the system. Given that both $H_{\mathcal{E}_f}$ and $H_{\mathcal{S}\mathcal{E}_f}$ can be interpreted as the entropies of the joint probability distributions of independent random variables, they can be expressed as the sum of their individual entropies, so we can write $H_{\mathcal{E}_f} - H_{\mathcal{S}\mathcal{E}_f} = P_k^{\mathrm{e}}(t)\log P_k^{\mathrm{e}}(t) + (1-P_k^{\mathrm{e}}(t))\log\left(1-P_k^{\mathrm{e}}(t)\right)$,

The resulting mutual information is

$$I_f = H_{\mathrm{b}}(P_n^{\mathrm{e}}(t)) - H_{\mathrm{b}}(P_k^{\mathrm{e}}(t)) \tag{3.27}$$

where $f = 1 - \frac{k}{n}$, and $H_{\mathrm{b}}(x) = -x\log x - (1-x)\log(1-x)$ is the binary entropy function. In fig. 3.3**a**, we show this curve for different dynamical regimes. Despite an almost linear dependence in some periods, it is mostly flat around null mutual information except for $f \approx 1$ when the system is highly mixed, which implies the absence of objective reality upon which observers can agree.

We now study the case in which the random process that governs the dynamics has a quantum source. In particular, we consider n emitters initially excited that relax to their ground state emitting an ancilla in the process. Moreover, we further assume that the ancilla is emitted in state $\rho_a = |0\rangle\langle 0|$ and, once emitted, it immediately collides with the system, flipping its state (since $\theta = \pi$). Hence, the emitter-ancilla dynamics is such that their joint state at time t can be written as $\sqrt{e^{-\lambda t/n}}|1\rangle_e \otimes |0\rangle_a + \sqrt{1-e^{-\lambda t/n}}|0\rangle_e \otimes |1\rangle_a$. The total state including system and environment is now the pure state

$$|\psi_{\mathcal{S}\mathcal{E}}(t)\rangle = \sum_{\alpha_1=0}^{1} \cdots \sum_{\alpha_n=0}^{1} \sqrt{\Lambda(\vec{\alpha}_n)} |\vec{\bar{\alpha}}_n\rangle_e \otimes |\vec{\alpha}_n\rangle_a \otimes \left(\delta_{\text{even}}(\vec{\alpha}_n)|+_t\rangle + \delta_{\text{odd}}(\vec{\alpha}_n)|-_t\rangle\right), \tag{3.28}$$

where $\bar{\alpha}_i = 1 - \alpha_i$ represents the state of emitter i. Tracing out all the emitters cancels all the coherences in the density matrix and leaves us with eq. (3.24). Therefore, despite the quantum super-environment, our previous result regarding the lack of information in the ancillae alone still holds. However, we are now interested in the mutual information as we trace out emitter-ancilla pairs. As we did in the previous subsection, we need the reduced state $\rho_{\mathcal{S}\mathcal{E}_f}(t)$ resulting from the partial trace of k pairs. Furthermore, since we must compute von Neumann entropies, our strategy consists in finding the orthogonal pure states whose convex sum leads to the reduced density operators; by doing so, the entropies are simply given by the Shannon entropies of the corresponding probabilities. To simplify the notation in what follows, let us define $|\beta_i\rangle \equiv |\bar{\alpha}_i\rangle_e \otimes |\alpha_i\rangle_a$, with $\beta_i = \alpha_i$, to account for the state of a pair. Now, to determine $\rho_{\mathcal{S}\mathcal{E}_f}(t)$, we proceed in the following way. First, we notice that, when summing over the states of the k ancillae $|\vec{\beta}_k\rangle$, if $\vec{\beta}_k$ represents an even number of collisions, $\delta_{\text{even}}(\vec{\beta}_{n-k}) = \delta_{\text{even}}(\vec{\beta}_n)$, so $\langle\vec{\beta}_k|\psi_{\mathcal{S}\mathcal{E}}(t)\rangle\langle\psi_{\mathcal{S}\mathcal{E}}(t)|\vec{\beta}_k\rangle$ yields $\Lambda(\vec{\beta}_k)|\psi_{\mathcal{S}\mathcal{E}_f,\text{e}}(t)\rangle\langle\psi_{\mathcal{S}\mathcal{E}_f,\text{e}}(t)|$, where

$$|\psi_{\mathcal{S}\mathcal{E}_f,\text{e}}(t)\rangle = \sum_{\beta_1=0}^{1} \cdots \sum_{\beta_{n-k}=0}^{1} \sqrt{\Lambda(\vec{\beta}_{n-k})}|\vec{\beta}_{n-k}\rangle \otimes \left(\delta_{\text{even}}(\vec{\beta}_{n-k})|+_t\rangle + \delta_{\text{odd}}(\vec{\beta}_{n-k})|-_t\rangle\right). \tag{3.29}$$

If $\vec{\beta}_k$ represents an odd number of collisions, the same operation yields $\Lambda(\vec{\beta}_k)\,|\psi_{\mathcal{S}\mathcal{E}_f,\text{o}}(t)\rangle\langle\psi_{\mathcal{S}\mathcal{E}_f,\text{o}}(t)|$ instead, with

$$|\psi_{\mathcal{S}\mathcal{E}_f,\text{o}}(t)\rangle = \sum_{\beta_1=0}^{1} \cdots \sum_{\beta_{n-k}=0}^{1} \sqrt{\Lambda(\vec{\beta}_{n-k})}|\vec{\beta}_{n-k}\rangle \otimes \left(\delta_{\text{odd}}(\vec{\beta}_{n-k})|+_t\rangle + \delta_{\text{even}}(\vec{\beta}_{n-k})|-_t\rangle\right). \tag{3.30}$$

Since we must sum over all $|\vec{\beta}_k\rangle$, the resulting state can be written as

$$\rho_{\mathcal{S}\mathcal{E}_f}(t) = P_k^{\text{e}}(t)|\psi_{\mathcal{S}\mathcal{E}_f,\text{e}}(t)\rangle\langle\psi_{\mathcal{S}\mathcal{E}_f,\text{e}}(t)| + \left(1 - P_k^{\text{e}}(t)\right)|\psi_{\mathcal{S}\mathcal{E}_f,\text{o}}(t)\rangle\langle\psi_{\mathcal{S}\mathcal{E}_f,\text{o}}(t)|. \tag{3.31}$$

From this expression, we can immediately see that the reduced state of the system is, as in the case without emitters, $\rho_{\mathcal{S}}(t) = P_n^{\text{e}}(t)|+_t\rangle\langle+_t| + \left(1 - P_n^{\text{e}}(t)\right)|-_t\rangle\langle-_t|$. As for the reduced state of the environment, $\rho_{\mathcal{E}_f}(t)$, we observe that

$$\langle +_t|\psi_{\mathcal{S}\mathcal{E}_f,\mathrm{e}}(t)\rangle\,\langle\psi_{\mathcal{S}\mathcal{E}_f,\mathrm{e}}(t)|+_t\rangle = \langle -_t|\psi_{\mathcal{S}\mathcal{E}_f,\mathrm{o}}(t)\rangle\langle\psi_{\mathcal{S}\mathcal{E}_f,\mathrm{o}}(t)|-_t\rangle = P^{\mathrm{e}}_{n-k}(t)|\psi_{\mathcal{E}_f,\mathrm{e}}(t)\rangle\langle\psi_{\mathcal{E}_f,\mathrm{e}}(t)|, \tag{3.32}$$

where

$$|\psi_{\mathcal{E}_f,\mathrm{e}}(t)\rangle = \sum_{\{\vec{\beta}_{n-k}|\delta_{\mathrm{even}}(\vec{\beta}_{n-k})=1\}} \sqrt{\frac{\Lambda(\vec{\beta}_{n-k})}{P^{\mathrm{e}}_{n-k}(t)}}|\vec{\beta}_{n-k}\rangle. \tag{3.33}$$

Similarly,

$$\langle -_t|\psi_{\mathcal{S}\mathcal{E}_f,\mathrm{e}}(t)\rangle\langle\psi_{\mathcal{S}\mathcal{E}_f,\mathrm{e}}(t)|-_t\rangle = \langle +_t|\psi_{\mathcal{S}\mathcal{E}_f,\mathrm{o}}(t)\rangle\langle\psi_{\mathcal{S}\mathcal{E}_f,\mathrm{o}}(t)|+_t\rangle = \left(1-P^{\mathrm{e}}_{n-k}(t)\right)|\psi_{\mathcal{E}_f,\mathrm{o}}(t)\rangle\langle\psi_{\mathcal{E}_f,\mathrm{o}}(t)|, \tag{3.34}$$

where

$$|\psi_{\mathcal{E}_f,\mathrm{o}}(t)\rangle = \sum_{\{\vec{\beta}_{n-k}|\delta_{\mathrm{odd}}(\vec{\beta}_{n-k})=1\}} \sqrt{\frac{\Lambda(\vec{\beta}_{n-k})}{1-P^{\mathrm{e}}_{n-k}(t)}}|\vec{\beta}_{n-k}\rangle. \tag{3.35}$$

Finally, using eq. (3.31), we obtain

$$\begin{aligned}\rho_{\mathcal{E}_f}(t) &= P^{\mathrm{e}}_k(t)\left(P^{\mathrm{e}}_{n-k}(t)|\psi_{\mathcal{E}_f,\mathrm{e}}(t)\rangle\langle\psi_{\mathcal{E}_f,\mathrm{e}}(t)| + \left(1-P^{\mathrm{e}}_{n-k}(t)\right)|\psi_{\mathcal{E}_f,\mathrm{o}}(t)\rangle\langle\psi_{\mathcal{E}_f,\mathrm{o}}(t)|\right)\\ &\quad + (1-P^{\mathrm{e}}_k(t))\left(\left(1-P^{\mathrm{e}}_{n-k}(t)\right)|\psi_{\mathcal{E}_f,\mathrm{o}}(t)\rangle\langle\psi_{\mathcal{E}_f,\mathrm{o}}(t)| + P^{\mathrm{e}}_{n-k}(t)|\psi_{\mathcal{E}_f,\mathrm{e}}(t)\rangle\langle\psi_{\mathcal{E}_f,\mathrm{e}}(t)|\right)\\ &= P^{\mathrm{e}}_{n-k}(t)|\psi_{\mathcal{E}_f,\mathrm{e}}(t)\rangle\langle\psi_{\mathcal{E}_f,\mathrm{e}}(t)| + \left(1-P^{\mathrm{e}}_{n-k}(t)\right)|\psi_{\mathcal{E}_f,\mathrm{o}}(t)\rangle\langle\psi_{\mathcal{E}_f,\mathrm{o}}(t)|.\end{aligned} \tag{3.36}$$

Hence, in this case, we have

$$\begin{aligned}H_{\mathcal{S}} &= -P^{\mathrm{e}}_n(t)\log P^{\mathrm{e}}_n(t) - (1-P^{\mathrm{e}}_n(t))\log\left(1-P^{\mathrm{e}}_n(t)\right),\\ H_{\mathcal{E}_f} &= -P^{\mathrm{e}}_{n-k}(t)\log P^{\mathrm{e}}_{n-k}(t) - \left(1-P^{\mathrm{e}}_{n-k}(t)\right)\log\left(1-P^{\mathrm{e}}_{n-k}(t)\right),\\ H_{\mathcal{S}\mathcal{E}_f} &= -P^{\mathrm{e}}_k(t)\log P^{\mathrm{e}}_k(t) - (1-P^{\mathrm{e}}_k(t))\log\left(1-P^{\mathrm{e}}_k(t)\right),\end{aligned} \tag{3.37}$$

From this, the mutual information takes the form

$$I_f = H_{\mathrm{b}}(P^{\mathrm{e}}_n(t)) + H_{\mathrm{b}}(P^{\mathrm{e}}_{n-k}(t)) - H_{\mathrm{b}}(P^{\mathrm{e}}_k(t)). \tag{3.38}$$

Comparing this result with eq. (3.27), we see that the presence of the emitters introduces the term $H_{\mathrm{b}}(P^{\mathrm{e}}_{n-k}(t))$, which corresponds to the entropy of the environment, $H_{\mathcal{E}_f}$. Figure 3.3**b** depicts the mutual information in this new setting. In this case, there is a clear plateau at $I_f/H_{\mathcal{S}} = 1$, revealing a structure of the total state of system and environment compatible with QD.

Due to the finite size effects, the plateau is only present at times in which the reduced state of the system is highly mixed. As time progresses, the probability that all ancillae collided with the system grows closer to one, in which case system and environment will be in a product state and no information can be obtained through environmental measures. This, along with our previous discussion regarding the separability of the system and the ancillae alone, can be interpreted as further evidence that, assuming that system and environment both start in pure states, the emergence of objectivity requires entanglement.

We have noticed that, after the system has recohered (due to its non-Markovianity), quantum Darwinism features are lost, as the system effectively decouples from the environment. This seems to feed into the observation that non-Markovianity hinders the emergence of quantum Darwinism [66, 67, 51], motivated by the fact that information backflow would degrade the correlations between the system and the surrounding environment. However, in other works a connection between the two phenomena was not found [68, 69]. In general, the interplay between non-Markovianity and quantum Darwinism seems highly model dependent, and no general conclusion has been proven so far.

3.2 SCM approach to transport phenomena in quantum networks

The potential applications of stochastic collision models go way beyond the examples proposed in section 3.1, and the exploration of models with similar features is still in its early stage (see [70, 71, 72] for some relevant examples). To further highlight the versatility of the model, we will use it to study transport phenomena in (open) quantum networks. We will investigate the consequences of spatial and temporal heterogeneity of noise on transport efficiency in a fully connected graph and in the Fenna-Matthews-Olson complex, and show how our approach allows to meaningfully formulate questions, and provide answers, on important open issues such as the properties of optimal noise.

3.2.1 Introduction

Despite markedly different predictions of quantum mechanics with respect to the classical description of reality, speculations on its possible role in key biological processes date back to its founding fathers. More recently, with the formidable advances in experimental and numerical approaches, fields like quantum biology and quantum complex science have highlighted the existence and persistence of quantum coherence even in complex macroscopic systems. Nonetheless, whether quantumness plays a functional role in biological complexes remains to date a most fascinating open question.

Initial investigations on the quantum measurement problem suggested that the emergence of a classical description of reality from the underlying quantum one could be explained in the framework of environment-induced decoherence [4]. Within this approach, the larger the quantum system, the faster the loss of quantumness due to the interaction with the environment. More recently, however, it has become evident that environmental noise need not be an enemy to the preservation of quantumness [73]. On the contrary, it may sustain the persistence of quantum coherence and, as a consequence, improve the efficiency of quantum transport in complex systems [74, 75, 76, 77]. In this sense, the initial scepticism on the presence of quantum phenomena in macroscopic "hot and dirty" systems, due to their very short coherence time, has been overcome [78]. Nonetheless, complex quantum systems such as, e.g., the extensively studied photosynthetic complexes, are undoubtedly strongly interacting with complex environments, the characteristics of which are very hard to model microscopically.

The enormous challenge of a fully quantum microscopic description of the environment of biological complexes stems both from experimental difficulties in extracting its detailed features and from the exponential increase in the resources needed to simulate quantum many-body systems of large size. Moreover, standard approaches of open quantum systems theory rely on approximations, such as weak-coupling and Markovian [1], which are generally not satisfied in quantum biology or not justified for complex many-body quantum systems, where even the division between the open system and its environment may be somewhat arbitrary. Because of these considerations, effective models combining quantum and classical aspects of noise while retaining strong physical insight and flexibility in the noise parameters are crucial for advancing our understanding on the role of quantumness in biological or chemical processes.

To demonstrate the usefulness, flexibility, and descriptive power of the SCM, we apply it to the study of noisy transport in quantum networks, considering two paradigmatic examples: the fully connected graph and the Fenna-Matthews-Olson (FMO) complex [79, 80]. In the first case, we bring to light the interplay between spatial/temporal noise heterogeneity and the presence of system-environment entanglement in the efficiency of transport. In the second case, we also focus on the features of noise optimality. We discover that optimality constraints unveil the existence of two classes of nodes. Specifically, transport efficiency is optimised when certain nodes are subjected to strong noise, while the others to very low levels. Remarkably, these two communities are consistent, to a high degree, with the recent discovery of two classes of site-dependent fluctuations in the FMO complex [81].

3.2.2 The model

We use a generalized version of the SCM for N-qubit systems driven by some Hamiltonian H, so that each of the system qubits is subject to its own SCM. The collision between an ancilla — initially in the state $|\nu\rangle$ — and a system qubit m is modeled through the unitary dynamics generated by the local interaction Hamiltonian $H^{(I)}_{\mathrm{anc},m} = (\eta/2)\sigma_x^{\mathrm{a}} \otimes \sigma_z^m$ during a short period of time τ, after which the ancilla drifts away and never interacts with the system again. We assume the interaction time τ to be much shorter than any relevant time scale in the free system dynamics, so that collisions can be regarded as instantaneous processes resulting in the application of unitary transformations $U_m = \exp\{-i(\theta/2)\sigma_x^{\mathrm{a}} \otimes \sigma_z^m\}$, with $\theta = \tau\eta$ being the interaction strength. As already seen in section 3.1, this parameter controls the entanglement between the system and the ancilla. For instance,

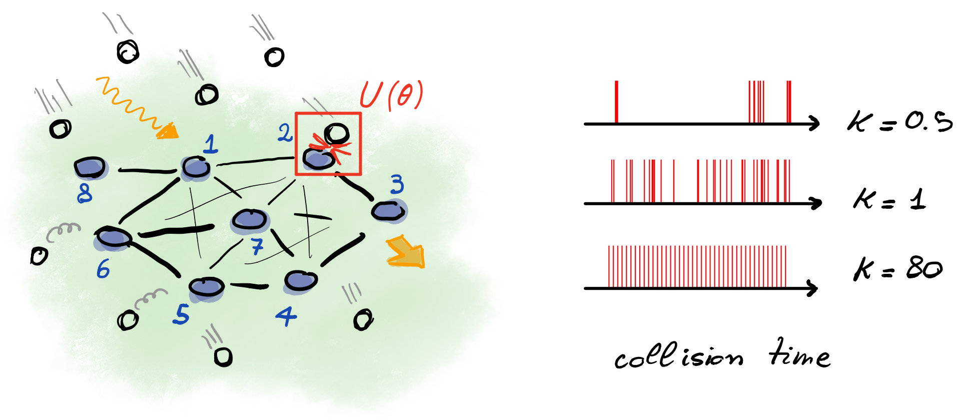

FIGURE 3.4: **Pictorial representation of the Stochastic Collision Model.** The sketch illustrates environmental ancillae colliding with the eight sites of the FMO complex. Each ancilla collides only once with one node of the FMO complex, while the time between two consecutive collisions follows the Weibull Renewal Process. On the right side we show how changing the value of $k \equiv k_i$ — which for simplicity we assume here to be independent on the node i — we can describe the cases of heterogeneous ($k < 1$), Poisson ($k = 1$), and regular ($k \gg 1$) collision time interval distribution.

for $\theta = (2k+1)\pi$, $k \in \mathbb{Z}$, the interaction is non-entangling, while it can be maximally entangling for $\theta = (2k+1)\pi/2$, $k \in \mathbb{Z}$. In any case, the fact that the ancilla does not collide again with the system deems its degrees of freedom irrelevant after the collision event, so it can be safely "traced out". The effect of the composition of U_m and the consequent partial trace results in a single quantum channel $\Phi_m\left[\rho(t)\right] = K_m\rho(t)K_m^\dagger + K_m^\dagger\rho(t)K_m$, with $K_m = e^{-i(\theta/2)\sigma_z^m}/\sqrt{2}$. While the system-ancilla interaction outlined here has been designed to account for dephasing, other interactions can result in dissipation through the same mechanism as well.

The collision time dynamics can in principle be any stochastic process of our choice. Here, we focus on the case in which the collisions on all the system qubits occur independently following a Weibull Renewal Process (WRP) [82]. For every qubit i, the probability density for the interval between two consecutive collisions on i, t_i is then given by a Weibull distribution,

$$p(t_i) = \frac{k_i}{\lambda_i}\left(\frac{t_i}{\lambda_i}\right)^{k_i-1} e^{-(t_i/\lambda_i)^{k_i}}, \tag{3.39}$$

in which k_i and λ_i are the shape and scale parameters, respectively. The main motivation for this choice is that it allows us to control the intensity and the heterogeneity in the collision statistics locally, that is, on each qubit independently. In particular, for a fixed value of k_i, the mean intercollision time $\langle t_i\rangle = \lambda_i\Gamma(1+1/k_i)$ (where Γ stands for the gamma function) is proportional to λ_i, so we can control the *spatial heterogeneity* of the noise across the system simply by choosing different scale parameters for each qubit. At the same time, we can interpret the shape parameter as enabling the control of the *temporal heterogeneity* of the noise, since

$\mathrm{Var}(t_i) = \lambda_i^2 \left[\Gamma(1+2/k_i) - \Gamma(1+1/k_i)^2\right]$. For $k_i < 1$, the collision dynamics is heterogeneous, characterized by bursts of collisions separated by long intervals of inactivity. As k_i increases above 1, collisions become increasingly regular, as shown in fig. 3.4. For $k_i = 1$, they follow a Poisson point process with rate $1/\lambda_i$. Therefore, in that case, the dynamics of the system, when averaged over stochastic realizations, is described by a the master equation in Gorini-Kossakowski-Sudarshan-Lindblad form [63, 64], and the system therefore undergoes Markovian dynamics [83]. For a general waiting time distribution, such process evolves as a master equation with a memory kernel that is not trivial to solve [83, 84, 85]. In all cases, however, the dynamics can be efficiently simulated by sampling the individual time intervals between collisions from eq. (3.39).

In this paper, we apply the SCM to the study of transport phenomena in the framework of Continuous Time Quantum Walks (CTQW). In CTQW, one typically considers N qubits interacting through a Hamiltonian that preserves the number of excitations, such as

$$H = \sum_{i=1}^{N} \omega_i \sigma_+^i \sigma_-^i + \sum_{i \neq j} g_{ij} (\sigma_+^i \sigma_-^j + \sigma_+^j \sigma_-^i), \tag{3.40}$$

where $\omega_i \in \mathbb{R}$ and $\sigma_\pm^i$ are the site energies and ladder operators of qubit i, respectively, and $g_{ij} \in \mathbb{R}$ are the hopping strengths between nodes i and j. The fact that the hopping strengths can be set independently for every pair of qubits brings about an interpretation of the Hamiltonian in terms of a network, in which qubits are associated with its nodes and hopping strengths with weighted connections among them. Hence, the dynamics of a single excitation (see Box 2) through the network — a quantum walker — is reminiscent of classical random walks on graphs. Furthermore, like in the case of classical random walks, the structural properties of the underlying network generally have non-trivial effects on the propagation of the quantum walker [86].

Among the many fields in which CTQW find applications, they are widely used in quantum biology to model the propagation of energy across light-harvesting complexes [87, 75, 76, 88]. In these complexes, excitations must travel from a specific *initial node* r towards a *target node* s, where they are finally captured. This last part of the process can be modeled by adding a sink, an extra node attached to the target node from which excitations decay irreversibly. Mathematically, this can be achieved without de facto increasing the dimension of the system by phenomenologically including in the Hamiltonian the non-Hermitian term $-i\gamma\sigma_+^s\sigma_-^s$, with γ the *sink rate*. Indeed, this term results in a leak of probability, which models the transfer of probability to the sink (its population). In other words, the sink's population at any time t is given by $1 - \mathrm{Tr}\left[\rho(t)\right]$, where $\rho(t)$ is the state of the system at that time, further details can be found in Box 3. The transfer dynamics is slowed down due to quantum Zeno effect for $\gamma \gg g_{ij}$ [89], while in the opposite regime $\gamma \ll g_{ij}$ the dynamics is effectively unitary. We use a non-Hermitian Hamiltonian instead of an irreversible decay channel because we wish to be able to compute a time evolution

Box 2: Single-excitation subspace

The Hamiltonian of the system, eq. (3.40), preserves the number of excitations. This means that, for any state with k excitations $|\psi_k\rangle = \sigma_+^{i_1} \cdots \sigma_+^{i_k} |0\rangle^{\otimes N}$, the vector $H|\psi_k\rangle$ is orthogonal to any state with a number of excitations different from k. As a result, the Hamiltonian can be written as a direct sum of operators, each living in a k-excitation subspace, that is, $H = \bigoplus_{k=0}^{N} H^{(k)}$. This significantly reduces the computational complexity of the problem, as we do not need to consider the full 2^N-dimensional Hilbert space to study the dynamics of an initially localized single excitation. Instead, we can restrict our attention to the N-dimensional single-excitation subspace and its corresponding Hamiltonian $H^{(1)}$. It is convenient to introduce the basis of single-excitation localized states $\left\{|i\rangle \equiv \sigma_+^i |0\rangle^{\otimes N}\right\}$, in which the matrix representation of $H^{(1)}$ has elements $H_{ij}^{(1)} = \langle i| H |j\rangle = g_{ij}(1-\delta_{ij}) + \omega_i \delta_{ij}$, which coincides with the adjacency matrix of the graph.

Box 3: Simulating the effect of the sink

For simulating the effect of the sink, using a non-Hermitian Hamiltonian is equivalent to the use of an irreversible decay channel.
Suppose we have a general n level system undergoing free evolution as well as an irreversible decay from state $|s\rangle$ towards the state $|t\rangle$. In the free evolution, state $|t\rangle$ is decoupled by the rest of the system i.e. the Hamiltonian H does not include any $|t\rangle$ term. The state of the system ρ undergoes the evolution described by the master equation $\dot{\rho} = -i[H,\rho] + \gamma(K\rho K^\dagger - \frac{1}{2}\{K^\dagger K, \rho\})$ with $K = |t\rangle\langle s|$ and $\{,\}$ the anti-commutator. If we project over the system minus the state $|t\rangle$, the resulting reduced density operator ρ_R evolves according to $\dot{\rho}_R = -i[H,\rho_R] - \frac{1}{2}\gamma(|s\rangle\langle s|\rho_R + \rho_R |s\rangle\langle s|)$, defining $\widetilde{H} = H - i\frac{1}{2}\gamma$ we see how it is possible to rewrite the previous equation as $\dot{\rho}_R = \frac{d}{dt}(e^{-i\widetilde{H}t}\rho e^{i\widetilde{H}^\dagger t})$, this way we can describe the time evolution of ρ_R as the free evolution under the non-Hermitian Hamiltonian $\widetilde{H}$.

operator, without relying on a master equation. The sink further allows us to define a figure of merit to quantify the effectiveness of the excitation transport. We define the *performance* ε as the inverse of the time required for the population of the sink to reach a certain value (which we set to 0.95). It should be noted that the fact that the evolution is non-unitary even in the absence of noise does not prevent us from applying the SCM to this system in any way.

The dynamics of a system subjected to a SCM can be evaluated by averaging over all possible stochastic realizations. This may not be easy to do analytically, but can always be numerically simulated.

We initially set $t = 0$, and define τ_i as values sampled form the waiting time distribution W_i that is in principle different for each node i. We build a list S containing the collision times for each node $S = \{\tau_i, i \in [1, N]\}$ with N the number of nodes of the network. The node of the network that will receive the first collision is simply the node i such that $S_i = min(S)$. At this point the state undergoes the following evolution $\rho(S_i) = \Phi_i[U(S_i - t)\rho(t)U^\dagger(S_i - t)]$ where Φ_i is the channel representing the collision of an ancilla with the node i, and $U(t)$ is the time evolution operator defined as $U(t) = e^{-iHt}$ with H the Hamiltonian of the network. At this point the value of t is updated $t = S_i$ and so is the value of S_i by sampling another value from the waiting time distribution, $S_i = t + \tau_i$. Now that we have an updated list of the collision times, we find where and when the next collision is going to happen and repeat the process. In our case the process goes on as long as the population of the sink is inferior to the threshold value.

This scheme integrates a single realization of the dynamic in an exact way, however, it gives us the state of the system only at the time of the collisions. If the collision times are far away from one another, then the resulting "resolution" may not be the desired one. However, since the state undergoes only free Hamiltonian evolution between collisions, it is always possible to interpolate exactly the state of the system at any time between the collisions.

3.2.3 Fully connected graph

We first apply our noise model to study the energy transport in the fully connected network, where each node is connected with all others with the same hopping strength, $g_{ij} = g$, and the site energies are homogeneous (which we set to zero without loss of generality). The fully connected network is an interesting case study, considering that it is a system where, as we show in Box 4, the energy transfer is strongly suppressed in the absence of noise. In a network with N nodes, only $1/(N-1)$ of the population of an initially localized excitation is able to reach the sink, most of it being trapped in the initial node [75]. This is because a localized state in a fully connected network is mostly composed of energy eigenstates with no spatial overlap with the sink. Such states evolve according to a unitary dynamics and are hence effectively decoupled from the sink.

By adding dephasing noise, which maps states decoupled from the sink into mixtures of decoupled and coupled states, we can break the energy confinement and let the excitation flow through the network until it eventually reaches the sink. In fig. 3.5, we show the performance ε as a function of the *collision rate* $\zeta \equiv 1/\langle t_i \rangle$ for different spatial and temporal heterogeneity, as well as for different interaction strengths θ. In particular, fig. 3.5**a** corresponds to spatially homogeneous noise ($\lambda_i = \lambda$, $\forall i$), while fig. 3.5**b** shows the results for maximally heterogeneous spatial noise, in which collisions only occur on the initial node r (in this case, $\zeta = 1/\langle t_r \rangle$). Figure 3.5**c** shows the effect of the interaction strength for fixed spatial and temporal heterogeneity. Overall, the curves are characterized by a low performance for small collision rates, which are not effective in breaking the energy confinement, as well as for high rates, Box 4: Noiseless dynamics in the fully connected network

Using the expression for the time-evolution operator in the absence of sink and collisions presented in the main text, $e^{-itH^{(1)}} = e^{igt}\left(e^{-igNt}\left|\phi\right\rangle\left\langle\phi\right| + P_\perp\right) = e^{igt}\left[\left(e^{-igNt}-1\right)\left|\phi\right\rangle\left\langle\phi\right| + \mathbb{1}\right]$, we see that the state of an excitation initially localized at node r at time t is $e^{-itH^{(1)}}\left|r\right\rangle = e^{igt}\left[\left(e^{-igNt}-1\right)\frac{1}{\sqrt{N}}\left|\phi\right\rangle + \left|r\right\rangle\right]$. The population on some node k is thus

$$\left|\left\langle k\right| e^{-itH^{(1)}}\left|r\right\rangle\right|^2 = \delta_{rk}\left[1 + \frac{2}{N}\left(\cos(gNt)-1\right)\right] + \frac{2}{N^2}\left[1-\cos(gNt)\right]. \tag{3.41}$$

Since the term multiplying the Kronecker delta is positive for $N > 4$, we see that, for large networks, the initial node has the largest population throughout the dynamics. Let us now turn our attention to the interference-induced coherence trapping, which results in a strong suppression of the energy transfer to the sink in this graph. The same argument that we present here can be found in [75]. As before, we consider an excitation initially localized on node r and the sink to be attached to node s. If we ignore the sink for a moment, we can see that $\left|\varphi_i\right\rangle = \left|r\right\rangle - \left|i\right\rangle, \forall i \notin \{r,s\}$, along with $\left|\phi\right\rangle$, form a complete set of eigenstates of the Hamiltonian. Moreover, it is easy to show that

$$\left|r\right\rangle = \frac{1}{N-1}\left(\sum_{i\notin\{r,s\}}\left|\varphi_i\right\rangle + \sqrt{N}\left|\phi\right\rangle - \left|s\right\rangle\right). \tag{3.42}$$

The vector $\sum_{i\notin\{r,s\}}\left|\varphi_i\right\rangle$ is an eigenstate of the Hamiltonian and has no overlap with the target node state $\left|s\right\rangle$. Hence, its population is protected from the sink, while the population on the other two terms is unprotected and can eventually flow to the sink. Given that $\left\langle\varphi_i|\varphi_j\right\rangle = 1 + \delta_{ij}$, we can write $\sum_{i\notin\{r,s\}}\left|\varphi_i\right\rangle = \sqrt{(N-1)(N-2)}\left|\Psi\right\rangle$ with $\left\langle\Psi|\Psi\right\rangle = 1$. Introducing this into eq. (3.42), yields

$$\left|r\right\rangle = \sqrt{\frac{N-2}{N-1}}\left|\Psi\right\rangle + \left|\text{unprotected}\right\rangle. \tag{3.43}$$

The unprotected population, that is, the maximum amount of population that can reach the sink, can be readily computed from the expression above as $\left\langle\text{unprotected}|\text{unprotected}\right\rangle = \left\langle r|r\right\rangle - (N-2)/(N-1)\left\langle\Psi|\Psi\right\rangle = 1/(N-1)$ (where we have used $\left\langle\Psi|\text{unprotected}\right\rangle = 0$ since $\left\langle\varphi_i|\phi\right\rangle = 0$ and $\left\langle\varphi_i|s\right\rangle = 0$). This trapping of coherence is due to the peculiar eigenstate structure of the Hamiltonian, which is in turn a consequence of the high symmetry of the fully connected network.

which slow down the excitation walk due to the Zeno effect [90, 91, 92][1]. Hence, we observe an optimal collision rate ζ, different in each case.

The comparison between fig. 3.5**a** and **b** reveals the strong effect of spatial heterogeneity. While collisions on all the qubits are able to break the confinement, the

[1]It should be noted that, while it is reasonable to assume the slowdown of excitation walk to be due to the Zeno effect, a full characterisation of the phenomenon is yet to be done.

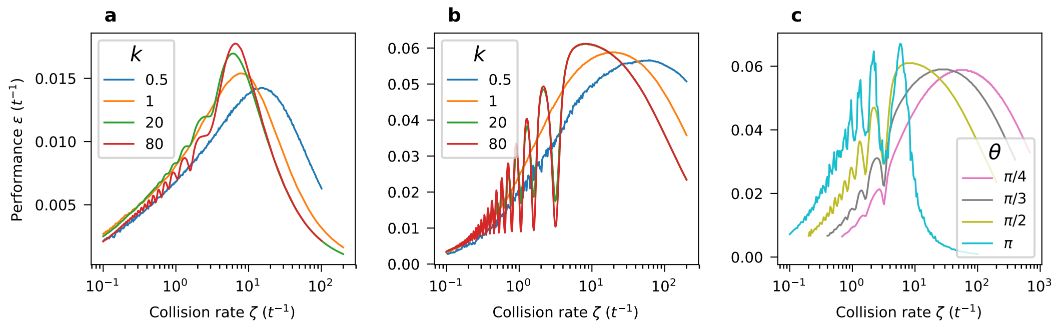

FIGURE 3.5: **Effect of noise heterogeneity and system-environment entanglement on transport performance.** In all cases, the curves show the performance ε as a function of the inverse intercollision time ζ for a fully connected network with $N = 20$ nodes. In **a**, ancillae collide with all nodes with equal shape and scale parameters. In **b**, collisions only take place with the initial node r. In both cases, $\theta = \pi/2$, and the legend indicates the shape parameter corresponding to each curve. In **c**, only node r is affected by collisions, and $k_r = 10$. Each curve corresponds to a different interaction strength.

process is much more efficient if the collisions are localized on the initial node r only. Moreover, numerical investigation shows that localized noise on a single node that is not the initial one is instead a sub-optimal strategy. This behavior is a consequence of the fact that the initial node remains the most populated one throughout the dynamics, which in turn implies that colliding with it is the most effective strategy to alter the coherences that give rise to the quantum interference-induced trapping.

In addition to the spatial heterogeneity, the curves also portray the effect of temporal heterogeneity in the collision statistics. Both with spatially localized and homogeneous collisions, large values of k_i give rise to a higher but narrower performance peak, while low k_i yields lower and wider peaks, with good performances even for very high dephasing rates. Therefore, temporal heterogeneity makes the dynamics more resilient to the Zeno effect. Both homogeneity and heterogeneity in the collision times can thus be regarded as resources, depending of the circumstances.

Another evident and interesting phenomenon is that, in the case of large values of k_i, the performance exhibits sudden drops for some specific collision rates. The periodicity of the corresponding collision rates suggests that they are related to some characteristic time of the network, and their origin can indeed be easily understood by looking at the unitary dynamics of the system (i.e., in the absence of noise and sink). By introducing the single-excitation localized states $\{|i\rangle \equiv \sigma_+^i |0\rangle^{\otimes n}\}$, which form a basis of the single-excitation subspace, the corresponding subspace Hamiltonian $H^{(1)}$ (that is, with matrix elements $H_{ij}^{(1)} = \langle i| H |j\rangle$) can be written as $H^{(1)} = g\left(N |\phi\rangle \langle\phi| - \mathbb{1}\right) = g\left[(N-1) |\phi\rangle \langle\phi| - P_\perp\right]$, where $|\phi\rangle = \left(\sum_{i=1}^N |i\rangle\right)/\sqrt{N}$ and $P_\perp = \mathbb{1} - |\phi\rangle \langle\phi|$ is the projector on the subspace orthogonal to $|\phi\rangle$. Consequently, the time evolution operator reads $e^{-itH^{(1)}} = e^{igt}\left(e^{-igNt} |\phi\rangle \langle\phi| + P_\perp\right)$, which equals identity (except for an irrelevant phase factor) at times

$$t = \frac{2\pi m}{gN}, \quad m \in \mathbb{Z}. \tag{3.44}$$

Therefore, in the limit of perfectly periodic collisions matching such periods, the ancillae always collide with a localized state — the initial one — with no effect, and the excitation remains trapped. In fig. 3.5**b**, however, the performance does not drop to zero. The reason is that, while large values of k_r result in nearly periodic collisions, they are ultimately random. In other words, even when the collision rate matches a characteristic time of the network, the actual collision times are noisy. Moreover, the width of the drops shows that a slightly detuned collision rate can still lead to a significant loss of performance, which suggests some robustness in this phenomenon. It should be mentioned that, when one of the nodes is attached to a sink, the state is not fully localized at times t given by eq. (3.44). Yet, at those times, the localization is highest, making the collisions as little effective as possible.

Finally, we also address the role of the interaction strength θ. In fig. 3.5**c**, we show the performance vs. collision rate curves with fixed spatial and temporal heterogeneity (collisions occur only with the initial node r with $k_r = 10$) for different values of θ. We can appreciate that, as the interaction strength increases, the curves are shifted towards lower collision rates and, at the same time, the optimality peak narrows. Interestingly, the highest performance is achieved for non-entangling qubit-ancilla interactions, which do not cause decoherence in any single realization of the noise dynamics. We can also see the periodic performance drops in all cases, the positions of which do not depend on θ whatsoever. This is consistent with our explanation of the phenomenon in terms of the periodicity of the free network dynamics, according to which we expect to observe it as long as the collisions take place when the population is localized on r and the interaction with such state has no effect (which is the case for any value of θ).

3.2.4 FMO complex

We now turn our attention to the Fenna-Matthews-Olson (FMO) complex, a real networked system widely studied in the quantum biology literature. This complex appears in green sulfur bacteria and assists energy migration from a chlorosome supercomplex to the reaction centre [93, 78]. It can be modeled as an 8-node fully connected network with non-homogeneous hopping strengths and non-homogeneous site energies. Using the values tabulated in Ref. [93], we can write the matrix representation of its single-excitation subspace Hamiltonian in the computational basis as (units in

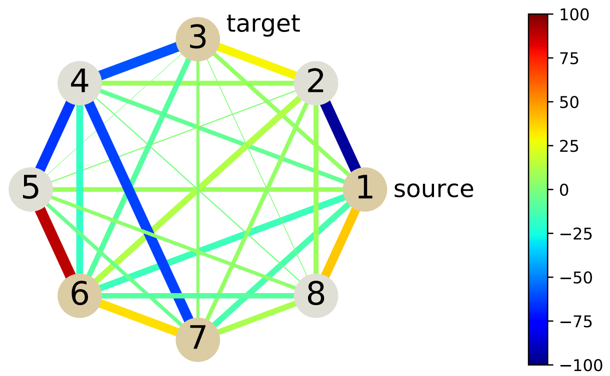

FIGURE 3.6: **Network representation of the FMO complex.** Nodes in the FMO are represented as circles, whereas the lines connecting them represent the hopping strengths. Every link's width is proportional to the logarithm of the corresponding matrix element, $\log|H^{(1)}_{ij}|$, while the color indicates the value according to the bar on the right. The colors of the nodes highlight their optimal noise level from fig. 3.8: high (pale grey) or low (dark yellow).

cm^{-1})

$$H^{(1)} = \begin{pmatrix} 200 & -94.8 & 5.5 & -5.9 & 7.1 & -15.1 & -12.2 & 39.5 \\ -94.8 & 230 & 29.8 & 7.6 & 1.6 & 13.1 & 5.7 & 7.9 \\ 5.5 & 29.8 & 0 & -58.9 & -1.2 & -9.3 & 3.4 & 1.4 \\ -5.9 & 7.6 & -58.9 & 180 & -64.1 & -17.4 & -62.3 & -1.6 \\ 7.1 & 1.6 & -1.2 & -64.1 & 405 & 89.5 & -4.6 & 4.4 \\ -15.1 & 13.1 & -9.3 & -17.4 & 89.5 & 320 & 35.1 & -9.1 \\ -12.2 & 5.7 & 3.4 & -62.3 & -4.6 & 35.1 & 270 & 11.1 \\ 39.5 & 7.9 & 1.4 & -1.6 & 4.4 & -9.1 & 11.1 & 505 \end{pmatrix}. \tag{3.45}$$

The site energies have been shifted so that the 3rd node, to which the sink is connected, has zero energy. A network representation of the complex is depicted in fig. 3.6. In many previous works [75, 76, 88, 94, 95] the FMO is modeled as a 7-node network, as the eighth node has recently been discovered [93, 96, 97]. In any case, the two networks have a highly similar topology and behavior, and all the results presented here are valid for both of them. It is worth clarifying that the FMO is a large biomolecule with a complex internal structure that interacts with a warm environment. Its purpose is to transfer excitations as fast as possible to the reaction center before it is lost to the environment due to dissipation. Modeling the FMO as an 8-node network, the energy transfer as a CTQW within the network, and the environmental interaction as pure dephasing — ignoring dissipation — all corresponds to an effective model. While such models are capable of capturing the core behavior of these systems [98, 99, 100], they are not adequate for accurate numerical computations.

We apply the SCM to the FMO with different spatial and temporal heterogeneity, as we did with the fully connected network. By comparing the two extremes of spatial

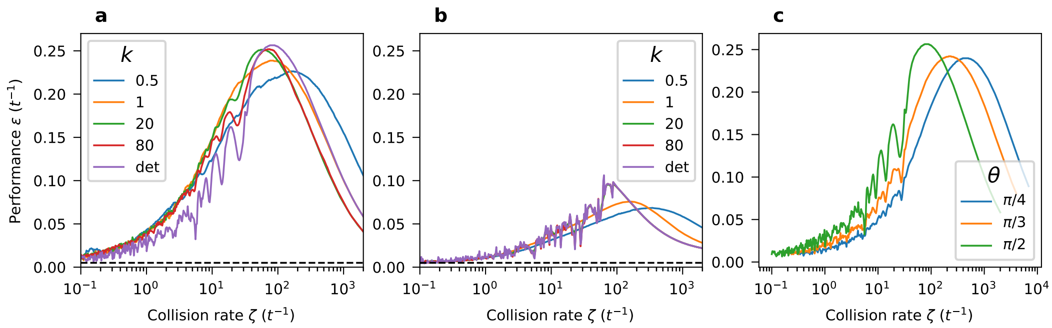

FIGURE 3.7: **Effect of noise heterogeneity on transport performance in the FMO complex.** Performance ε as a function of the inverse intercollision time ζ in the case of **a** spatially homogeneous noise and **b** maximally heterogeneous noise (collisions on the initial node $r = 1$ only). In both cases, $\theta = \pi/2$, and the legend indicates the shape parameter corresponding to each curve. The black dashed line shows the performance of FMO in the noiseless case. In **c**, it is shown the case of spatially and temporal homogeneous collisions for different interaction strengths.

homogeneity (collisions on all nodes) and heterogeneity (collisions only on the initial node $r = 1$) in fig. 3.7, we see that, in this system, localizing the collisions on the source node no longer is the most efficient strategy to drive the excitation to the sink. The FMO is a disordered system that does not experience strong population trapping in the initial node, so there is a priori no reason to expect localized dephasing to result in a better performance in this case. On the other hand, temporal heterogeneity has the same effect on the FMO as on the fully connected network: it leads to lower performance at optimal noise rates while resulting in increased resilience against the Zeno effect.

Surprisingly, we also observe drops in the performance of the process for some collision rates in this system. In the fully connected network, this was associated with the presence of characteristic times in the dynamics, which could be identified given the simplicity of the system. Finding the characteristic times of the FMO from the free dynamics would be far from trivial, but these performance drops signal their existence in such a disordered system, and raises questions regarding the generality of the phenomenon.

Given that the SCM is able to reveal this periodicity in the FMO dynamics, we now consider whether the versatility of the model can be further exploited to identify other properties of this real system. We have so far studied spatial heterogeneity by simulating the dynamics in two extreme cases, and the temporal one by jointly modifying the shape parameters of all nodes with non-zero collision rate. We now address the question of what the local scale and shape parameters maximising the performance in the FMO are. To find the optimal values of $\{\lambda_i, k_i\}$, we use a genetic optimisation algorithm [101], detailed in Box 5.

The results of the optimisation are displayed in fig. 3.8, where we show the distribution of the optimal mean collision rate ζ_i, fig. 3.8**a**, and of the shape parameters k_i,

Box 5: Genetic algorithms

The purpose of the genetic algorithm is to find the noise parameters that yield the highest performance for the given network. An initial pool of candidates is created by sampling random values (first generation). The pool is composed by a certain number of candidates, each consisting of the set of parameters that we wish to optimise. The performance of each component of the pool is evaluated, and the half with the best performance is promoted to be the parents of the next generation. The values of the parents are mixed to create an offspring, and the offspring is further subjected to random mutations. The parents and the offspring are now the members of the second generation, whose performance is evaluated and the process begins anew. By including the parents in the future generation we ensure that high performing members are never lost (the offspring do not always outperform their parents). This way, through each generation, we improve the overall quality of the genetic pool.
In our case we used a pool of 40 individuals, 20 of which were selected to be the parents at each iteration. Each individual corresponds to the shape and scale noise parameters for each qubit of the networks, so the total number of chromosomes is 16 when optimising for the FMO. Each offspring individual inherits 8 chromosomes from one parent and 8 from the other, and each parent mates twice with different partners. The mutation usually consists in adding randomly extracted values to the chromosomes, though we often found faster convergences by multiplying by random values instead, or using a hybrid model. The number of generations is not fixed, but rather the algorithm is stopped once the quality of the population reaches a plateau.

fig. 3.8**b**, for each node. Interestingly, we notice two clearly distinct behaviors, with nodes being subjected to either very strong noise (very high collision rate) or virtually no noise at all. Moreover, fig. 3.8**b** reveals that the noise is essentially deterministic. This result allows us to classify the nodes in the FMO into two classes according to their optimal SCM noise levels, and suggests a methodology for transport-based community detection [102]. It should also be stressed that this node classification is by no means evident from the structure of the network (see fig. 3.6).

To conclude our SCM-based analysis of the FMO complex, we focus on the structure of the Hamiltonian. Given that it is a biological system, one would expect eq. (3.40) to be the result of an evolutionary process driving the system towards an optimal performance in noisy environments, such that modifying the hopping strengths would lead to a lower performance. However, this does not seem to be the case. In fig. 3.9, we show the distribution of transport performance of networks obtained by randomly reshuffling (permuting) the hopping strengths — so that all the networks have exactly the same weight distribution —, along with the performance of the FMO. When subjected to homogeneous noise, as many as 40% of these random networks outperform the original Hamiltonian. Similar results (not shown) can be obtained by simply sampling the hopping strengths independently from a Gaussian

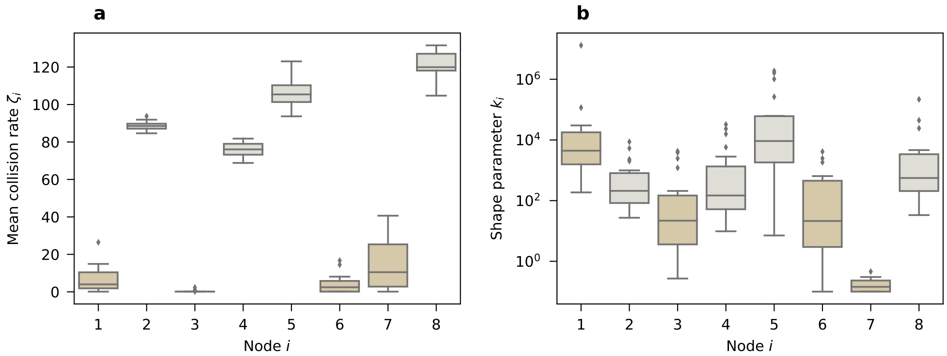

FIGURE 3.8: **Optimal noise for the FMO complex.** Distribution of **a** the mean collision rate ζ_i, and **b** the shape parameters k_i of node i in the last generation pool. The boxes show the first and third quartile, the middle bar being the median. The whiskers show an inter-quartile range of 1.5. Panel **a** shows that there are two classes of nodes (highlighted with two different colors): one with weak noise (small ζ_i) (nodes 1, 3, 6 and 7), and one with strong noise (large ζ_i). The optimal shape parameters k_i tend instead to be quite large, meaning that the collisions should be essentially deterministic.

distribution with the same mean and variance. This phenomenon depends on the noise model as well. As shown in the same figure, the fraction of networks outperforming the FMO is significantly reduced when subjected to the optimal noise from fig. 3.8. These rather surprising results do not necessarily contradict the assumption of the optimality of the FMO for excitation transfer. Although it seems relatively easy to outperform the actual FMO when allowed to choose the hopping rates freely, the actual physical system is subjected to constraints with which these randomized networks may be incompatible.

Overall, our results showcase the potential of the SCM for several purposes. On the one hand, considering an interaction with the environment in terms of collisions with the particles conforming it is a sensible assumption in many relevant situations. Needless to say, in these scenarios, collision events occur randomly in time. In its more general form, the SCM can accommodate a wide class of stochastic dynamics, for which efficient simulation techniques exist. On the other hand, the model can be useful for the analysis of general systems in which it may not seem physically adequate, as one can use parameter-optimisation techniques like the ones employed here to identify unknown dynamical phenomena in complex quantum systems.

3.3 Conclusions

We have introduced the stochastic collision model, a versatile noise model in which ancillae collide with the system qubits at random times.

We applied it to a single qubit to investigate the emergence of the classical reality from its quantum substrate, analytically deriving not only the master equation and the dynamical map, but also the relevant system-environment dynamical properties.

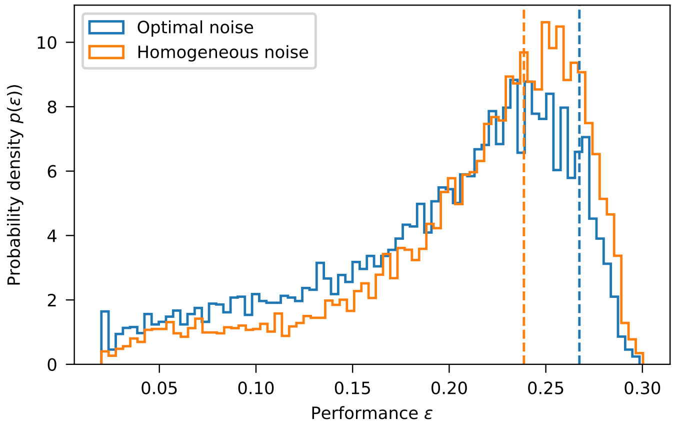

FIGURE 3.9: **Performance of the FMO upon link reshuffling.** The histograms shows the distribution of transport performance ε for 10^4 networks obtained by randomly reshuffling the links of the FMO. The orange histogram corresponds to spatially homogeneous and temporal Poissonian noise whereas, for the blue one, nodes were subjected to the optimal noise of fig. 3.8. The vertical dashed lines indicate the performance of the actual FMO complex under the corresponding noise. In the case of homogeneous noise, 40% of the reshuffled graphs are more efficient. Instead, for optimal noise, this is less common (9%).

The stochastic element introduced in the microscopic description of the collisions lends itself to an interesting generalization in terms of a super-environment that keeps track of the occurrence of the collisions. Due to these features, the underlying dynamics is dominated by simple fundamental physical mechanisms allowing us to shed new light on the role of quantum entanglement in three crucial phenomena: decoherence, non-Markovianity as information back-flow, and quantum Darwinism. The study of this model leads to the conclusion that system-environment entanglement is not necessary for decoherence or information back-flow, but plays a crucial role in the emergence of an objective reality.

By letting the collision-time dynamics be driven by a Weibull Renewal Process, the model is conferred with the capability to regulate the temporal heterogeneity of the noise. We have provided a thorough analysis of the effects of the noise heterogeneity on excitation transport in quantum networks both for the fully connected graph and the FMO light-harvesting complex. In the case of the fully connected network, the SCM reveals that, in the time-homogeneous regime, the transport performance is very sensitive to the periodicity of the system, a result that can be interpreted in terms of periodic coherence-induced excitation trapping. Remarkably, we observe a similar phenomenon in the FMO network, which suggest the existence of similar periodic excitation trappings in this real system. We have also exploited the versatility of our model to explore other non-trivial effects of the FMO structure on its dynamical properties. By optimising the transport performance over the noise parameters, we find that the best environmental conditions for this biological complex is given by high-rate nearly periodic collisions on some of its qubits, and no noise whatsoever on the rest, which does not seem to be expected from the structure of the underlying graph. Finally, we have addressed the question of whether the FMO structure is optimal, and we have found that a mere randomization of the hopping strengths often results in a more efficient system under homogeneous noise. Overall, our results showcase the potential of the SCM for several purposes. The SCM can accommodate a wide class of stochastic dynamics, and can be useful for the analysis of general systems, as one can use parameter-optimisation techniques like the ones employed here to identify unknown dynamical phenomena in complex quantum systems.

Chapter 4

Redundancy and consensus

In the previous chapter, we have explored the interplay between properties of the open system dynamics and the emergence of objectivity. In particular, by exploring a stochastic collision model we found evidence that points to the fact that system-environment entanglement must be established for objectivity to emerge. In that case however, we were not interested in quantifying the degree of objectivity, but simply assessing whether objectivity emerged or not. To this end, simply recovering the objectivity plateau for the QMI is by itself enough to certify that a given state is objective.

If, however, we do not simply wish for a witness of objectivity, but we also want to be able to measure the degree of objectivity of a quantum system, we need to find a suitable quantifier. As already mentioned in chapter 2, a reasonable measure of the degree of objectivity of a quantum state is the number of observers that can simultaneously agree on the properties of the system and reach a consensus, a quantity commonly referred to as "redundancy".

In this chapter, we show the existence of two different aspects of quantum objectivity, which we refer to as "redundancy" and "consensus". Though often used as synonyms in this context, we prove that they quantify different features of the degree of objectivity of a quantum state. More specifically, while redundancy measures how much information about the system was encoded into the environment, consensus measures how many observers can access said information. We also show that the two main frameworks used to measure quantum objectivity, namely spectrum broadcast structure and quantum Darwinism, naturally emerge from these two notions. Furthermore, by analysing explicit examples of nonlocal states, we highlight the potentially stark difference between the degrees of redundancy and consensus. In particular, this causes a break in the hierarchical relations, that we discussed at the end of chapter 2, between spectrum broadcast structure and quantum Darwinism.

A rigorous and well defined distinction between redundancy and consensus, also proves to be a valuable tool in giving an operative interpretations of mutual information plots, and in particular the operative meaning of the averaged mutual information, which we will discuss in the final part of this chapter. We will show that, whenever the information encoding into the environment is not uniform, computing the non-averaged mutual information may result in misleading interpretations of objectivity, while the average mutual information always offers results with a clear operative interpretation. This will also allow us to provide examples where a noticeable distinction between redundancy and consensus can be achieved even when the information encoding is purely local. The results presented here are based on two recent works [103, 104].

4.1 Introduction

As we have already discussed in chapter 2, "objectivity" is usually understood in the quantum domain as consensus between observers. More specifically, given a quantum system $\mathcal{S}$ interacting with an environment $\mathcal{E}$ composed of a number of constituents $\mathcal{E}_i$, we say that the system is objective when observers performing independent measurements on different $\mathcal{E}_i$ reach a consensus about some property of the system [5]. This is only possible if, due to prior interactions between system and environment, the relevant information was encoded with high *redundancy* into the environment.

The notion of "consensus" is also often found in the literature, and is usually used as a synonym of redundancy. We will see however, how in several situations these concepts ought to be carefully distinguished, and that redundancy is a necessary, but not sufficient, condition to achieve consensus. In particular, we show that in the presence of nonlocal information encoding, consensus and redundancy quantify significantly different features. In fact, even though some information about $\mathcal{S}$ might be redundantly encoded into the environment, it is possible that due to the nonlocality of such encoding, the observers might not be able to access it, and thus the redundancy might fail to realize into a corresponding amount of consensus. Such situations arise naturally whenever there are inter-environmental interactions [105, 106, 52, 51, 107]. While redundancy is an intrinsic property of a state, consensus is also a function of the particular scenario, and in particular of how the environment is distributed between observers.

To clarify the distinction between the superficially similar notions of redundancy and consensus, we propose a natural way to quantify them. We find that, remarkably, this approach leads naturally to the two main quantifiers of "quantum objectivity", namely, spectrum broadcast structures (SBS) [44] and quantum Darwinism (QD) [42, 43]. More precisely, we find QD and SBS to quantify consensus and redundancy, respectively.

Finally, we focus on the established hierarchy between SBS and QD: while SBS implies QD [44, 108], the opposite is only true under the additional assumption of *vanishing discord* and *strong independence* [55, 108]. We show that this hierarchy does not hold in scenarios where consensus and redundancy are distinct, a notable example being highly nonlocal states. In particular, SBS states need not satisfy the QD condition.

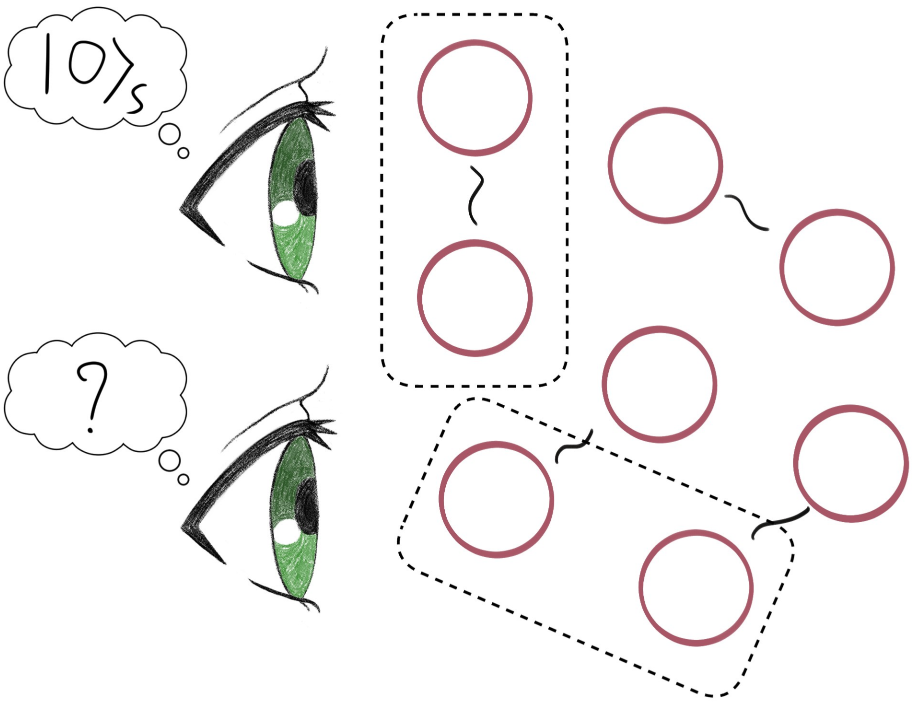

FIGURE 4.1: **Nonlocal information encoding.** When the information about the system is encoded into nonlocal states, it can only be recovered measuring suitable environmental macrofractions.

4.2 Definition of redundancy and consensus

To clarify the differences between the different aspects involved in the notion of *quantum objectivity*, we introduce here operative definitions of "redundancy" and "consensus" in quantum systems. Even though directly verifying these conditions might be hard in practice, we will show that they naturally reduce to QD and SBS in specific appropriate approximation regimes.

The idea of *redundancy* is that information about the system is encoded into several independent environmental fractions. More precisely, we thus say that a state ρ has redundancy n, and write $\mathrm{Red}(\rho) = n$, if n is the largest integer such that there is a partition $\mathcal{E} = \bigotimes_{i=1}^{n} \mathcal{E}_i$ such that $I_{\text{acc}}(\mathcal{S} : \mathcal{E}_i) \simeq S(\rho_S)$ for all $i = 1, ..., n$, where $S(\rho_S)$ is the von Neumann entropy of ρ_S, and $I_{\text{acc}}(\mathcal{S} : \mathcal{E}_i)$ is the *accessible* mutual information [11] between system and i-th environmental fraction $\mathcal{E}_i$. The accessible information is here defined as the mutual information between the probability distributions resulting from measuring $\mathcal{S}$ and $\mathcal{E}_i$, maximised over all possible choices of measurements. We use the accessible, rather than the full quantum mutual information, to ensure that correlations are actually observable from outcome probabilities.

This notion of redundancy is however unconcerned with the practical retrievability of the information. Even though information about a system can be encoded into its environment with high redundancy, actually accessing this information might require a careful partitioning of the environment, to avoid information being hidden in the correlations between different observers. To quantify the likelihood of actually observing information redundantly encoded into the environment, one ought to introduce the notion of *consensus*. While the redundancy is concerned with the maximum number of environmental fractions encoding information about $\mathcal{S}$, the notion of consensus is also concerned with how hard it is to find partitions realizing a set amount of redundancy. More precisely, we want to define the consensus of a state ρ as the largest number of observers that can, *with high probability*, retrieve information about the system from their measurement outcomes.

To this end, consider the probability $P(\rho, n)$ of finding a partition $\mathcal{E} = \bigotimes_{i=1}^n \mathcal{E}_i$ with redundancy n:

$$P(\rho, n) \equiv \mathrm{Prob}\big(I_{\mathrm{acc}}(\mathcal{S} : \mathcal{E}_i) \simeq S(\rho_S),\ i = 1, ..., n\big), \tag{4.1}$$

where the probability effectively counts the number of partitions $\mathcal{E} = \bigotimes_{i=1}^n \mathcal{E}_i$ such that $\dim(\mathcal{E}_i) = \dim(\mathcal{E}_j)$ for all i, j — and thus such that $\dim(\mathcal{E}_i) = f \dim(\mathcal{E})$ with $f = 1/n$. While in principle one could consider partitions with uneven fractions, we will focus on this simplest case, as it is the one usually considered in the topical literature. We can now define the "consensus" of ρ as the largest n such that $P(\rho, n) \simeq 1$. Thus ρ has a degree of consensus n *iff*, for any partition of the form $\mathcal{E} = \bigotimes_{i=1}^n \mathcal{E}_i$, each $\mathcal{E}_i$ is maximally correlated with $\mathcal{S}$, and the correlation is fully accessible[1]. $P(\rho, n)$ quantifies the probability that an observer is able, measuring a fraction of the environment of size $1/n$, to infer sufficient information about the system. In computing it, we assume that all the possible environmental fractions are sampled by the observers with equal probability. This is the simplest assumption one can make without going into the details of specific physical models. In specific scenarios, certain environmental fractions may be sampled with a higher probability than others (for example fractions with higher spatial connectivity), thus resulting in a different $P(\rho, n)$ that the one we would obtain assuming equiprobable fractions. However, even in this case our definition of consensus remains unchanged, as it does not depend on how $P(\rho, n)$ is computed.

In conclusion, redundancy is the maximum number of observers that could, in principle, infer information about the system. Consensus is instead the guaranteed number of observers that can infer information about the system with a random partition of the environment. Assuming a one-shot partition of the environment, the number of observers being able to retrieve information about the system will likely be higher than consensus, but lower than redundancy. Redundancy and consensus therefore capture two different, nonequivalent aspects of the objectivity of a system.

[1] It is possible to make the definitions of consensus and redundancy more mathematically rigorous by interpreting the equations $I_{\mathrm{acc}}(\mathcal{S} : \mathcal{E}_i) \simeq S(\rho_S)$ and $P(\rho, n) \simeq 1$ as standing for $I_{\mathrm{acc}}(\mathcal{S} : \mathcal{E}_i) \geq \mathcal{S}(\rho_S) - \epsilon$ and $P(\rho, n) \geq 1 - \delta$, respectively, for suitable choices of thresholds ϵ and δ.

4.3 Relations with known measures of objectivity

This formalization of the notions of redundancy and consensus makes it clear that they quantify distinct features of the emergence of quantum objectivity. In particular, it is possible to have high redundancy and low consensus, in situations where the redundant information encoding cannot be easily accessed by the observers without taking great care in how the environmental fractions are distributed. Furthermore, we will show here that the two main quantifiers of quantum objectivity used in the literature, SBS and QD, directly correspond to redundancy and consensus, respectively. For improved clarity, we will propose again some of the definitions first discussed in chapter 2, to better compare them with the recently introduced notions of redundancy and consensus.

An SBS state is one that admits a decomposition of the form

$$\rho_{\mathrm{SBS}} = \sum_i p_i \, |i\rangle\langle i| \otimes \bigotimes_{j=1}^{N} R_i^j, \tag{4.2}$$

for some collection of states R_i^j — referred to in this context as *macrofractions* [44] — such that $R_i^j R_{i'}^j = \delta_{ii'}(R_i^j)^2$ for all j. Such a decomposition is defined with respect to a specific partition $\mathcal{E} = \bigotimes_{j=1}^N \mathcal{E}_j$, of the environment, $R_i^j \in \mathcal{E}_j$, and the conditions on R_i^j ensure that different states of the system can be recovered from measurements in each $\mathcal{E}_j$. SBS states are thus always objective, provided observers are able to measure environmental fractions compatibly with the partitioning corresponding to the SBS structure. It follows that the redundancy of such a ρ_{SBS} is precisely N, the largest number of macrofractions that allow to write the state as an SBS.

QD defines "objectivity" via the quantum mutual information (QMI) between system $\mathcal{S}$ and an environment fraction $\mathcal{E}_f$ of size $f \dim(\mathcal{E})$, where $f \in (0,1)$ [42, 43]. For non-uniform environments, this QMI will depend on the choice of environmental fraction. In such instances, it is therefore warranted to consider the *average* QMI, defined as $\tilde{I}(\mathcal{S} : \mathcal{E}_f) \equiv \langle I(\mathcal{S} : \mathcal{E}_f)\rangle$, where the average is taken with respect to all environmental fractions $\mathcal{E}_f$ [53, 58, 9, 60]. A state is then said to be objective according to QD if there is $f \in (0,1)$ such that

$$\tilde{I}(\mathcal{S} : \mathcal{E}_f) \simeq S(\rho_S). \tag{4.3}$$

If f satisfies eq. (4.3), then there are at least $1/f$ observers that can simultaneously agree on some property of the system. We can then quantify *QD-objectivity* as $1/f$ for the smallest such f. One further possible issue arising in the context of QD is the presence of *quantum discord* [33, 109] in these QMI. Namely, in some scenarios computing $I(\mathcal{S} : \mathcal{E}_f)$ might falsely overestimate the actual accessible correlations between system and environment, which are the correlations that can be observed via some suitable choice of measurement basis on the environmental fractions. These arguably are, for the purpose of objectivity, the correlations one is actually interested

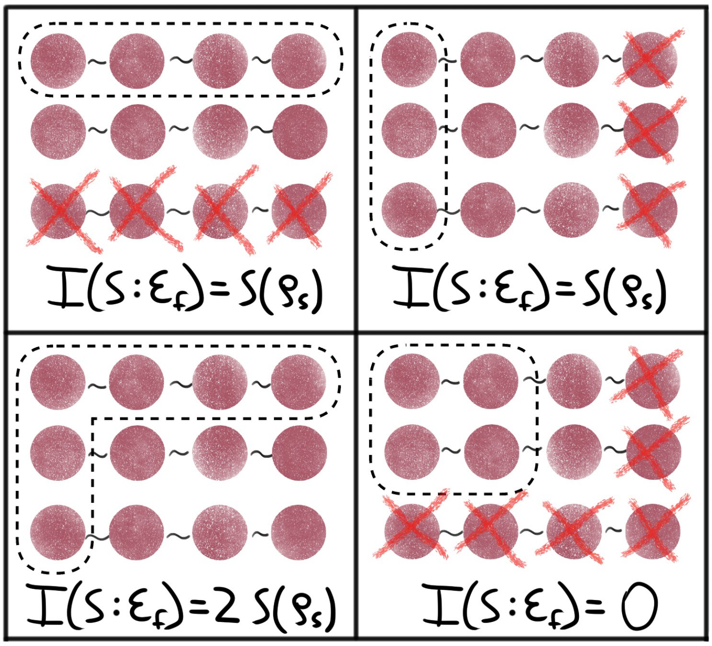

FIGURE 4.2: **How measuring different qubits affects the QMI**. In each figure, the three rows correspond to the three $|\mathrm{GHZ}_{\pm}^{(k)}\rangle$ macrofractions in the state $|\Psi\rangle_{k,N}$, with degree of nonlocality $k = 4$ and redundancy $N = 3$. The disks corresponds to the physical environmental qubits. In each scenario, depending on which subset of qubits is being measured, we get a different corresponding QMI. The dashed lines highlight qubits that are being measured, and the red crosses mark ones that have been traced out. Measuring qubits which are neither encircled nor crossed out does not affect the QMI. Measuring a full row (***top left***) or a full column (***top right***) we get $I(S : \mathcal{E}_f) = S(\rho_S)$, while measuring both a full row and a full column (***bottom left***), $I(S : \mathcal{E}_f) = 2S(\rho_S)$. If neither are true (***bottom right***), there is no correlation between system and the measured environmental fraction, corresponding to $I(S : \mathcal{E}_f) = 0$.

in, and therefore the use of *accessible* mutual informations might more accurately quantify the sought-after objectivity of states [55, 59].

We can now observe that QD-objectivity precisely corresponds to the degree of consensus previously introduced. In fact, if $P(\rho, n) \simeq 1$, then any macrofractioning of the environment of the form $\mathcal{E} = \bigotimes_{i=1}^{n} \mathcal{E}_i$ gives $I_{\mathrm{acc}}(\mathcal{S} : \mathcal{E}_i) \simeq S(\rho_S)$, and therefore the average accessible mutual information also satisfies $\tilde{I}_{\mathrm{acc}}(\mathcal{S} : \mathcal{E}_f) \simeq S(\rho_S)$ with $1/f = n$. Vice versa, if $\tilde{I}_{\mathrm{acc}}(\mathcal{S} : \mathcal{E}_f) \simeq S(\rho_S)$, then each $\mathcal{E}_i$ gives $I_{\mathrm{acc}}(\mathcal{S} : \mathcal{E}_i) \simeq S(\rho_S)$ —note that $S(\rho_S)$ is an upper bound for $\tilde{I}_{\mathrm{acc}}(\mathcal{S} : \mathcal{E}_f)$— and thus $P(\rho, n) \simeq 1$. A concise memorandum of the definitions of consensus and redundancy is given in Box 1.

4.4 States highlighting the difference between consensus and redundancy

A notable class of states highlighting the differences between redundancy and consensus are highly nonlocal states. Nonlocal states are understood here as those in which some information about the system can only be recovered by means of nonlocal measurements on several environmental constituents, as pictorially represented in fig. 4.1. While it is usually the case that a single element does not hold enough information about the system, we define nonlocality in terms of *fragility* of such information encodings with respect to loss of pieces of the environment, and show that it is tightly related with the departures between redundancy and consensus. We focus in particular on the extreme cases, where losing even a single environmental constituent results in a severe degradation of the correlations.

We focus here on many-qubit states for simplicity. To have both high redundancy and maximal nonlocality of the information encoding, we require the state of the system to be maximally correlated with a number of maximally nonlocal environmental states of the form

$$|\,\mathrm{GHZ}_{\pm}^{(k)}\rangle \equiv \frac{1}{\sqrt{2}}(|0\rangle^{\otimes k} \pm |1\rangle^{\otimes k}) \in (\mathbb{C}^2)^{\otimes k}. \tag{4.4}$$

While these two states are fully distinguishable when all k qubits are measured, they become completely indistinguishable if even only a single qubit is lost, as

$$\mathrm{tr}_i(\mathrm{GHZ}_{+}^{(k)}) = \mathrm{tr}_i(\mathrm{GHZ}_{-}^{(k)}),\ \forall i = 1, ..., k. \tag{4.5}$$

The integer k governs the degree of nonlocality of the states. Note that GHZ-like states are characterized by not being determined by their reduced density matrices. More explicitly, this means that for any pair of orthogonal states $|\psi\rangle, |\phi\rangle \in (\mathbb{C}^2)^{\otimes k}$ such that $\mathrm{tr}_i(|\psi\rangle\langle\psi|) = \mathrm{tr}_i(|\phi\rangle\langle\phi|)$ for all i, $|\psi\rangle$ and $|\phi\rangle$ are local unitary equivalent to $|\mathrm{GHZ}_{\pm}^{(k)}\rangle$ [110, 111].

We thus consider system-environmental states $|\Psi\rangle_{k,N} \in (\mathbb{C}^2)^{Nk+1}$ of the form

$$|\Psi\rangle_{k,N} \equiv \frac{1}{\sqrt{2}}(|0\rangle \otimes |\mathrm{GHZ}_{+}^{(k)}\rangle^{\otimes N} + |1\rangle \otimes |\mathrm{GHZ}_{-}^{(k)}\rangle^{\otimes N}). \tag{4.6}$$

These states have degree of redundancy N. If furthermore $k = 1$, the information encoding is local, and we also have a degree of consensus N. In fact, in this case, there is only one possible macrofractioning of the environment — which is composed of $Nk = N$ qubits — into N constituents, so that $P(\rho, N) = 1$.

However, as soon as $k > 1$, the two aspects of objectivity diverge. In such instances, the QMI depends on the way in which the kN environmental qubits are partitioned between observers. We recognize in particular two conditions that are sufficient to determine the QMI $I(\mathcal{S} : \mathcal{E}_i)$ corresponding to a given environmental fraction $\mathcal{E}_i$. The first condition is whether at least one full GHZ state is fully contained in $\mathcal{E}_i$. The second condition is whether at least one qubit from each GHZ state is in $\mathcal{E}_i$. If neither condition is satisfied $I(\mathcal{S} : \mathcal{E}_i) = 0$; if either condition is satisfied $I(\mathcal{S} : \mathcal{E}_i) = S(\rho_S)$; finally, if both conditions are satisfied, then $I(\mathcal{S} : \mathcal{E}_i) = 2S(\rho_S)$. The corresponding four possible scenarios are pictorially represented in fig. 4.2. We refer to section 4.6 for the full derivation of these quantities, where we also show that performing the same calculations for the accessible mutual information gives

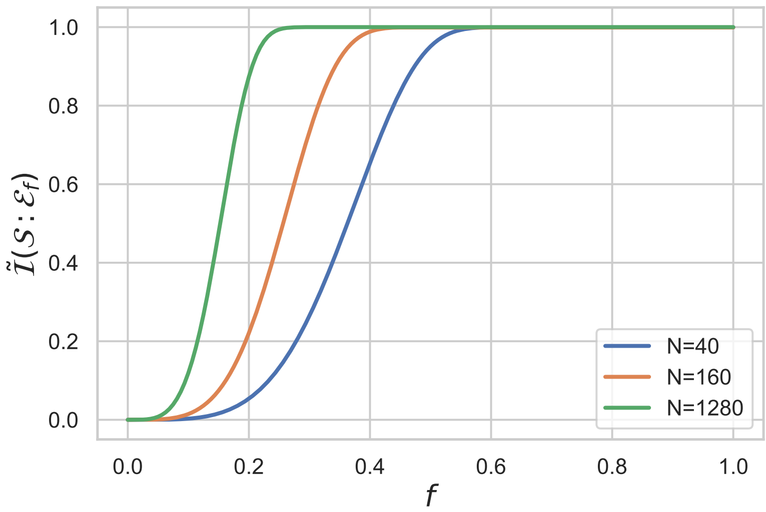

FIGURE 4.3: **Average accessible mutual information for different values of redundancy**. Notice how high redundancy does not always result in the typical objectivity plateau of quantum Darwinism. In particular, redundancy values of 40, 160 and 1280 correspond to consensus values of 1, 2 and 4, respectively. In all cases the degree of nonlocality is $k = 4$.

$I_{\text{acc}}(S : \mathcal{E}_i) = S(\rho_S)$ in all cases except when neither condition is satisfied. With these results, computing average QMI and accessible mutual information reduces to a combinatorial problem, which we also detail in section 4.6.

In fig. 4.3 we give the values of $\tilde{I}_{\text{acc}}(\mathcal{S} : \mathcal{E}_f)$ as a function of f for different values of N, for $k = 4$. As clear from these results, a large degree of redundancy does not guarantee an equal amount of consensus. Therefore, it could be possible that, on average, observers will not measure any intact *macrofraction*, and will be unable to recover information about the system, rendering the redundant information inaccessible. In particular, redundancy values of 40, 160 and 1280 correspond to consensus values of 1, 2 and 4. This choice of states thus highlights how nonlocal information encoding results in non-equivalence between redundancy and consensus. We also see that the consensus increases with the size of the environment, which is a consequence of the fact that for large N the probability of selecting at least $k \ll N$ qubits belonging to the same macrofraction tends to unity. In the macroscopic limit, the system exhibits objectivity even in the worst-case scenario of maximally nonlocal information encoding. As discussed previously, it is possible to recover information about the system by measuring a single element from each $|\text{GHZ}\rangle$ — that is, reading each element of a column in fig. 4.2. However, in the macroscopic limit of $N \gg k$, the probability of picking such partition goes to zero.

We have shown that maximally nonlocal information encoding is only possible for states that are local unitary equivalent to the GHZ state. Nonetheless, many entangled states also feature a high degree of nonlocality. One such standard example of three-qubit nonlocal states are W states [112]. These can be seen as an intermediate

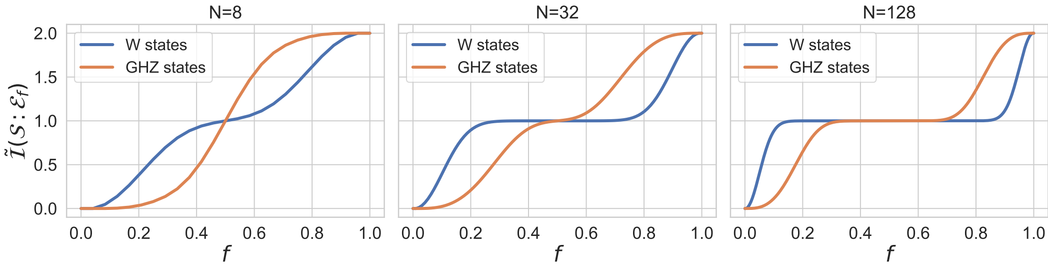

FIGURE 4.4: **Averaged QMI encoding the information in GHZ states and W states.** While the overall effects of nonlocal information encoding remain unaltered, encoding information in W states always results in higher consensus compared to GHZ states. In each figure, the degree of nonlocality is $k = 3$, while the redundancy is $N = 8, N = 32$, and $N = 128$, respectively. GHZ states result in consensus values of 1, 2 and 3 respectively, while W states result in consensus values of 2, 3 and 6 respectively.

case bewteen maximally local and maximally nonlocal information encoding. We then consider system-environment states of the form

$$\frac{1}{2}(\,|0\rangle \otimes |W_+^{(k)}\rangle^{\otimes N} + |1\rangle \otimes |W_-^{(k)}\rangle^{\otimes N}), \tag{4.7}$$

with $|W_\pm^{(k)}\rangle$ a pair of W-like orthogonal many-qubit states. In the case of $k = 3$, these read

$$\begin{aligned} |W_+^{(3)}\rangle &\equiv \frac{1}{\sqrt{3}}(|001\rangle + |010\rangle + |100\rangle), \\ |W_-^{(3)}\rangle &\equiv \frac{1}{\sqrt{3}}(|001\rangle + \omega_3\,|010\rangle + \omega_3^2\,|100\rangle), \end{aligned} \tag{4.8}$$

with $\omega_3 \equiv e^{2\pi i/3}$. These definitions are straightforwardly generalized to general k.

In this case, the mutual information between system and environmental fraction does not reduce to the four possible cases as with the GHZ state structure, as now it becomes relevant how many qubits are selected from each macrofraction. In any case, it is still possible to reduce the QMI calculation to a combinatorial, albeit more complex, problem. Again, the full calculation can be found in section 4.6.

While the individual qubits still carry no information about the system, a partially surviving $|W_+^{(k)}\rangle$ state is slightly distinguishable from the $|W_-^{(k)}\rangle$ counterpart, meaning that an observer may be able to determine the state of the system without having access to a full macrofraction. For this reason we expect it to be easier to achieve state objectivity in this case compared to the maximally nonlocal one.

This is confirmed by fig. 4.4, where we compare the average QMI between W-state and GHZ-state encodings for a nonlocality degree of $k = 3$. We can see that the W-state encoding always results in a higher QMI compared with the GHZ case. In particular, redundancy values of 8, 32 and 128 correspond to consensus values of 2, 3 and 6 for W-states and 1, 2 and 3 for GHZ-states. In any case, even though a W-state encoding allows to reach state objectivity with a smaller environmental size, the qualitative behaviour and relative implications are the same as with the GHZ

Box 1: Definitions of redundancy and consensus

Redundancy— how many times information about the system is encoded into the environment. It is the maximum number of fractions into which we can divide the environment, such that every fraction is highly correlated with the system. Therefore, it is the highest n such that $\mathcal{E} = \bigotimes_{i=0}^{n} \mathcal{E}_i$ and $I(\mathcal{S} : \mathcal{E}_i) \simeq S(\rho_{\mathcal{S}})\ \forall i$.

Consensus— how many observers can simultaneously access information about the system. It is the maximum number of fractions into which we can randomly divide the environment, being confident that each fraction will be highly correlated with the system. We define $P(\rho, n)$ as the probability that, given a random environmental partition $\mathcal{E} = \bigotimes_{i=0}^{n} \mathcal{E}_i$, then $I(\mathcal{S} : \mathcal{E}_i) \simeq S(\rho_{\mathcal{S}})\ \forall i$. Consensus is then the highest n such that $P(\rho, n) \simeq 1$

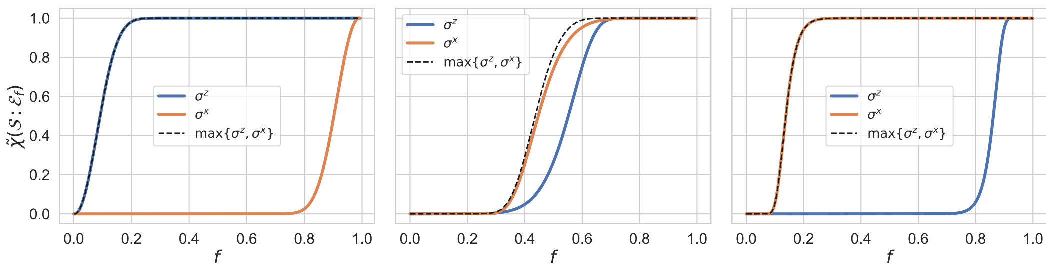

FIGURE 4.5: **Averaged QMI encoding the information in GHZ states and W states.** While the overall effects of nonlocal information encoding remain unaltered, encoding information in W states always results in higher consensus compared to GHZ states. In each figure, the degree of nonlocality is $k = 3$, while the redundancy is $N = 8, N = 32$, and $N = 128$, respectively. GHZ states result in consensus values of 1, 2 and 3 respectively, while W states result in consensus values of 2, 3 and 6 respectively.

case.

4.4.1 Reading the environment in more bases

The classical mutual information is usually computed by maximising the Holevo χ with respect to the measurements performed on the system. In the context of quantum objectivity, it is often the case that the Holevo χ is always maximised by measuring the system in the same basis, and this in turn is sufficient to define it as the pointer basis of the system. However, we will show here that this is not always the case, as for the states in eq. (4.6), the Holevo χ is not always maximised by measuring the system in the same basis.

If instead of computing the maximised Holevo χ, we choose to compute the Holevo χ with respect to one specific measurement basis, we are able to recover how much information the environmental fractions hold about that basis. The detailed calculation is left at the end of the chapter, but we summarise the results here. Considering once again the four possible scenarios represented in fig. 4.2, $\chi(\mathcal{S} : \mathcal{E}_i)$ computed with respect to the $\{|0\rangle, |1\rangle\}$ basis is $S(\rho_{\mathcal{S}})$ if at least one full GHZ state is fully contained in $\mathcal{E}_i$ (***top left*** and ***bottom left*** of fig. 4.2). Instead, $\chi(\mathcal{S}:\mathcal{E}_i)$ computed with respect to the $\{|+\rangle, |-\rangle\}$ basis is $S(\rho_{\mathcal{S}})$ if at least one qubit from each GHZ state is in $\mathcal{E}_i$ (***top right*** and ***bottom left*** of fig. 4.2). The environment then holds redundant information about the system simultaneously in two different bases. It should be noted however, that only one basis can be measured at any given time: if a specific $\mathcal{E}_i$ fraction holds information about the system in one basis, the rest of the environment will hold no information about the system in the other basis. This is because it is impossible for one environmental fraction to satisfy the condition represented in ***top left*** of fig. 4.2 and for another, distinct fraction to safisfy the condition represented in ***top right*** of fig. 4.2.

Figure 4.5 shows a comparison between $\chi(\mathcal{S}:\mathcal{E}_f)$ computed with respect to the $\{|0\rangle, |1\rangle\}$ and the $\{|+\rangle, |-\rangle\}$ bases, as well as the maximised $\chi(\mathcal{S}:\mathcal{E}_f)$, as a function of f. All plots are for a redundancy value of $N=80$, while the degree of nonlocality is, from left to right, $k=2$, $k=8$, and $k=32$. We can see how, as the degree of nonlocality increases, the environment "knows" more about the $\{|+\rangle, |-\rangle\}$ basis compared to the computational one, and it even takes over as the one containing the most information for $N=80$ and $k=32$ (rightmost plot of fig. 4.5).

4.5 The importance of using the average mutual information

As we have already mentioned in chapter 2, $I(\mathcal{S}:\mathcal{E}_f)$ is the mutual information between the system and a specific fraction $\mathcal{E}_f$, and for any value of f there are of course multiple possible environmental fractions $\mathcal{E}_f$ of the same size. Objectivity is often assessed by plotting $I(\mathcal{S}:\mathcal{E}_f)$ as a function of f, making a choice of $\mathcal{E}_f$ for each value of f, which intrinsically implies choosing a sequence of environmental fractions of increasing size. When the degree of correlations between the system and the various environmental constituents is not homogeneous, the value of $I(\mathcal{S}:\mathcal{E}_f)$ as a function of f will depend on the specific chosen sequence of environmental fractions. It is therefore warranted to use the averaged QMI, defined as $\tilde{I}(\mathcal{S}:\mathcal{E}_f) = \langle I(\mathcal{S}:\mathcal{E}_f)\rangle_{\mathcal{E}_f}$ where the mean is taken with respect to all environmental fractions of the same size $f \dim \mathcal{E}$.

In many studied scenarios [54, 113, 114, 115, 116, 117, 118], the state ρ is assumed to be the result of a unitary dynamics in which different environmental fractions only directly interact with the system, so that the overall state is driven by a Hamiltonian of the form $H_I = \sum_k A^{\mathcal{S}} \otimes B^{\mathcal{E}_k}$, with the different $B^{\mathcal{E}_k}$ acting identically to their respective subsystems. In such cases, the QMI $I(\mathcal{S}:\mathcal{E}_f)$ depends only on the size of $\mathcal{E}_f$, rather than the specific group of environmental constituents considered, therefore, performing the average is unneeded, and the average QMI is identical to the QMI with respect to any chosen sequence. However, this condition does not hold in other cases of interest, where the system is correlated asymmetrically with the environmental

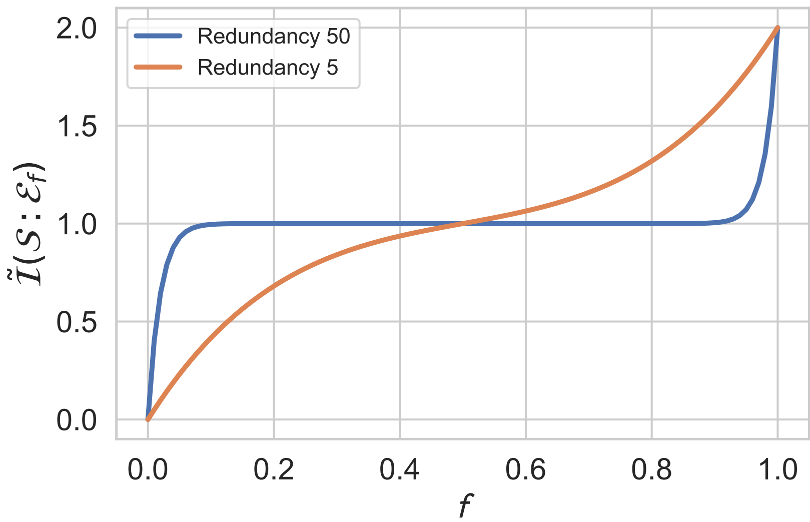

FIGURE 4.6: **Averaged mutual information as a function of the fraction size**. The environment consists of some qubits perfectly correlated with the system, and others entirely uncorrelated ("junk" qubits). We compare the case in which there are 50 correlated qubits, where we can see a clear signature of objectivity, with the case in which there are only 5 correlated qubits, where objectivity does not emerge. In both cases, for every correlated qubit there are 20 "junk" qubits. The value of redundancy is precisely the number of correlated qubits.

fractions [53, 58, 9, 60, 105, 51, 52]. We will show how, in such cases, not using the averaged QMI could prove to be misleading for the task of witnessing objectivity.

4.5.1 Uneven degree of correlations

We first show an example that illustrates some possible issues that arise when computing the QMI in cases with asymmetric information encoding, and how these issues do not arise when using the averaged QMI. Suppose we wish to measure the degree of objectivity of the following state

$$|\Psi\rangle = \frac{1}{\sqrt{2}}(|0\rangle_{\mathcal{S}} \otimes |0\rangle^{\otimes m} + |1\rangle_{\mathcal{S}} \otimes |1\rangle^{\otimes m}) \otimes |+\rangle^{\otimes N-m}\,, \tag{4.9}$$

there are m environmental qubits that are perfectly correlated with the system, but there are also $N-m$ environmental qubits that are entirely uncorrelated, so that the total number of environmental qubits is N. Measuring even just one of the m correlated qubits is sufficient to recover the required information about the system, that is, information about the system is encoded redundantly into m different qubits.

Let us now proceed to compute the averaged QMI of the state in eq. (4.9). If we randomly extract i qubits from the environment, the number of possible extractions where all the selected qubits are uncorrelated with the system is $\binom{N-m}{i}$, whereas the overall number of possible extractions is $\binom{N}{i}$. The probability that, with a random extraction, all selected qubits are uncorrelated with the system is therefore

$\binom{N-m}{i}\binom{N}{i}^{-1}$, in which case the QMI between the selected qubits and the system is zero. The probability for the complementary event, that at least one of the selected qubits is correlated with the system, is therefore $1-\binom{N-m}{i}\binom{N}{i}^{-1}$, in which case the QMI is $S(\rho_{\mathcal{S}})$. There is also the probability that, provided $i > m$, all the correlated qubits haven been selected, which we obtain by preemptively selecting the correlated qubits and then randomly extracting the $i-m$ remaining ones, the probability is therefore $\binom{N-m}{i-m}\binom{N}{i}^{-1}$, in which case the QMI is $2S(\rho_{\mathcal{S}})$. Notice that, if this second condition is met, the first one surely is, so that the two events are not independent. Given that selecting i environmental qubits correspond to selecting a fraction of size $fN = i$, we can explicitly write the average mutual information between system and a fraction $\mathcal{E}_f$.

$$\tilde{I}(\mathcal{S}:\mathcal{E}_f) = \left(1 - \frac{\binom{N-m}{fN} + \binom{N-m}{fN-m}}{\binom{N}{fN}}\right) S(\rho_{\mathcal{S}}), \tag{4.10}$$

The plots of eq. (4.10) as a function of f are shown in fig. 4.6 for the case where $N = 1000$ and $m = 50$ as well as for $N = 100$ and $m = 5$, so that in both cases only one in twenty qubits is actually correlated with the system. We can see how in the first case $I(\mathcal{S}:\mathcal{E}_f) \simeq S(\rho_{\mathcal{S}})$ even for small values of f, which is represented by the QMI plot exhibiting the typical plateau of objective states. In the second case however, said plateau is not present, and the state is therefore not objective. In general, from eq. (4.10) it can be seen that, given a value of f, the corresponding value of QMI depends mostly on m, and only marginally on N. Regardless the amount of "junk" qubits, objectivity emerges provided that the number of correlated qubits is sufficiently large.

By choosing a required threshold value for the QMI, it is possible to compute the minimum size $f_0 \dim \mathcal{E}$ for the environmental fractions, such that each observer can independently infer information about the system by measuring a single fraction. The number of resulting environmental fractions -the consensus-, quantified as $1/f_0$, would then be strictly less than the redundancy m. We therefore have another example where consensus and redundancy are not equivalent.

In general, whenever there are hindrances to the information recovering from the observers' part, consensus will be less than redundancy. Said hindrances may arise when the information encoding is not symmetrical or not local, precisely the cases where it is deemed to use the average mutual information. In the scenario presented here, since only some environmental constituents are correlated with the system, it is not unlikely that observers measuring certain environmental fractions will only measure "junk" qubits. To minimise the probability of this event occurring, we have to increase the size of the environmental fractions, ending up with a value of consensus that is strictly less than the redundancy. In the case under study here, by choosing a threshold value of $0.99S(\rho_{\mathcal{S}})$, we obtain a consensus value of 11 when the redundancy is 50, and 1 (no objectivity) when the redundancy is 5.

If, on the other hand, we do not perform the average, to compute the QMI plot

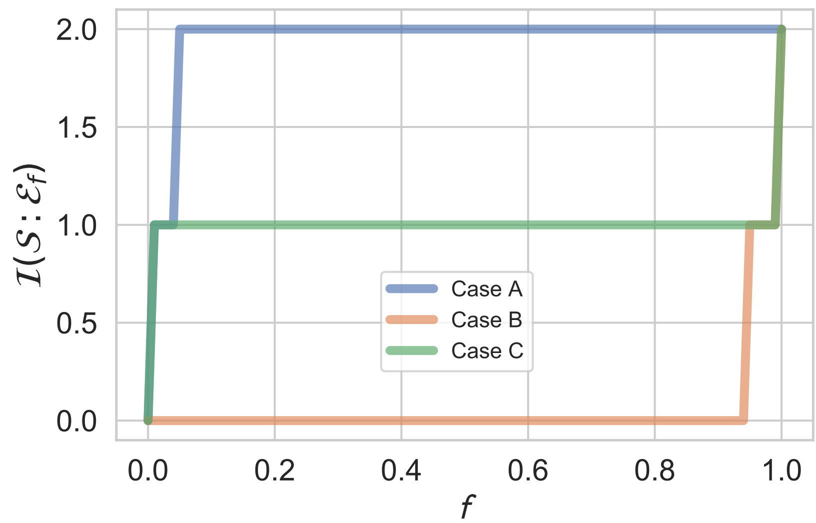

FIGURE 4.7: **Different plots for the mutual information as a function of the fraction size**. All plots refer to the same system-environment state, where however no average was performed. In case A every fraction of size fN contains only correlated qubits, in case B every fraction of size fN contains only "junk" qubits, and in case C every fraction contains at least one correlated qubit, but at least one of the correlated qubits is always left out of each fraction. Not performing the average results in outcomes that are contradicting among themselves and misleading compared to the physical scenario. Since the ratio between correlated and "junk" is the same, the presented plots are the same whether the total number of environmental qubits is $N = 100$ or $N = 1000$.

we have to choose a specific environmental fraction of size fN, for each value of f. Usually, each fraction of a larger size fully contains the fractions of smaller size. The scaling of the QMI as a function of f will thus depend on the chosen sequence of environmental fractions of increasing size. If we try to quantify objectivity by using the non-averaged QMI, then we may end up with contradicting results, as a matter of fact, we present in fig. 4.7 three extreme examples of such cases.

In case A, every fraction of size fN contains only correlated qubits, unless $fN > m$, in which case the fractions contain all the correlated qubits and some of the "junk" qubits. In case B, every fraction of size fN contains only "junk" qubits, unless $fN > N - m$, in which case the fractions contain all the "junk" qubits and some of the correlated qubits. In case C, every fraction contains at least one correlated qubit, but at least one of the correlated qubits is always left out of each fraction (unless of course the whole environment is taken into account). Notice how the mutual information plots for these three specific cases are identical whether the environment is made by $m = 5$ or $m = 50$ correlated qubits, this is because the ratio between the correlated qubits and the "junk" qubits is the same. The fact that the plots shown in fig. 4.7 are the same both for a case where quantum objectivity emerges ($m = 50$), and one where quantum objectivity does not emerge ($m = 5$), already shows how non-averaged QMI plots are unable to distinguish between two very different outcomes.

In cases A and B the typical plateau of objective states is not present, but while in case A the QMI is consistently higher than one, in case B it is consistently lower than one. While both cases seem to suggest that there is a disproportion between the degree of correlations of the various environmental fractions, they do not allow to reach a conclusion on whether objectivity is present or not. Regardless, it is interesting to notice that, in both cases, the QMI exhibits a very small plateau, whose width is exactly m/N. This suggests that, even for non-averaged QMI, a minimum plateau that is at least as large as the redundancy must be present. Case C is somewhat more tricky, as there is a clear objectivity plateau, but given that the QMI is $S(\rho_{\mathcal{S}})$ even for a fraction of one qubit, the natural interpretation would be that the overall redundancy is N, while only m qubits are actually correlated with the system. Aside from grossly overestimating the degree of redundancy, case C would suggest that objectivity emerges both when $m = 5$ and when $m = 50$, which we know to be false from fig. 4.6.

The scenario proposed here arises whenever, aside from the environment that acquired information about the system, extra environmental elements are taken into account, whose correlations with the system are negligible. For objective states in the macroscopic limit, it is reasonable to assume that several uncorrelated environmental fractions enter the picture. One would assume that these extra fractions should not modify the degree of objectivity, and indeed in our model, regardless of how many "junk" qubits are present, objectivity always emerges provided that redundancy is sufficiently large. Indeed, a similar conclusion was also obtained in a recent work [119]. However, even in this simple example, not using the average QMI results in grossly misleading results.

4.5.2 Asymmetric quantum mutual information

We have seen with a simple example how failing to compute the averaged QMI may results in false positives or false negatives witnesses of objectivity, as well as misquantifying the degrees of redundancy and consensus. Let us focus now on cases where the non-averaged quantum mutual information between system and a small environmental fraction $\mathcal{E}_f$ is larger than $S(\rho_\mathcal{S})$, that is $I(\mathcal{S}:\mathcal{E}_f) > S(\rho_\mathcal{S})$ for $f < \frac{1}{2}$. This is analogous to the scenario represented in fig. 4.7, case A, and is only possible if the information encoding is asymmetrical [2], and some environmental constituents are more correlated with the system than others. Assuming that $\mathcal{E} = \mathcal{E}_f \otimes \mathcal{E}_{\overline{f}}$ and $\dim(\mathcal{E}_f) < \dim(\mathcal{E}_{\overline{f}})$, we have

$$I(\mathcal{S}:\mathcal{E}_f) = S(\rho_\mathcal{S}) + \Delta, \tag{4.11}$$

the two fractions $\mathcal{E}_f$ and $\mathcal{E}_{\overline{f}}$ can, of course, have their own internal structure, what is relevant for our discussion is that the fraction $\mathcal{E}_f$ corresponds to a small portion of the environment. Provided that the system-environment state $\rho_{\mathcal{S}\mathcal{E}}$ is pure, we can compute the QMI between the system and the rest of the environment: $I(\mathcal{S}:\mathcal{E}_{\overline{f}}) = S(\rho_\mathcal{S}) + S(\rho_{\mathcal{E}_{\overline{f}}}) - S(\rho_{\mathcal{S}\mathcal{E}_{\overline{f}}})$. Since $\rho_{\mathcal{S}\mathcal{E}}$ is pure, we can write $I(\mathcal{S}:\mathcal{E}_{\overline{f}}) = S(\rho_\mathcal{S}) + S(\rho_{\mathcal{S}\mathcal{E}_f}) - S(\rho_{\mathcal{E}_f})$, moreover, from eq. (4.11) we have that $S(\rho_{\mathcal{E}_f}) = S(\rho_{\mathcal{S}\mathcal{E}_f}) + \Delta$. Combining all this we have that

$$I(\mathcal{S}:\mathcal{E}_{\overline{f}}) = S(\rho_\mathcal{S}) - \Delta. \tag{4.12}$$

Measuring the whole $\mathcal{E}_{\overline{f}}$ environmental fraction, i.e. the majority of the environment, still does not allow to recover enough information about the system.

While there is a consistently growing interest in measuring objectivity using accessible quantities [44, 55], rightfully motivated by the fact that the QMI contains discordant [33] quantities that do not translate in information recoverable by the observers, it is interesting to notice how the QMI contains relevant information even in the context of quantum objectivity, in particular, witnessing quantum correlations with one environmental fraction puts a bound on the accessible information with all other fractions.

The fact that the QMI between system and most of the environment is smaller than $S(\rho_S)$ does not allow, in itself, to conclude that $\rho_{\mathcal{S}\mathcal{E}}$ exhibits quantum objectivity or not. Interpreting objectivity as consensus, information about the system could be present in $\mathcal{E}_f$ with a high degree of redundancy, so that an observer measuring a random fraction of the environment will (on average) be able to infer information about the system, as was the case in fig. 4.6. However, it could also be that information

[2] We recall that, if the information encoding is symmetrical, or the average is performed, the QMI plot has the property of being anti-symmetric with respect to $f = \frac{1}{2}$, therefore $I(\mathcal{S}:\mathcal{E}_{f_0}) > S(\rho_\mathcal{S})$ is possible only for $f_0 > \frac{1}{2}$

about the system has been encoded only once in a small portion of the environment, in which case quantum objectivity would not be present.

Witnessing values of $I(\mathcal{S} : \mathcal{E}_f) > S(\rho_{\mathcal{S}})$ signals that the system is mostly correlated with only a part of the environment, and that the use of the averaged QMI is needed. Using the accessible information instead of the QMI (which would in general be desirable as a more precise measure of objectivity [55]) could bizarrely prove even more misleading in this case, since the accessible information is never higher than $S(\rho_{\mathcal{S}})$, this phenomenon would be more difficult to uncover. This analysis provides further evidence for the fact that the non-averaged QMI can be a misleading quantifier for quantum objectivity. Notwithstanding, it also shows us that the QMI with respect to a specific environmental fraction provides interesting information about accessible quantities, bounding the possible correlations with respect to the rest of the environment. This further shows how a quantum system cannot be correlated with QMI higher than one simultaneously with more than one element, therefore, objectivity requires that the QMI between the system and the environmental fractions is exactly $S(\rho_{\mathcal{S}})$. The existence of even a partial objectivity plateau is then a crucial feature of objective states. Since, as previously noted, the width of the objectivity plateau is at least the value of redundancy, the lack of a QMI plateau is sufficient to infer a complete lack of redundancy, and thus of objectivity.

4.5.3 Random degrees of correlations

We have provided an example to show the importance of using the averaged QMI to witness objectivity. The proposed example, however explanatory, was nonetheless related to a very specific scenario. To further highlight the importance of averaging the QMI to witness objectivity, we will consider here more general scenarios with random degrees of correlation between system and environmental fractions. We expect that the results presented so far, namely the non equivalence between redundancy and consensus, as well as the potentially misleading results from failing to perform the average, would hold even in this case.

In the proposed example, instead of considering qubits that are either perfectly correlated of totally uncorrelated with the system, each qubit interacts with the system with an imperfect CNOT (iCNOT) gate: if the system qubit is in the $|0\rangle_{\mathcal{S}}$ state, the gate acts as an identity on the environmental qubit, if the system is in the $|1\rangle_{\mathcal{S}}$ state, the gate coherently flips the state of the qubit imperfectly, with an associated probability p. In matrix form, the iCNOT reads

$$i\,\mathrm{CNOT} = \begin{pmatrix} 1 & 0 & 0 & 0 \\ 0 & 1 & 0 & 0 \\ 0 & 0 & \sqrt{1-p} & \sqrt{p} \\ 0 & 0 & \sqrt{p} & -\sqrt{1-p} \end{pmatrix}, \tag{4.13}$$

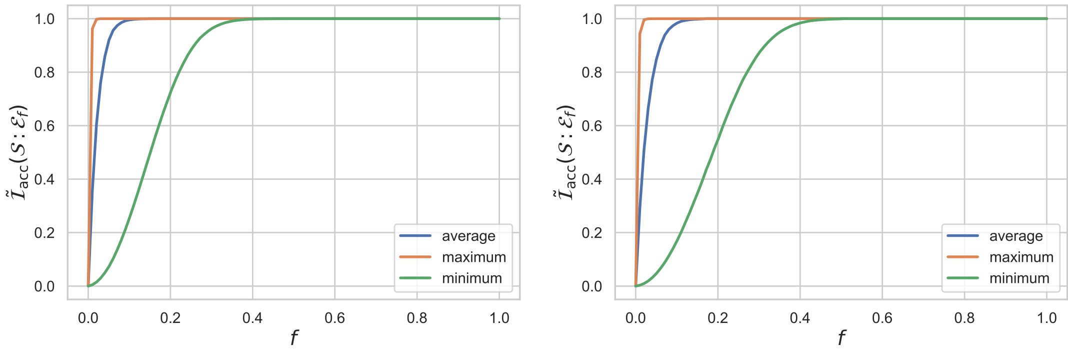

(A) Flat distribution (B) Exponential distribution

FIGURE 4.8: **Mutual information plots for random degrees of correlation**. The environment consists of $N = 100$ qubits, and each qubit has a random level of correlations with the system. **(a)** The correlations for each qubit follow a flat distribution, against a degree of redundancy of Red = 15, the average mutual information gives a degree of consensus of Cons = 11. We also show the possible results of non averaged mutual information, which would suggest degrees of consensus of 2 and 50 respectively. **(b)** The correlations follow an exponential distribution, the degree of redundancy is Red = 12, while the degree of consensus of Cons = 9. Non averaged mutual information, suggest degrees of consensus of 2 and 50 respectively.

with $p \in (1, 0)$. This type of system-environment interaction is standard when studying objective states resulting from collision models [113, 115]. The element of novelty here is that, for each qubit the value of p is randomly extracted from a probability distribution.

If the initial state is $|+\rangle_{\mathcal{S}} |0\rangle^{\otimes N}$, after each environmental qubit has interacted with the system, the state becomes

$$|0\rangle_{\mathcal{S}} |0\rangle^{\otimes N} + |1\rangle_{\mathcal{S}} \otimes \bigotimes_{i=1}^{N} \left(\sqrt{1-p_i}\, |0\rangle + \sqrt{p_i}\, |1\rangle \right), \tag{4.14}$$

with each p_i value a random number. Assuming that the observers restrict themselves to measuring the environmental qubits and the system in the computational basis, we can compute the redundancy and the mutual information of the state in eq. (4.14).

The mutual information between the system and a set of fN environmental qubits is computed as follows. Upon performing projective measurements on the system and the environmental qubits, there are three possible measurement outcomes.

- The system is in the $|0\rangle_{\mathcal{S}}$ state and the environmental qubits are in the $|0\rangle^{\otimes m}$ state, with probability $\frac{1}{2}$.
- The system is in the $|1\rangle_{\mathcal{S}}$ state and the environmental qubits are in the $|0\rangle^{\otimes m}$ state, with probability

$$P_f = \frac{1}{2} \prod_{i}^{fN} (1 - p_i). \tag{4.15}$$

- The system is in the $|1\rangle_{\mathcal{S}}$ state and the environmental qubits are in any state that is not $|0\rangle^{\otimes m}$, with probability $\frac{1}{2}(1 - P_f)$.

From these three possible outcomes, we can compute the marginal probability distribution for the system and for the environmental fraction, and recover the mutual information

$$I_{\mathrm{acc}}(\mathcal{S} : \mathcal{E}_f) = \frac{1}{2}\ln(2) + P_f \ln(P_f) - \left(\frac{1}{2} + P_f\right)\ln\left(\frac{1}{2} + P_f\right) \tag{4.16}$$

The average mutual information between the system and m environmental qubits is obtained by extracting m values of p_i from a chosen probability distribution, and computing the resulting mutual information. The value is averaged over 10^4 extractions. The maximised (minimised) mutual information is obtained by extracting N values of p_i and computing the mutual information with the m highest (lowest) values, again averaging over 10^4 extractions. The threshold value of $0.99S(\rho_{\mathcal{S}})$ is used to compute the resulting values of consensus.

Just like in the previous example, also in this case it would be desirable to compare the degree of consensus with the degree of redundancy. Given the simple structure of the state in eq. (4.9), computing its redundancy was straightforward. However, in more general cases, computing the redundancy from its definition is a far from trivial task, as it requires to find the largest n such that there is an environmental partition $\mathcal{E} = \bigotimes_{i=0}^{n} \mathcal{E}_i$ that allows to cast the state in SBS form. This would be computationally demanding in most scenarios.

Here we compute redundancy by simply creating environmental fractions, whose mutual information with the system is at least $0.99S(\rho_{\mathcal{S}})$, also in this case averaging over 10^4 extractions. Admittedly, this is a rather crude method to compute the redundancy, and it likely results in an underestimation, as no optimisation procedure is involved. However, the redundancy thus computed, even if underestimated, still results higher than consensus, thus proving our initial expectations.

In fig. 4.8 we show a comparison between the average accessible information, and the maximised, as well as minimised accessible information. Both results are for an environment composed by $N = 100$ qubits. In fig. 4.8 (a) the degrees of correlation between the environmental qubits and the system are given by a flat probability distribution, the redundancy is $\mathrm{Red} = 15$, and consensus is $\mathrm{Cons} = 11$. The non-averaged mutual information plots would instead lead to grossly overestimating or underestimating the degree of objectivity. Similar results are obtained in fig. 4.8 (b), where the degrees of correlation between environmental qubits and system are given by an exponential distribution, the redundancy is $\mathrm{Red} = 12$ while consensus is $\mathrm{Cons} = 9$. We can see how even in this more realistic scenarios, not performing the average can lead to misleading results. Furthermore, this case offers yet another example where we can appreciate the numerical difference between consensus and redundancy.

4.6 Average mutual information for nonlocal encodings

Here we show how to obtain the average mutual information between system $\mathcal{S}$ and environmental fraction $\mathcal{E}_f$, when the global system-environment state is the one in eq. (4.6) (information encoded in GHZ-like states) and eq. (4.7) (information encoded in W-like states). In both cases, we will first have to compute all possible values of $I(\mathcal{S}:\mathcal{E}_f)$, which depend on the environmental constituents making up $\mathcal{E}_f$. We will then make combinatorial considerations to compute the probability associated with each $I(\mathcal{S}:\mathcal{E}_f)$ value, thus computing the averaged mutual information. The obtained results correspond to the ones shown in fig. 4.3 and fig. 4.4.

4.6.1 Mutual information for GHZ encodings

Here we consider all possible states resulting from tracing out environmental components from the global state, when information about the system is encoded in GHZ-like states, and compute the QMI between the system and the resulting environmental fraction. We are interested in computing the accessible information, but we will see how, in this specific case, we can easily recover the accessible information by computing the QMI first. The global state is the same as in eq. (4.6)

$$|\Psi\rangle = \frac{1}{\sqrt{2}}\left(|0\rangle \otimes |\tilde{+}\rangle^{\otimes N} + |1\rangle \otimes |\tilde{-}\rangle^{\otimes N}\right), \tag{4.17}$$

where $|\tilde{\pm}\rangle = \frac{1}{\sqrt{2}}(|0\rangle^{\otimes k} \pm |1\rangle^{\otimes k})$ are the same as in eq. (4.4), the GHZ states into which the information is encoded.

Depending on which qubits are traced out from the global state, four different scenarios may arise, which we will analyse individually.

First case

So long as we trace out entire GHZ states, so that only fN remain ($f \in [0,1]$), the resulting state is the following:

$$\rho_{\mathcal{S}\mathcal{E}_f^{(0)}} = \frac{1}{2}\left(|0\rangle\langle 0| \otimes |\tilde{+}\rangle\langle\tilde{+}|^{\otimes fN} + |1\rangle\langle 1| \otimes |\tilde{-}\rangle\langle\tilde{-}|^{\otimes fN}\right), \tag{4.18}$$

whose entropy is 1 bit. If we trace out the system as well we obtain the following

$$\rho_{\mathcal{E}_f^{(0)}} = \frac{1}{2}\left(|\tilde{+}\rangle\langle\tilde{+}|^{\otimes fN} + |\tilde{-}\rangle\langle\tilde{-}|^{\otimes fN}\right), \tag{4.19}$$

whose entropy is also 1. Hence the mutual information is $I(\mathcal{S}:\mathcal{E}_f^{(0)}) = 1$.

Let's consider the case in which we trace out only some qubits from a GHZ state. We can rewrite eq. (4.18) as follows

$$\rho_{\mathcal{S}\mathcal{E}_f^{(0)}} = \frac{1}{2}\left(|0\rangle\langle 0| \otimes |\tilde{+}\rangle\langle\tilde{+}|^{\otimes fN-1} \otimes |\tilde{+}\rangle\langle\tilde{+}| + |1\rangle\langle 1| \otimes |\tilde{-}\rangle\langle\tilde{-}|^{\otimes fN-1} \otimes |\tilde{-}\rangle\langle\tilde{-}|\right), \tag{4.20}$$

and after tracing out m ancillae from the same group (with $m < k$) we obtain

$$\rho_{\mathcal{S}\mathcal{E}_f^{(0)}} = \frac{1}{4}\Big(|0\rangle\langle 0| \otimes |\tilde{+}\rangle\langle\tilde{+}|^{\otimes fN-1} + |1\rangle\langle 1| \otimes |\tilde{-}\rangle\langle\tilde{-}|^{\otimes fN-1}\Big)\otimes\Big(|0\rangle\langle 0|^{\otimes k-m} + |1\rangle\langle 1|^{\otimes k-m}\Big). \tag{4.21}$$

This is the tensor product of two states of entropy 1, meaning it itself has entropy 2. Similarly after tracing out the system we have

$$\rho_{\mathcal{E}_f^{(0)}} = \frac{1}{4}\Big(|\tilde{+}\rangle\langle\tilde{+}|^{\otimes fN-1} + |\tilde{-}\rangle\langle\tilde{-}|^{\otimes fN-1}\Big) \otimes \Big(|0\rangle\langle 0|^{\otimes k-m} + |1\rangle\langle 1|^{\otimes k-m}\Big), \tag{4.22}$$

also of entropy 2. The procedure can be generalized: so long as we trace individual qubits from a complete GHZ state, we increase the entropy of $\mathcal{S}\mathcal{E}_f^{(0)}$ and $\mathcal{E}_f^{(0)}$ by one. The mutual information is $I(\mathcal{S} : \mathcal{E}_f^{(0)}) = 1$ as long as there is still an intact GHZ state remaining.

Second case

The previous results correspond to the case were at least one GHZ state is entirely traced out, and that at least one GHZ state remained intact. Let's now consider the case where we trace out a single qubit from the global (pure) state. The initial state is:

$$\rho_{\mathcal{S}\mathcal{E}} = \frac{1}{2}\mathbb{P}\left(|0\rangle \otimes |\tilde{+}\rangle^{\otimes N-1} \otimes |\tilde{+}\rangle + |1\rangle \otimes |\tilde{-}\rangle^{\otimes N-1} \otimes |\tilde{-}\rangle\right), \tag{4.23}$$

where we have used $\mathbb{P}(|\psi\rangle)$ as a shorthand for $|\psi\rangle\langle\psi|$. We will make use of this notation throughout the current section. By tracing out a single environmental qubit we obtain

$$\begin{aligned}\rho_{\mathcal{S}\mathcal{E}_f^{(1)}} =& \frac{1}{2}\mathbb{P}\left(|0\rangle \otimes |\tilde{+}\rangle^{\otimes N-1} + |1\rangle \otimes |\tilde{-}\rangle^{\otimes N-1}\right) \otimes |0\rangle\langle 0|^{\otimes k-1} \\ &+ \frac{1}{2}\mathbb{P}\left(|0\rangle \otimes |\tilde{+}\rangle^{\otimes N-1} - |1\rangle \otimes |\tilde{-}\rangle^{\otimes N-1}\right) \otimes |1\rangle\langle 1|^{\otimes k-1},\end{aligned} \tag{4.24}$$

this is a state on entropy 1. If we trace out the system as well we obtain

$$\rho_{\mathcal{E}_f^{(1)}} = \frac{1}{4}\Big[\,|\tilde{+}\rangle\langle\tilde{+}|^{\otimes N-1} + |\tilde{-}\rangle\langle\tilde{-}|^{\otimes N-1}\Big] \otimes \Big[\,|0\rangle\langle 0|^{\otimes k-1} + |1\rangle\langle 1|^{\otimes k-1}\Big], \tag{4.25}$$

that is instead of entropy 2, meaning that the mutual information is $I(\mathcal{S} : \mathcal{E}_f^{(1)}) = 2$ even if the global state is not pure. We write the generic state in the case where n qubits, pertaining to different GHZ groups, have been traced out

$$\rho_{\mathcal{S}\mathcal{E}_f^{(1)}} = \frac{1}{2^n}\sum_{a_1=0}^{1}\cdots\sum_{a_n=0}^{1}\mathbb{P}\left(|0\rangle \otimes |\tilde{+}\rangle^{\otimes N-n} + (-)^{\sum a_i}\,|1\rangle \otimes |\tilde{-}\rangle^{\otimes N-n}\right)\bigotimes_{i=0}^{n}|a_i\rangle\langle a_i|. \tag{4.26}$$

Since all the terms in the sum are orthogonal with one another, we have a statistical mixture of 2^n states, all with equal probability, so that the entropy of this state is n.

By tracing out the system we obtain

$$\rho_{\mathcal{E}_f^{(1)}} = \frac{1}{2^{n+1}} \Big[\big|\tilde{+}\big\rangle \big\langle\tilde{+}\big|^{\otimes N-n} + \big|\tilde{-}\big\rangle \big\langle\tilde{-}\big|^{\otimes N-n} \Big] \sum_{a_1=0}^{1} \cdots \sum_{a_n=0}^{1} \bigotimes_{i=0}^{n} |a_i\rangle \langle a_i| , \tag{4.27}$$

that instead has entropy $n+1$. This means that even as we trace out environmental qubits, as long as me make sure that no GHZ state is traced out entirely, the mutual information between system and environment is $I(\mathcal{S} : \mathcal{E}_f^{(1)}) = 2$.

Third case

We can also consider the scenario when qubits are traced out from all GHZ states but no GHZ state is traced out entirely, in this case the resulting state is

$$\rho_{\mathcal{S}\mathcal{E}_f^{(2)}} = \frac{1}{2^N} \sum_{a_1=0}^{1} \cdots \sum_{a_n=0}^{1} \mathbb{P} \Big(|0\rangle + (-)^{\sum a_i} |1\rangle \Big) \bigotimes_{i=0}^{N} |a_i\rangle \langle a_i| , \tag{4.28}$$

of entropy N, and when tracing out the system we obtain

$$\rho_{\mathcal{E}_f^{(2)}} = \frac{1}{2^N} \sum_{a_1=0}^{1} \cdots \sum_{a_n=0}^{1} \bigotimes_{i=0}^{N} |a_i\rangle \langle a_i| , \tag{4.29}$$

Also of entropy N, meaning that in this case the mutual information is $I(\mathcal{S} : \mathcal{E}_f^{(2)}) = 1$.

Fourth case

There is only one scenario we have yet not considered, the case in which at least one qubit has been traced out from each GHZ state, and at least one GHZ state has been traced out entirely. in this case system and environment are in a tensor product, meaning that there are no correlations and that the mutual information is $I(\mathcal{S} : \mathcal{E}_f^{(3)}) = 0$:

$$\rho_{\mathcal{S}\mathcal{E}_f^{(3)}} = \frac{1}{2^{n+1}} \left(|0\rangle \langle 0| + |1\rangle \langle 1| \right) \otimes \Big(|0\rangle \langle 0|^{\otimes k-m} + |1\rangle \langle 1|^{\otimes k-m} \Big)^{\otimes n} . \tag{4.30}$$

For simplicity, we have considered the case where the global state is in an equal weight superposition between $|0\rangle \otimes \big|\tilde{+}\big\rangle^{\otimes N}$ and $|1\rangle \otimes \big|\tilde{-}\big\rangle^{\otimes N}$. All the calculations remain correct even for different superposition weights, as long as the resulting mutual information is not measured in bits, but in units of the system entropy.

Here we have computed the quantum mutual information. If one is interested in the accessible mutual information, it is worth noting how, whenever the quantum mutual information between system and environment is 1, the corresponding states are classical-classical, meaning that the accessible information is also 1. This also implies that when the quantum mutual information is 2, the accessible information is 1.

4.6.2 Holevo χ

Here we compute the Holevo χ between the system and the various environmental fractions. The Holevo χ is computed with respect to measuring the system in a given basis $\{|j\rangle\}$, as

$$\chi_{\{|j\rangle\}} = H(\sum_j p_{|j\rangle}\rho_{|j\rangle}) - \sum_j p_{|j\rangle}H(\rho_{|j\rangle}), \tag{4.31}$$

with $\rho_{|j\rangle}$ the environmental state after the system has been measured in the $|j\rangle$ state, and $p_{|j\rangle}$ the respective probability. We will call $\rho_{|j\rangle}$ the conditioned states and $\sum_{|j\rangle} p_{|j\rangle}\rho_{|j\rangle}$ the unconditioned state. Computing the Holevo χ is then nothing more than comparing the entropies of the conditioned states with the entropy of the unconditioned state. We wish to compute the Holevo χ with respect to two different system measurement bases: the computational basis $\{|0\rangle, |1\rangle\}$ and the $\{|+\rangle, |-\rangle\}$ basis that we will call "alternative".

Here we go through the four possible cases depicted in fig. 4.5, and for each we compute the Holevo χ in both bases for an environmental fraction $\mathcal{E}_i$.

1. At least one full GHZ state is fully contained in $\mathcal{E}_i$.

   Computational base: the conditioned states are pure, and the unconditioned state has entropy 1, $\chi = 1$.

   Alternative base: the conditioned states have the form $1/2\,|\tilde{+}\rangle^{\otimes n} + 1/2\,|\tilde{-}\rangle^{\otimes n}$, so they have entropy 1. The unconditioned state has entropy 1 so that $\chi = 0$.

2. At least one qubit from each GHZ state is in $\mathcal{E}_i$.

   Computational basis: the conditioned states ha the following form

$$\sum_{a_1=0}^{1} \cdots \sum_{a_n=0}^{1} \bigotimes_{i=0}^{N} |a_i\rangle\langle a_i| \tag{4.32}$$

   which happens to be the same form of the unconditioned state, meaning that the Holevo χ is 0.

   Alternate basis: the unconditioned states are

$$\sum_{a_1=0}^{1} \cdots \sum_{a_n=0}^{1} \frac{(1 + (-1)^{\sum a_1})}{2} \bigotimes_{i=0}^{N} |a_i\rangle\langle a_i| \tag{4.33}$$

   for $|+\rangle$ and

$$\sum_{a_1=0}^{1} \cdots \sum_{a_n=0}^{1} \frac{(1 - (-1)^{\sum a_1})}{2} \bigotimes_{i=0}^{N} |a_i\rangle\langle a_i| \tag{4.34}$$

   for $|-\rangle$. These are states of entropy N-1 (2^{N-1}distinguishable states), the unconditioned state has entropy N, so the Holevo χ is 1.

3. At least one full GHZ state and one qubit from each GHZ state are in $\mathcal{E}_i$. We will consider the simplest case, but it is easy to generalise.

Computational base: the conditioned sttaes are $|\tilde{+}\rangle\langle\tilde{+}|^{\otimes N-1}\otimes[|0\rangle\langle 0|^{\otimes k-1}+|1\rangle\langle 1|^{\otimes k-1}]$ and $|\tilde{-}\rangle\langle\tilde{-}|^{\otimes N-1}\otimes[|0\rangle\langle 0|^{\otimes k-1}+|1\rangle\langle 1|^{\otimes k-1}]$, clearly of entropy 1 and the unconditioned state has entropy 2, so the Holevo χ is 1.

Alternative base: the conditioned states are

$$\begin{aligned}&[|\tilde{+}\rangle^{\otimes N-1}+|\tilde{-}\rangle^{\otimes N-1}][\langle\tilde{+}|^{\otimes N-1}+\langle\tilde{-}|^{\otimes N-1}]\otimes|0\rangle\langle 0|^{\otimes k-1}\\ +&[|\tilde{+}\rangle^{\otimes N-1}-|\tilde{-}\rangle^{\otimes N-1}][\langle\tilde{+}|^{\otimes N-1}-\langle\tilde{-}|^{\otimes N-1}]\otimes|1\rangle\langle 1|^{\otimes k-1}\end{aligned} \tag{4.35}$$

for $|+\rangle$ and

$$\begin{aligned}&[|\tilde{+}\rangle^{\otimes N-1}-|\tilde{-}\rangle^{\otimes N-1}][\langle\tilde{+}|^{\otimes N-1}-\langle\tilde{-}|^{\otimes N-1}]\otimes|0\rangle\langle 0|^{\otimes k-1}\\ +&[|\tilde{+}\rangle^{\otimes N-1}+|\tilde{-}\rangle^{\otimes N-1}][\langle\tilde{+}|^{\otimes N-1}+\langle\tilde{-}|^{\otimes N-1}]\otimes|1\rangle\langle 1|^{\otimes k-1}\end{aligned} \tag{4.36}$$

for $|-\rangle$. these are states of entropy 1, so even in this base the Holevo χ is 1.

4. None of the above.

Since the mutual information between system and environment is 0, the Holevo χ in any basis will be 0 as well.

4.6.3 Combinatorial computation for GHZ encodings

Following the considerations in the previous section, we can see that, given a specific environmental fraction $\mathcal{E}_f$, there are two conditions that define the mutual information $I(\mathcal{S}:\mathcal{E}_f)$.

- Condition A: $\mathcal{E}_f$ contains at least one complete GHZ state
- Condition B: $\mathcal{E}_f$ contains at least one qubit from each GHZ state

If only one of the two conditions is satisfied, then $I(\mathcal{S}:\mathcal{E}_f)=S(\rho_\mathcal{S})$. If both conditions are satisfied then $I(\mathcal{S}:\mathcal{E}_f)=2S(\rho_\mathcal{S})$. If neither condition is satisfied, then $I(\mathcal{S}:\mathcal{E}_f)=0$. The probabilities associated with the two conditions are independent from one another, and can thus be computed separately.

We will think of the environment as being made of boxes, each box can contain at most k qubits, and the total number of boxes is N. We randomly fill the boxes with m qubits, where m is the size of the environmental fraction. Condition A corresponds to the case where at least one box is completely full. Condition B correspond to the case where no box is empty. The issue now is understanding the probabilities of the boxes being empty or full when we randomly fill them with qubits.

We wish to know how many configurations correspond to having at least one box full, $\mathcal{N}_A$. We assume that we entirely fill one box beforehand, and distribute the remaining qubits in the remaining free slots. The number of possible combinations is $\binom{Nk-k}{m-k}$, but we must also take into account that the initial choice of the full box was arbitrary, so that the total number of combinations is $N\binom{Nk-k}{m-k}$. However, this corresponds to an over-counting, because we are counting multiple times the cases where more than one box is completely filled. We correct this over-counting by subtracting all the possible combinations where two boxes are completely filled beforehand, keeping in mind that this also corresponds to an over-counting of the number of events with more than two boxes completely filled, and so on. The total number of configurations that fulfill condition A results in a sum of alternating sign, that reads

$$\mathcal{N}_A = \sum_{j=1}^{N} (-1)^{1+j} \binom{N}{j} \binom{Nk - jk}{m - jk}. \tag{4.37}$$

The total number of possible configurations is simply $\mathcal{N} = \binom{Nk}{m}$, so that the probability that condition A is fulfilled is $p_A = \frac{\mathcal{N}_A}{\mathcal{N}}$.

Instead of computing the number of configurations where none of the boxes are empty, $\mathcal{N}_B$, it's easier to compute the number of configurations where there is at least an empty box, $\mathcal{N}_{\overline{B}}$, by following a similar reasoning to the previous case: we keep an entire box empty, and then distribute the qubits in the remaining boxes, also in this case we need to take care of the resulting over-counting, leading to

$$\mathcal{N}_{\overline{B}} = \sum_{j=1}^{N} (-1)^{1+j} \binom{N}{j} \binom{Nk - jk}{m}. \tag{4.38}$$

Since we are interested in the number of configurations where none of the boxes are empty, we have that $\mathcal{N}_B = \mathcal{N} - \mathcal{N}_{\overline{B}}$, and the probability that condition B is fulfilled is $p_B = \frac{\mathcal{N}_B}{\mathcal{N}}$.

Based on these results we can finally compute the averaged mutual information between the system $\mathcal{S}$ and an environmental fraction $\mathcal{E}_f$ as $\tilde{I}(\mathcal{S} : \mathcal{E}_f) = (p_A + p_B) S(\rho_{\mathcal{S}})$.

If we want to compute the averaged accessible information $I_{\mathrm{acc}}(\mathcal{S} : \mathcal{E}_f)$, we should take into account that when both conditions A and B are satisfied, the accessible information is only $I_{\mathrm{acc}}(\mathcal{S} : \mathcal{E}_f) = S(\rho_{\mathcal{S}})$. therefore

$$\tilde{I}_{\mathrm{acc}}(\mathcal{S} : \mathcal{E}_f) = (p_A + p_B - p_A p_B) S(\rho_{\mathcal{S}}) \tag{4.39}$$

4.6.4 Mutual information for W encodings

Here we consider all possible states resulting from tracing out environmental components from the global state, when information about the system is encoded in W-like states, and compute the QMI between the system and the resulting environmental fraction. In the case of W encodings, it is not trivial to compute the accessible information, we will therefore compute the QMI, using it as an upper bound for the accessible information.

For simplicity, we will focus on the case of nonlocality degree $k = 3$. The global state (eq. (4.7) in the main text) is

$$|\Psi\rangle = \sqrt{p}\, |0\rangle \otimes |w^+\rangle^{\otimes N} + \sqrt{1-p}\, |1\rangle \otimes |w^-\rangle^{\otimes N}. \tag{4.40}$$

Where $|w^+\rangle = \frac{1}{\sqrt{3}}(|001\rangle + |010\rangle + |100\rangle)$ and $|w^-\rangle = \frac{1}{\sqrt{3}}(|001\rangle + \omega_3 |010\rangle + \omega_3^2 |100\rangle)$ are the states in eq. (4.8), with $\omega = e^{2\pi i/3}$. We will use a compact notation with $\left|\tilde{0}\right\rangle_N = |0\rangle \otimes |w^+\rangle^{\otimes N}$ and $\left|\tilde{1}\right\rangle_N = |1\rangle \otimes |w^-\rangle^{\otimes N}$.

As with the GHZ-like encoding, depending on which qubits are traced out, we will compute the resulting QMI for four different cases.

First case

We will first consider the case where at least one W state has been fully traced out. In this case, if two qubits are traced out from a W states, the last one will be in a product state with everything else, and will not influence the QMI because it will cause the same increase of entropy for both $\rho_{\mathcal{S}\mathcal{E}_f}$ and $\rho_{\mathcal{E}_f}$. When we trace out a qubit from a W state, we create a mixture between two pure state. More specifically, if we trace out the i-th qubit $\mathrm{tr}_i\{|w^\pm\rangle\langle w^\pm|\} = \rho_\pm^{(i)} = 1/k\,|0\rangle\langle 0|^{\otimes k-1} + \frac{k-1}{k}\left|w_i^\pm\right\rangle\left\langle w_i^\pm\right|$, with $|0\rangle\langle 0|^{\otimes k-1}$ and $\left|w_i^\pm\right\rangle\left\langle w_i^\pm\right|$ orthogonal to one another.

When we trace out one W state from the global state, but at least one W state remains intact, the states are the following:

$$\rho_{\mathcal{S}\mathcal{E}_f^{(0)}} = p\left|\tilde{0}\right\rangle\left\langle\tilde{0}\right|_n \otimes \rho_+^{(i)\otimes m} + (1-p)\left|\tilde{1}\right\rangle\left\langle\tilde{1}\right|_n \otimes \rho_-^{(i)\otimes m}, \tag{4.41}$$

$$\rho_{\mathcal{E}_f^{(0)}} = p\left|w^+\right\rangle\left\langle w^+\right|^{\otimes n} \otimes \rho_+^{(i)\otimes m} + (1-p)\left|w^-\right\rangle\left\langle w^-\right|^{\otimes n} \otimes \rho_-^{(i)\otimes m}, \tag{4.42}$$

It is actually not needed to compute the entropies of the states above. The two states clearly have the same entropy, so the mutual information is $I(\mathcal{S} : \mathcal{E}_f^{(0)}) = S(\rho_{\mathcal{S}})$.

Second case

If at least one group is traced out entirely, and all other groups have been traced out partially, the states are the following:

$$\rho_{\mathcal{S}\mathcal{E}_f^{(1)}} = p\,|0\rangle\langle 0| \otimes \rho_+^{(i)\otimes m} + (1-p)\,|1\rangle\langle 1| \otimes \rho_-^{(i)\otimes m}, \tag{4.43}$$

$$\rho_{\mathcal{E}_f^{(1)}} = p\rho_+^{(i)\otimes m} + (1-p)\rho_-^{(i)\otimes m}, \tag{4.44}$$

We can explicitly rewrite eq. (4.43) in the following way

$$\begin{aligned}\rho_{\mathcal{S}\mathcal{E}_f^{(1)}} =& p\,|0\rangle\langle 0| \otimes \left[1/k\,|0\rangle\langle 0|^{\otimes k-1} + (k-1)/k\left|w_i^+\right\rangle\left\langle w_i^+\right|\right]^{\otimes m} \\ &+(1-p)\,|1\rangle\langle 1| \otimes \left[1/k\,|0\rangle\langle 0|^{\otimes k-1} + (k-1)/k\left|w_i^-\right\rangle\left\langle w_i^-\right|\right]^{\otimes m},\end{aligned} \tag{4.45}$$

all the terms in the above states are pure and orthogonal to one another, so the resulting entropy is only due to classical mixing. The entropy of this state results from the probability vector $(p, 1-p) \otimes (1/k, (k-1)/k)^{\otimes m}$, whose entropy is straightforward to compute.

In the case of eq. (4.44) we end up having states of the form $p\left|w_i^+\middle\rangle\!\middle\langle w_i^+\right|^{\otimes m} + (1-p)\left|w_i^-\middle\rangle\!\middle\langle w_i^-\right|^{\otimes m}$, the eigenvalues of such states are $\lambda = (1 \pm \sqrt{1+4p(1-p)(f-1)})/2$ with $f = |\left\langle w_i^+\right|^{\otimes m}\left|w_i^-\right\rangle^{\otimes m}|^2$, in the case of $p = 1/2$ they reduce to $\lambda = (1 \pm \sqrt{f})/2$.

The entropy for the state in eq. (4.44) is thus

$$S[(1/3, 2/3)^{\otimes m}] + \sum_{j=0}^{m}(1/3)^{m-j}(2/3)^j\binom{m}{j}S(p\left|w_i^+\middle\rangle\!\middle\langle w_i^+\right|^{\otimes j} + (1-p)\left|w_i^-\middle\rangle\!\middle\langle w_i^-\right|^{\otimes j}), \tag{4.46}$$

where $S[(1/3, 2/3)^{\otimes n}]$ is the entropy of the probability vector $(1/3, 2/3)^{\otimes n}$. The QMI is thus

$$I(\mathcal{S} : \mathcal{E}_f^{(1)}) = H'(m) = \sum_{j=0}^{m}(1/3)^{m-j}(2/3)^j\binom{m}{j}S(p\left|w_i^+\middle\rangle\!\middle\langle w_i^+\right|^{\otimes j} + (1-p)\left|w_i^-\middle\rangle\!\middle\langle w_i^-\right|^{\otimes j}). \tag{4.47}$$

Notice how it is necessary to know the number of W states from which only one qubit has been traced out.

Third case

Let's now focus on the alternate scenario, where we never entirely trace out a W-group. We start once again from the global state eq. (4.40), assuming $p = \frac{1}{2}$

$$\frac{1}{2}[|\tilde{0}\rangle_{N-1}|w^+\rangle + |\tilde{1}\rangle_{N-1}|w^-\rangle][\langle\tilde{0}|_{N-1}\langle w^+| + \langle\tilde{1}|_{N-1}\langle w^-|]. \tag{4.48}$$

After tracing out one qubit we obtain the following state:

$$\frac{1}{3}\mathbb{P}\left(|\tilde{0}\rangle_{N-1} + |\tilde{1}\rangle_{N-1}\right) \otimes |0\rangle\!\langle 0|^{\otimes 2} + \frac{2}{3}\mathbb{P}\left(|\tilde{0}\rangle_{N-1}|w_i^+\rangle + |\tilde{1}\rangle_{N-1}|w_i^-\rangle\right), \tag{4.49}$$

so we have a statistical mix of pure distinguishable states. So long as we trace out at most one qubit from each W-group, the procedure can be easily generalised and we end up with a sum of pure distinguishable states where $(1/3,\ 2/3)^{\otimes m}$ is the resulting probability vector from which we can compute the entropies. To be precise, relative phases may come up depending on which qubit is traced out. As we keep tracing out qubits, these phases may build up, making the exact writing of the states non trivial. However, these relative phases are of no consequence for us as we are always left with distinguishable states (notice that in the previous cases such phases did not exist, since we always had at least one fully traced-out W state). This is no longer true when we trace out more than one qubit from each W-group, as in this case such relative phases influence the entropy of the resulting states.

To illustrate this, we start from the initial state

$$|\Psi\rangle = |\tilde{0}\rangle_N + |\tilde{1}\rangle_N, \tag{4.50}$$

after tracing out one qubit we have (from now on, we will use $\mathbb{P}\left(|\psi\rangle\right)$ as a compact notation for $|\psi\rangle\langle\psi|$)

$$\frac{1}{3}\mathbb{P}\left(|\tilde{0}\rangle_{fN}|0\rangle+\phi_i^0|\tilde{1}\rangle_{fN}|0\rangle\right)+\frac{2}{3}\mathbb{P}\left(|\tilde{0}\rangle_{fN}|w_i^+\rangle+|\tilde{1}\rangle_{fN}|w_i^-\rangle\right). \tag{4.51}$$

ϕ_i^0 is the relative phase of the i-th qubit of the $|w^-\rangle$ state, the superscript 0 indicates that it refers to the first W state we are tracing out. To be precise, $[\phi_0^j,\ \phi_1^j,\ \phi_2^j]=[1,\ e^{i\frac{2}{3}\pi},\ e^{-i\frac{2}{3}\pi}]$. If we trace out another qubit from another W state we have

$$\begin{aligned}&\frac{1}{9}\mathbb{P}\left(|\tilde{0}\rangle_{fN}|00\rangle+\phi_i^0\phi_j^1|\tilde{1}\rangle_{fN}|00\rangle\right)+\frac{2}{9}\mathbb{P}\left(|\tilde{0}\rangle_{fN}\left|0w_j^+\right\rangle+\phi_i^0|\tilde{1}\rangle_{fN}\left|0w_j^-\right\rangle\right)+\\&\frac{2}{9}\mathbb{P}\left(|\tilde{0}\rangle_{fN}|w_i^+0\rangle+\phi_j^1|\tilde{1}\rangle_{fN}|w_i^-0\rangle\right)+\frac{4}{9}\mathbb{P}\left(|\tilde{0}\rangle_{fN}\left|w_i^+w_j^+\right\rangle+|\tilde{1}\rangle_{fN}\left|w_i^-w_j^-\right\rangle\right),\end{aligned} \tag{4.52}$$

See how this procedure always keeps the resulting states distinguishable, so that the entropy of the resulting state is only due to the relative probabilities. Now we trace another qubit from one of the surviving pairs, resulting in

$$\begin{aligned}&\frac{1}{9}\mathbb{P}\left(|\tilde{0}\rangle_{fN}|00\rangle+\phi_i^0\phi_j^1|\tilde{1}\rangle_{fN}|00\rangle\right)+\frac{1}{9}\mathbb{P}\left(|\tilde{0}\rangle_{fN}|00\rangle+\phi_i^0\phi_{j'}^1|\tilde{1}\rangle_{fN}|00\rangle\right)\\&+\frac{1}{9}\mathbb{P}\left(|\tilde{0}\rangle_{fN}|01\rangle+\phi_j^1\phi_{j''}^1|\tilde{1}\rangle_{fN}|01\rangle\right)+\frac{2}{9}\mathbb{P}\left(|\tilde{0}\rangle_{fN}|w_i^+0\rangle+\phi_j^1|\tilde{1}\rangle_{fN}|w_i^-0\rangle\right)\\&+\frac{2}{9}\mathbb{P}\left(|\tilde{0}\rangle_{fN}|w_i^+0\rangle+\phi_{j'}^1|\tilde{1}\rangle_{fN}|w_i^-0\rangle\right)+\frac{2}{9}\mathbb{P}\left(|\tilde{0}\rangle_{fN}|w_i^+1\rangle+\phi_{j''}^1|\tilde{1}\rangle_{fN}|w_i^-1\rangle\right).\end{aligned} \tag{4.53}$$

In this case some of the resulting projectors are not distinguishable from one another anymore, resulting in mixed states. The coherence factor of the resulting mixed projector will be $\frac{1}{2}(\phi_j^1+\phi_{j'}^1)$, whose absolute value is $\frac{1}{2}\ \forall j\neq j'$. By tracing out a qubit from the other W state we have

$$\begin{aligned}&\frac{1}{9}\mathbb{P}\left(|\tilde{0}\rangle_{fN}|00\rangle+\phi_i^0\phi_j^1|\tilde{1}\rangle_{fN}|00\rangle\right)+\frac{1}{9}\mathbb{P}\left(|\tilde{0}\rangle_{fN}|00\rangle+\phi_i^0\phi_{j'}^1|\tilde{1}\rangle_{fN}|00\rangle\right)\\&+\frac{1}{9}\mathbb{P}\left(|\tilde{0}\rangle_{fN}|01\rangle+\phi_j^1\phi_{j''}^1|\tilde{1}\rangle_{fN}|01\rangle\right)+\frac{1}{9}\mathbb{P}\left(|\tilde{0}\rangle_{fN}|00\rangle+\phi_{i'}^0\phi_j^1|\tilde{1}\rangle_{fN}|00\rangle\right)\\&+\frac{1}{9}\mathbb{P}\left(|\tilde{0}\rangle_{fN}|00\rangle+\phi_{i'}^0\phi_{j'}^1|\tilde{1}\rangle_{fN}|00\rangle\right)+\frac{1}{9}\mathbb{P}\left(|\tilde{0}\rangle_{fN}|01\rangle+\phi_{i'}^0\phi_{j''}^1|\tilde{1}\rangle_{fN}|01\rangle\right)\\&+\frac{1}{9}\mathbb{P}\left(|\tilde{0}\rangle_{fN}|10\rangle+\phi_{i''}^0\phi_j^1|\tilde{1}\rangle_{fN}|10\rangle\right)+\frac{1}{9}\mathbb{P}\left(|\tilde{0}\rangle_{fN}|10\rangle+\phi_{i''}^0\phi_{j'}^1|\tilde{1}\rangle_{fN}|10\rangle\right)\\&+\frac{1}{9}\mathbb{P}\left(|\tilde{0}\rangle_{fN}|11\rangle+\phi_{i''}^0\phi_{j''}^1|\tilde{1}\rangle_{fN}|11\rangle\right).\end{aligned} \tag{4.54}$$

Once again some projectors are not distinguishable from one another, resulting in mixed states. The coherence factor of the resulting projectors is either $\frac{1}{2}(\phi_j^1+\phi_{j'}^1)$ or $\frac{1}{4}(\phi_i^0+\phi_{i'}^0)(\phi_j^1+\phi_{j'}^1)$. In general the absolute value of the resulting coherence factor will be $\frac{1}{2^l}$, where l is the number of $|0\rangle$ states corresponding to W states were two qubits have been traced out. Interestingly enough, the entropy of such states is the same one of the states of the form $\frac{1}{2}\mathbb{P}\left(|w_i^+\rangle^{\otimes l}\right)+\frac{1}{2}\mathbb{P}\left(|w_i^-\rangle^{\otimes l}\right)$.

To sum things up, whenever we have a state where we have not traced out more than one qubit per pair, then the probability vector of the resulting state is

$(1/3, 2/3)^{\otimes m}$. All the states are pure and distinguishable, so the entropy is only the entropy resulting from the probability. If we further trace out qubits from the surviving W states, we end up with a probability vector of the form $(2/3, 1/3)^{\otimes k} \otimes (1/3, 2/3)^{\otimes m-k}$, where k is the number of W states from which we have traced out two qubits, and $m-k$ is the number of W states from which we have traced out only one qubit. So actually, while the individual probabilities have changed, the entropy of the probability vector remains the same. However, now the states are still distinguishable but not necessarily pure. The mixed states are mixtures with a coherence factor of $\frac{1}{2^l}$ with $0 \leq l \leq k$. The entropy of the state $\rho_{\mathcal{S}\mathcal{E}_f^{(2)}}$ is thus

$$\begin{aligned} S(\rho_{\mathcal{S}\mathcal{E}_f^{(3)}}) =& S\left[\left(\frac{1}{3}, \frac{2}{3}\right)^{\otimes n}\right] + \sum_{i=0}^{m-k} \left(\frac{1}{3}\right)^i \left(\frac{2}{3}\right)^{m-k-i} \binom{m-k}{i} \times \\ &\times \sum_{j=0}^{k} \left(\frac{2}{3}\right)^k \left(\frac{1}{3}\right)^{k-j} \binom{k}{j} S\left(\frac{1}{2}\mathbb{P}\left(|w_i^+\rangle^{\otimes j}\right) + \frac{1}{2}\mathbb{P}\left(|w_i^-\rangle^{\otimes j}\right)\right). \end{aligned} \tag{4.55}$$

We will refer to the second term of eq. (4.55) as $\tilde{H}$. When we trace out the system as well, all the relative phases are lost, and we end up once again with a collection of pure distinguishable states with a resulting probability vector of $(p, 1-p) \otimes (1/3,\ 2/3)^{\otimes n}$, this leads to a mutual information of $I(\mathcal{S} : \mathcal{E}_f^{(2)}) = 2S(\rho_{\mathcal{S}}) - \tilde{H}$.

Fourth case

In the fourth and final case, at least one ancilla has been traced out from all groups, but no group has been entirely traced out. The state structure of the resulting state is exactly the same as in the previous scenario, so that the entropy is also the same. Instead, when tracing out the system as well the state structure is the same one as eq. (4.44). Combining our previous results, the mutual information in this case is $I(\mathcal{S} : \mathcal{E}_f^{(3)}) = S(\rho_{\mathcal{S}}) + H' - \tilde{H}$, where we need to keep track of the number of surviving pairs as well as the number of surviving singlets.

4.6.5 Combinatorial computation for W encodings

In the case of the W states, the combinatorial calculation is now more complicated compared to the GHZ encoding. Using the parallelism introduced earlier, it is no longer sufficient to know the probabilities for the boxes to be empty or full, but we also need to know the probabilities for a certain number of boxes to have exactly one qubit or two qubits, as this now influences the corresponding mutual information.

We can think of the combinatorial calculation in this way: once we fix the number of qubits of the environmental fraction m, we can go through all the possible integer partitions of that specific number (for example, two integer partitions of 5 are $1^1 2^2$ and 1^5), these partitions correspond to the possible ways in which we can distribute the qubits in different boxes. Some partitions however are not compatible with the physical problem at hand: for example, we cannot have integers larger than k, and the total number of integers making up our partitions cannot be larger than N. We may also wish to impose extra conditions: for example, if we wish that no W state is fully selected, we can impose that no integers in the partitions should be larger than $k-1$, and if we wish that no W state is entirely traced out, we can impose that the total number of integers in the partition is exactly N. If a partition $\mathbf{i}$ is $1^{i_1}2^{i_2}...$ the number of possible combinations is given by the polynomial $\binom{\sum_j i_j}{i_0,i_1,i_2...}$, if we also consider the degeneracy resulting from shuffling the qubits inside a box, we have that for every integer partition $\mathbf{i}$ of m, the number of possible configurations is

$$\mathcal{N}_{\mathbf{i}} = \binom{\sum_j i_j}{i_0, i_1, i_2 \dots} \Pi_j \binom{k}{j}^{i_j}, \tag{4.56}$$

with an associated probability $p_{\mathbf{i}} = \frac{\mathcal{N}_{\mathbf{i}}}{\mathcal{N}}$

4.7 Conclusions

In this chapter, we have shown that objectivity in quantum systems can be quantified as redundancy or consensus, two different notions of which we have given operative definitions. We further showed that these two notions can be quantified by means of SBS and QD, respectively. While redundancy and consensus often reduce to the same quantity, they can be very different, in particular in highly nonlocal scenarios, such as when the information is encoded in GHZ or W states. Our results highlight the role of nonlocality in the emergence of objectivity, and show that in general nonlocally encoded information tends to hinder the emergence of consensus. This is due to the fact that, even if redundancy is high, it will be difficult for observers to extract relevant information about the system. On the other hand, based on probabilistic considerations, the hindering effects of nonlocality is compensated by large environments, which suggests that, in the limit of macroscopic environments, high values of consensus are reached even with nonlocal information encoding.

Furthermore, we discussed how the difference between redundancy and consensus breaks the previously established relations between SBS and QD, since there are wide classes of states where being SBS does not necessarily imply QD. We note however, that said relation could be reestablished, provided that some extra care is taken whenever redundancy and consensus do not coincide: if a state is SBS for (on average) all environmental macrofractionings of a certain minimum size, then SBS would imply QD even in the nonlocal scenario. Our framework allows for a clearer interpretation of results obtained using quantifiers such as SBS and QD.

Having established operative definitions for both redundancy and consensus, as well as their non-equivalence, we used them as tools to shed further light on some features of objective states. More specifically, we discussed the need to use the averaged mutual information for measures of quantum objectivity, as well as the possible implications resulting from failing to do so. Aside from the already discussed example of nonlocal states, we have seen that performing the average is fundamental even when the information about the system is locally encoded. This also resulted in further evidence of the potentially stark difference between redundancy and consensus, even with locally encoded information.

We first provided an example with a clear physical interpretation, and showed the possible results of using the non-averaged mutual information, that would result in inaccurate measures of the degree of objectivity. The average mutual information, on the other hand, always has a clear operative meaning. We then analysed a more generic model, and obtained similar results even in a more complex scenario. Aside from advocating for the use of the averaged mutual information, this work offers interpretational tools for the analysis of (averaged and non-averaged) mutual information plots that can help navigate results for similar scenarios in future works. Overall, the results presented in this chapter pave the way for a more thorough understanding of the different aspects of quantum objectivity, and thus the emergence of classicality from the quantum world.

Chapter 5

Witnessing objectivity on a quantum computer

Quantum objectivity has been studied extensively from a theoretical point of view, several models and case studies have been made, and some of its features are now well understood. It still generally lack, however, a proper phenomenological characterization, which makes experimental investigations of quantum objectivity particularly needed.

So far, quantum objectivity has been experimentally studied in some pioneering works. More precisely, in [6] the authors use two-photon four-qubit photonic cluster states to simulate an environment of three qubits. In [7] they use a six-photons photonic quantum simulator to simulate an environment of five qubits. In [8] they use diamond NV centers to simulate an environment of five qubits, the state preparation and readout are done optically. In all these works, the system is composed by a single qubit.

Experimental investigations of QD requires a high level of control of the system as well as the environment, as well as the ability to preserve the purity of the total system-environment state. This strongly limits our ability to generate objective states in a lab. For these reasons, exploring alternative or complementary approaches to objectivity measures is highly needed. Here we propose the first realization of objective states on a superconducting quantum computer. More details can be found in our publication [9].

From the very beginning of their conception, quantum computers were thought as simulators for physical quantum systems [120, 121], considering that the very structure of the quantum theory makes simulations of quantum systems using classical resources particularly challenging.

In recent years, the development of Noisy Intermediate-Scale Quantum (NISQ) devices reached a level that makes their usage as quantum simulators possible. This has been shown in several topics including chemistry [122, 123] and quantum machine learning [124]. With the fast technological advancement it is reasonable to assume that NISQ devices will soon enable quantum simulations currently unattainable with classical resources alone. Our purpose is to investigate their potential to simulate quantum dynamics leading to the emergence of objectivity in the context of QD.

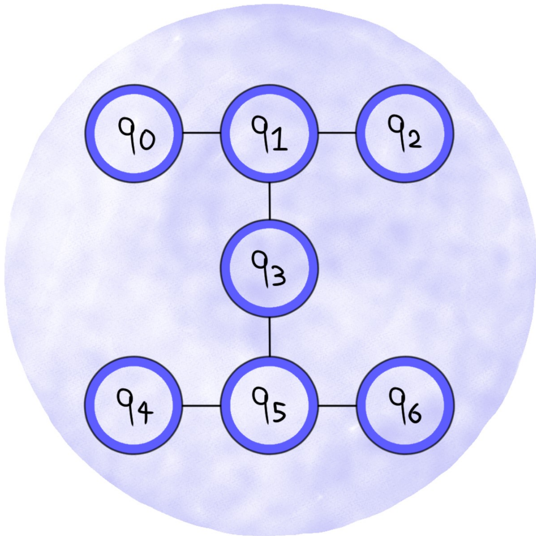

FIGURE 5.1: **Topology of the `ibmq_casablanca` quantum computer**. Each blue circle represents a qubit, the fact that two qubits are connected by a line means that it is possible to apply two-qubit gates between them. The symbols ranging from q_0 to q_6 are the labels by which the qubits are referred to.

For this purpose we simulate the SCM discussed in section 3.1. The model is particularly rich because it can exhibit QD and non-Markovianity, and the information encoding is strictly nonlocal. Being an exactly solvable model makes it an ideal use-case to benchmark the possibility to realise objective states in a quantum computer.

5.1 Simulation on a NISQ device

We study the case where the system, a single qubit, interacts with an environment made of ancillae, each a qubit, according to a SCM. Each ancilla is initially in the $|0\rangle$ state and collides with the system at a random moment in time, such that at any time t there is the probability $p = 1 - e^{-\lambda t}$ for the ancilla to have already collided with the system. In all simulations we set $\lambda = 1$, there is thus a unique correspondence between the physical time t and the probability p, we will use this to control the value of the physical time by changing the collision probability.

Given the $\sigma_x^{\mathrm{a}} \otimes \sigma_z^{\mathcal{S}}$ form of the interaction Hamiltonian, the SCM is a model of pure dephasing in the computational basis. Because of this, the most interesting scenario is the one where the system is initially in an equal weight superposition of the pointer basis (the computational one). We will thus focus on the case where the initial state of the system is $|+\rangle_{\mathcal{S}} = \frac{1}{\sqrt{2}}(|0\rangle_{\mathcal{S}} + |1\rangle_{\mathcal{S}})$.

We will only consider the case of a finite environment, given that the quantum computer has a finite number of qubits.

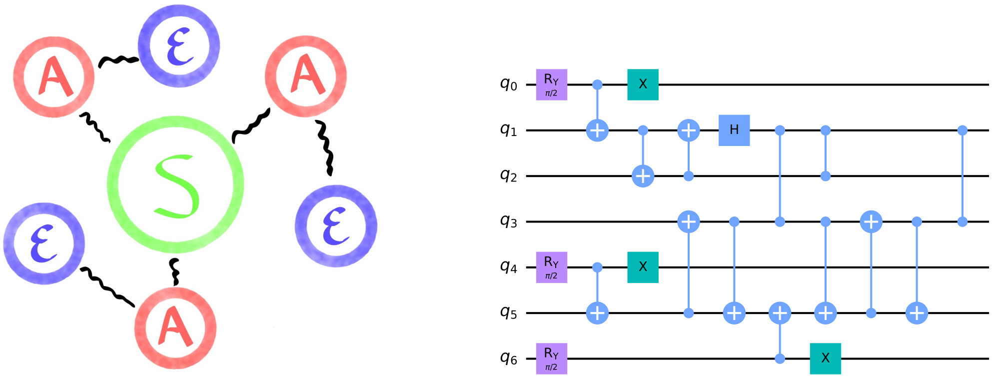

FIGURE 5.2: (a) Visual representation of the process: $\mathcal{S}$ represents the system, $\mathcal{A}$ the ancillae and $\mathcal{E}$ the emitters, the black lines represent the interaction between the different qubits. (b) Circuit representing the gate decomposition of the process: each line represents one of the qubits of the quantum computer. The ancilla-emitter states are prepared with a rotation along the Y axis followed by a CNOT and a local NOT gate. The interaction between the system and each ancilla is a Z gate on the ancilla controlled by the state of the system. The circuit uses several SWAP gates (represented by two or three consecutive CNOTs) in order to transfer the states of the qubits in the appropriate positions. At the end of the circuit, q1 is the system qubit; q2, q3 and q5 are the ancilla qubits; q0, q4 and q6 are the emitter qubits

The studied model is stochastic in nature, thus it cannot be straightforwardly simulated in a quantum computer, which only simulates unitary dynamics. This issue can be overcome by performing a purification of the global state. By introducing an appropriate super-environment as the cause behind the random collision times, one obtains a system-environment-superenvironment model whose resulting dynamics are, overall, unitary.

All the experiments presented here are performed using `ibmq_casablanca`, which is one of the IBM Quantum Falcon Processors with 7 qubits, schematically represented in fig. 5.1.

5.2 Purification

The constituents of the super-environment take the name of the emitters of the ancillae. Each ancilla is in an entangled state with its emitter, in a superposition between being un-emitted and being emitted. The weight of the superposition reflects the probability of the ancilla being emitted (and having collided) at any given time. We assume that each ancilla is emitted in the $|0\rangle_{\mathcal{A}}$ state, and once emitted it immediately collides with the system. For a single emitter-ancilla pair, the global state would then be the following:

$$\begin{aligned} |\psi(t)\rangle =& \sqrt{1-p(t)}\,|1\rangle_{\mathcal{E}}\,|0\rangle_{\mathcal{A}}\,|+\rangle_{\mathcal{S}} + \\ & i\sqrt{p(t)}\big(\cos\theta/2\,|0\rangle_{\mathcal{E}}\,|0\rangle_{\mathcal{A}}\,|+\rangle_{\mathcal{S}} - i\sin\theta/2\,|0\rangle_{\mathcal{E}}\,|1\rangle_{\mathcal{A}}\,|-\rangle_{\mathcal{S}}\big), \end{aligned} \tag{5.1}$$

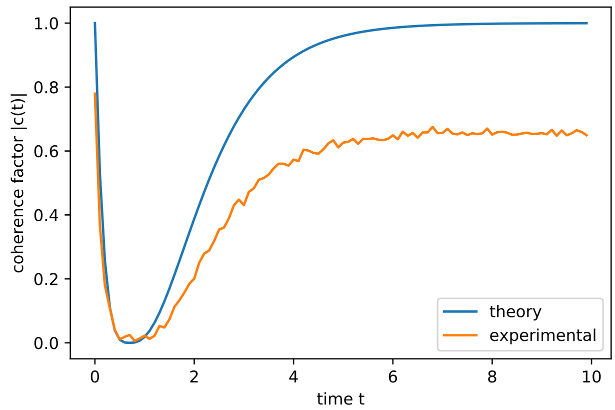

FIGURE 5.3: **coherence factor for the system as a function of time.** Results obtained in the case of three ancillae and three emitters, each represented by an individual qubit. The coherence factor is obtained by performing state tomography at each time step. In this model the non-monotonic behaviour of the coherence factor implies a non-monotonic behaviour of the trace distance between two initially distinguishable states, and can therefore be seen as a signature of non-Markovianity.

with $p(t) = 1 - e^{-\lambda t}$. The vectors $|0\rangle_{\mathcal{E}}$ and $|1\rangle_{\mathcal{E}}$ represent the ground and excited states of the emitter, respectively. Each ancilla thus requires the use of two qubits in the simulation: one for the ancilla itself and one for its emitter. We will focus on studying the case of non-entangling collisions, as it represents one of the most interesting scenarios described by the model. Moreover, the non-entangling scenario is the only one that can be simulated without system-ancilla unitaries controlled by the emitter, three-qubit gates that would make the simulation too noisy. We are thus able to simulate a stochastic collision model with three ancillae and three emitters, whose resulting circuit is shown in fig. 5.2.

At the start of the simulations all qubits are in the $|0\rangle$ state. It is then necessary to prepare the states of ancillae, emitters and system before letting them interact. The state of each ancilla-emitter pair is prepared by applying a $R_y(2\alpha)$ gate on the emitter followed by a CNOT gate on the ancilla controlled by the state of the emitter and finally a NOT gate on the emitter, this results in states of the form $\sqrt{1-p}\,|1\rangle_{\mathcal{E}}\,|0\rangle_{\mathcal{A}} + \sqrt{p}\,|0\rangle_{\mathcal{E}}\,|1\rangle_{\mathcal{A}}$. The NOT gate corresponds to the σ_x operator. The CNOT($\mathcal{C}$,$\mathcal{T}$) is a two-qubit gate that requires a control $\mathcal{C}$ and a target $\mathcal{T}$, it acts as a NOT gate on the target if the state of the control is $|1\rangle$, identity if it is $|0\rangle$, so it takes the form of $|0\rangle\langle 0|^{\mathcal{C}} \otimes \mathbb{1}^{\mathcal{T}} + |1\rangle\langle 1|^{\mathcal{C}} \otimes \sigma_x^{\mathcal{T}}$. The gate $R_y(2\alpha) = e^{-i\alpha\sigma_y/2}$ is a rotation around the Y axis of the Bloch sphere. The angle α is the parameter through which we can control the physical time and is given by $\alpha = \arccos\left(e^{-\lambda t/2}\right)$, so that the probability amplitude for the state in which the ancilla has not been emitted is $\sqrt{1-e^{-\lambda t}}$. The state of the system is prepared using a Hadamard gate, resulting in a $|+\rangle_{\mathcal{S}}$ state. The interaction between system and environment is a Z gate applied on the ancilla controlled by the state of the system, and has the form $|0\rangle\langle 0|^{\mathcal{S}} \otimes \mathbb{1}^{\mathcal{A}} + |1\rangle\langle 1|^{\mathcal{S}} \otimes \sigma_z^{\mathcal{A}}$.

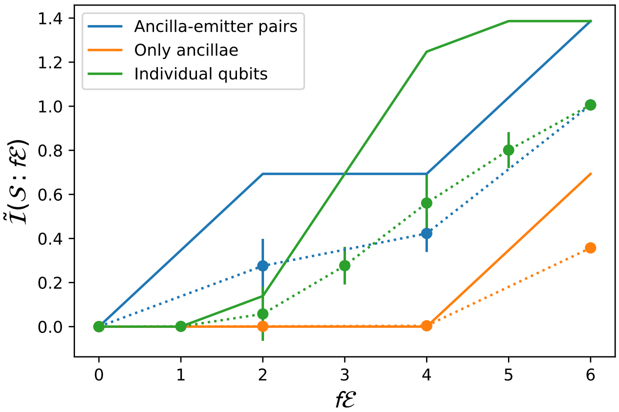

FIGURE 5.4: **Averaged mutual information between system and environmental fraction as a function of the size of the environmental fraction, for an environment of three ancilla-emitter pairs.** The dotted lines represent experimental values, while the continuous lines represent the theoretical expectations. The error bars are the standard error of the mean of the mutual information. Notice how the experimental values are consistently lower than the theoretical expectations: this is due to the decoherence the quantum computer is subject to, which erodes the mutual information between its components. In the blue line the environment is partitioned into ancilla-emitter pairs, in the orange line the emitters are traced out and only the ancillae are taken into account, in the green line the environemnt is partitioned into the individual environmental qubits. The structure of the partitioning of the environment plays an important role in the emergence of QD.

In the `ibmq_casablanca` quantum computer, it is not possible for all qubits to interact with one another and the list of possible two-qubit interactions defines the topology of the quantum computer, shown in fig. 5.1. To implement all the desired two-qubit gates it is thus necessary to use SWAP gates, in order to transfer the states of the qubits in the appropriate positions. The choice of qubit $q1$ as the system qubit is motivated as being the one that allowed us, given the specific topology of the `ibmq_casablanca` quantum computer, to minimise the overall number of SWAP gates.

The SWAP gate between two generic qubits q1 and q2 is usually obtained by applying three consecutive CNOT gates of the type CNOT(q1, q2) $\rightarrow$ CNOT(q2, q1) $\rightarrow$ CNOT(q1, q2). However, if the state of one of the two qubits is $|0\rangle$, one of the CNOTs is superfluous (an easy way to visualize this is to have the first CNOT controlled by the $|0\rangle$ qubit, which simply results in the identity gate). This helps in reducing the overall number of gates used in the circuit.

Since the SCM with a finite number of ancillae corresponds to a non-Markovian pure dephasing model, the system undergoes decoherence and recoherence, we show this by running the circuit for different values of the parameter α, corresponding to different values of the physical time. For each run of the circuit we perform state tomography of the system qubit, in order to experimentally recover the coherence

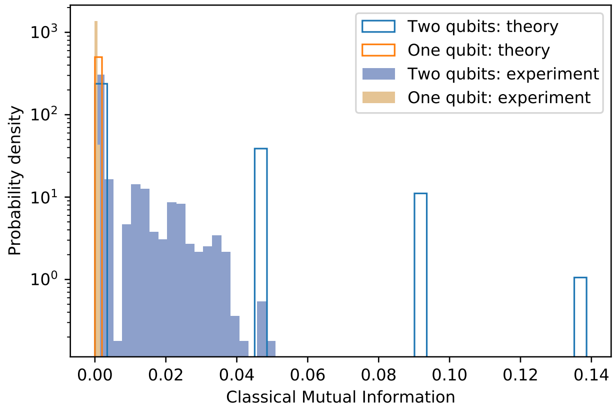

FIGURE 5.5: **Comparison of system-environment correlations between a one-qubit and a two-qubit environment.** In this histogram we represent statistical correlations (classical mutual information) between measurement outcomes of the system and a one-qubit environment (orange), and between measurements of the system and a two-qubit environment (blue). Values are always averaged between all combinations of one-qubit and two-qubit environmental fractions. Measurements are performed in all possible combination of the Pauli basis. Notice how one single qubit holds no correlations with the system: it is necessary to consider at least two qubits simultaneously to witness some correlations with the system.

factor of the system as a function of time, shown in fig. 5.3. Since this is a pure dephasing model, non-monotonicity of the coherence factor implies non-monotonicity in the trace distance between any pair of distinguishable states, and it can thus be seen as a genuine signature of non-Markovianity.

In order to witness QD, we obtain the global state by performing a full-state diluted maximum-likelihood tomographic reconstruction [125], explained in Box 1. We recover the state at the physical time $t = t_{\max}$ at which, according to the theory, the system should be in a maximally mixed state, and there should be objectivity according to QD.

From the global state it is possible to compute the QMI between the system $\mathcal{S}$ and a fraction of the environment $\mathcal{E}_f$ using the formula $\mathcal{I}(\mathcal{S} : \mathcal{E}_f) = S(\mathcal{S}) + S(\mathcal{E}_f) - S(\mathcal{S}\mathcal{E}_f)$. We stress again that in order to witness objectivity we must evaluate the averaged mutual information $\tilde{\mathcal{I}}(\mathcal{S} : \mathcal{E}_{\{})$, obtained by averaging over all environmental fractions of the same size. We show in fig. 5.4 $\tilde{\mathcal{I}}(\mathcal{S} : \mathcal{E}_f)$ as a function of the environmental size f.

The objectivity of the resulting state according to QD strongly depends on whether we treat each environmental qubit as independent, or if we consider each ancilla and its emitter together as indivisible environmental constituents. When the individual qubits are taken as the environmental fractions, the mutual information does not exhibit a plateau and objectivity does not seem to emerge. When, however, the environment is partitioned into ancilla-emitter pairs, the resulting mutual information plot is much closer to the one of an objective state. It thus seems to be necessary,

Box 1: Diluted maximum-likelihood tomography

Here we briefly outline the method used to perform the tomographic reconstruction of the global state, the used algorithm can be found in [125]. Tomography is performed by means of a POVM Π, using the measurement outcomes to reconstruct the original state.

If N is the total number of measurements, and f_i is the number of times a particular measurement outcome Π_i occurred, the logarithm of the likelihood of a particular set of outcomes $\{f_i\}$ for the state ρ is given by $\log \mathcal{L}(\rho) = \sum_i f_i \log p_i$ with $p_i = \mathrm{tr}(\Pi_i \rho)$. We can increase the likelihood of a state by iteratively applying the operator R

$$\rho^{(k+1)} = \frac{R(\rho^{(k)})\rho^{(k)}R(\rho^{(k)})}{\mathrm{tr}\left(R(\rho^{(k)})\rho^{(k)}R(\rho^{(k)})\right)}, \tag{5.2}$$

where R is defined as $R(\rho) = \frac{1}{N}\sum_i \frac{f_i}{p_i}\Pi_i$. This is justified by the fact that, if ρ_0 is a state that maximises the likelihood, then $\rho_0 = R(\rho_0)\rho_0 R(\rho_0)$. To ensure better convergence, a diluted version of R is used, by mixing it with the identity operator: $\tilde{R} = \frac{\mathbb{1}+\epsilon R}{1+\epsilon}$. We start from the maximally mixed state $\rho^{(0)} = \frac{1}{2}\left(|0\rangle\langle 0| + |1\rangle\langle 1|\right)$, iteratively applying the map $\tilde{R}$ until the log-likelihood reaches convergence.

for this model, to add an extra degree of information (the partitioning structure) to witness objectivity. Finally, by tracing out the emitters we recover the mutual information between the system and only the ancillae, where as expected the mutual information is zero unless all three ancillae are simultaneously taken into account.

Having the global state also allows us to address the following point: The non-Markovian features are present even in the absence of pairwise entanglement between the system and the environmental qubits. This is manifest not only by concurrence being zero (not shown), but also by the complete absence in statistical correlations in the measurement outcomes of the system and one environmental qubit in all the tomographic measuring bases. It is necessary to take into account at least two environmental qubits at the same time in order to witness any statistical correlations, as shown in fig. 5.5, where we show the classical mutual information between measurement outcomes of the system and one (two) environmental qubit(s) for all tomographic measurement settings. We can therefore conclude that none of the six environmental qubits has any information of the system when taken individually. It is only when taking account of them together that information about the system manifests, which means that for this model information about the system is encoded in a strictly nonlocal way.

The situation is analogous to the one considered in section 4.4, where we noticed how high levels of redundancy may compensate for the detrimental effects of nonlocality in the emergence of objectivity. In the specific case considered here however, the number of emitter-ancilla pairs is not enough to compensate for the effects of nonlocality, meaning that QD does not merge unless we consider the emitter-ancilla

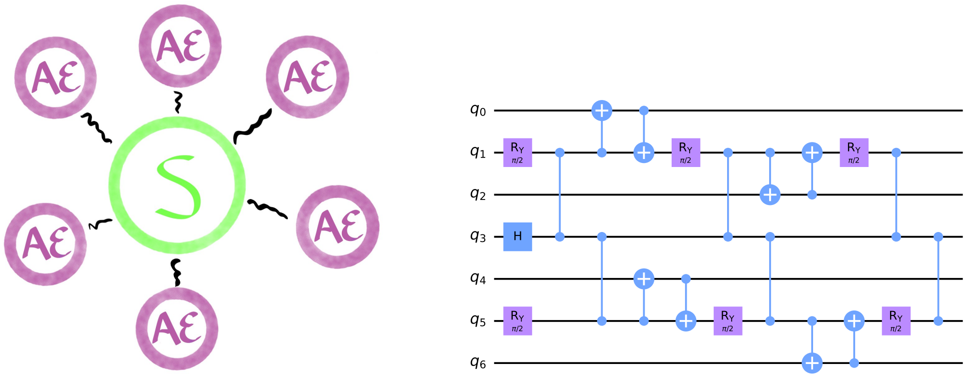

FIGURE 5.6: (a) Visual representation of the process in the condensed scenario: $\mathcal{S}$ represents the system, $\mathcal{AE}$ the condensed ancilla-emitter pairs, the black lines represent the interaction between the different qubits. (b) Circuit representing the gate decomposition of the process in the condensed scenario: each line represents one of the qubits of the quantum computer. The states of the ancilla-emitter pairs are prepared with a rotation along the Y axis. The interaction between the system and each ancilla-emitter pair is a Z gate on the pair controlled by the state of the system. The circuit uses several SWAP gates (represented by two consecutive CNOTs) in order to transfer the states of the qubits in the appropriate positions. Throughout the circuit, q3 is the system qubit, all others are the ancilla-emitter pairs.

pairs as indivisible entities.

While it may seem highly artificial that it is necessary to consider the emitters and the ancillae together in order to witness QD, this is strongly dependant on the physical scenario one has in mind. A physical system may be intrinsically partitioned with this structure, allowing a completely ignorant observer to witness objectivity. The opposite may be true as well: if the ancillae are photons emitted by some atoms, it may be physically impossible to measure the ancillae and the emitters together, let alone with the appropriate partition, so that witnessing objectivity would be impossible.

5.3 Condensation protocol

When collisions are non-entangling, $\theta = \pi$ and $\cos(\theta/2) = 0$, from eq. (5.1) we can see how the states assumed by the emitter-ancilla pair are spanned by $|1\rangle_{\mathcal{E}} |0\rangle_{\mathcal{A}}$ and $|0\rangle_{\mathcal{E}} |1\rangle_{\mathcal{A}}$. Any physical system that can live in superpositions of only two states is effectively a qubit, so it is possible to encode the information represented by the pair into a single qubit, remapping the previous states into the new $|0\rangle_{\mathcal{C}}$ and $|1\rangle_{\mathcal{C}}$ states. We will call this the *condensed* scenario.

This operation offers a great computational advantage, considering that quantum computers are still strongly limited in the number of qubits available and, more importantly, are more susceptible to decoherence the more qubits are used in the same circuit. What was previously a series of one and two qubit gates necessary

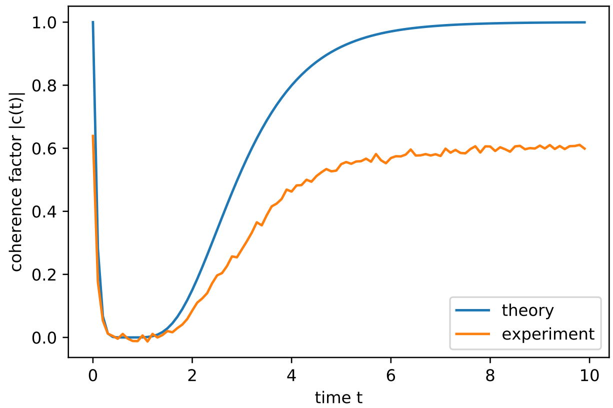

FIGURE 5.7: **Coherence factor of the system as a function of time.** Results obtained in the case of six ancilla-emitter pairs, with each pair represented by a single qubit. The coherence factor is obtained by performing state tomography at each time step. In this model the non-monotonic behaviour of the coherence factor implies a non-monotonic behaviour of the trace distance between two initially distinguishable states, and can therefore be seen as a signature of non-Markovianity.

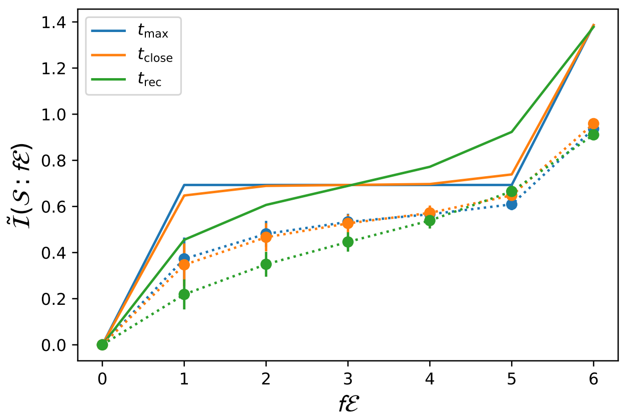

FIGURE 5.8: **Averaged mutual information between system and environmental fraction as a function of the size of the environmental fraction, for an environment of six ancilla-emitter pairs.** The dotted lines represent the experimental values, while the continuous lines represent the theoretical expectations. Notice how the experimental values are consistently lower than the theoretical expectations, this is due to the intrinsic decoherence the quantum computer is subject to, which erodes the mutual information between its components. The three different plots correspond to three different physical times: $t = t_{\rm max}$ for which the Darwinistic features should be very sharp, a time $t = t_{\rm close}$ close to $t_{\rm max}$, and a time in the "recoherence regime" $t = t_{\rm rec}$, for which the global state should have lost its Darwinistic features. The exact values are $t_{\rm max} = \ln 2$, $t_{\rm close} = \ln \frac{2}{1.3}$ and $t_{\rm rec} = \ln 6$.

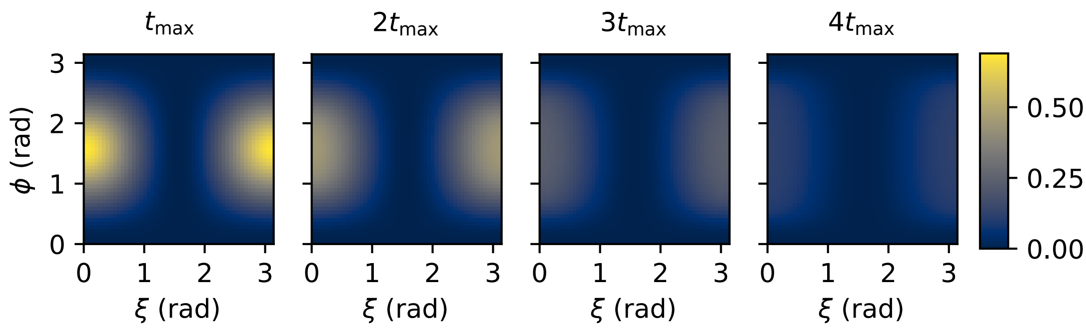

Figure 5.9: **Classical mutual information between the system and an ancilla-emitter pair recovered for all possible local measurement bases.** Results are obtained from the analytical solution of the model. ϕ and ξ define a measurement basis according to $|0'\rangle = \cos(\phi/2)|0\rangle + e^{i\xi}\sin(\phi/2)|1\rangle$ and $|1'\rangle = \sin(\phi/2)|0\rangle - e^{i\xi}\cos(\phi/2)|1\rangle$. The peaks correspond to measuring the ancilla-emitter pair in the $\{|+\rangle, |-\rangle\}$ base. The physical times are, from left to right, $t = t_{max}$, $t = 2t_{max}$, $t = 3t_{max}$, $t = 4t_{max}$, with $t_{max} = \ln 2$. The further we are from t_{max} the less is the obtainable CMI.

to prepare the state of an ancilla-emitter pair is now just a single qubit gate in the condensed scenario. More specifically, the state of each ancilla-emitter pair is prepared using a $R_y(2\alpha)$ gate, where the angle α has the same meaning as in the previous case. The interaction between system and environment is once again a Z gate applied on the condensed pair controlled by the state of the system. In this case the number of SWAP gates is minimised by choosing qubit $q3$ as the system. The circuit corresponding to the model is shown in fig. 5.6.

This way, using the same quantum computer we are able to simulate six environmental emitter-ancilla pairs.

We once again run the circuit for different values of the parameter α corresponding to different values of the physical time and perform state tomography of the system qubit for each run of the circuit. Figure 5.7 shows the coherence factor of the system as a function of time, and also in this case there is a clear non-Markovian behaviour.

We recover the global state though tomographic reconstruction for three different values of the physical time. In fig. 5.8 we show the averaged mutual information $\tilde{\mathcal{I}}(\mathcal{S} : \mathcal{E}_f)$ as a function of the environmental size f for different values of the physical times. The chosen times are: $t = t_{max}$ for which the Darwinistic features should be very sharp, a time $t = t_{close}$ close to t_{max}, and a time in the "recoherence regime" $t = t_{rec}$, for which a significant amount of information has already flown back to the system and the global state should have lost its Darwinistic features. The exact values are $t_{max} = \ln 2$, $t_{close} = \ln \frac{2}{1.3}$ and $t_{rec} = \ln 6$.

We can clearly see the presence of a "objectivity" plateau, even if lower than the theoretical expectations. Nonetheless, one of the key features of quantum Darwinism (redundancy) is reproduced, which allows us to say that, while the emergence of QD is less manifest compared to the theoretical expectations, there is a state structure clearly reminiscent of QD.

5.4 Accessible classical information

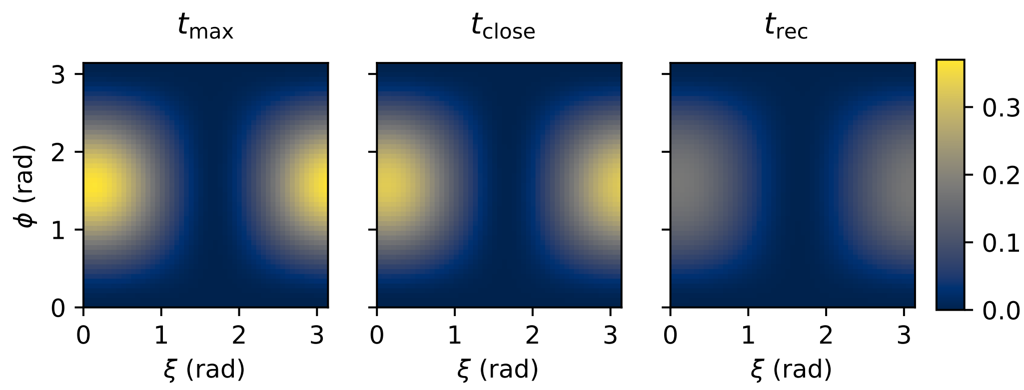

FIGURE 5.10: **Classical mutual information between the system and an ancilla-emitter pair recovered for all possible local measurement bases.** Results are obtained from the tomographically reconstructed states. ϕ and ξ define a measurement base according to $|0'\rangle = \cos(\phi/2)|0\rangle + e^{i\xi}\sin(\phi/2)|1\rangle$ and $|1'\rangle = \sin(\phi/2)|0\rangle - e^{i\xi}\cos(\phi/2)|1\rangle$. The peaks correspond to measuring the ancilla-emitter pair in the $\{|+\rangle, |-\rangle\}$ base. The leftmost figure corresponds to $t = t_{max}$, the central to $t = t_{close}$ and the one on the right is for $t = t_{rec}$. Values are $t_{max} = \ln 2$, $t_{close} = \ln \frac{2}{1.3}$ and $t_{rec} = \ln 6$.

While quantum Darwinism is concerned with the necessary conditions to achieve system objectivity, it is worth asking how much information can actually be inferred on the system by observers making measurements of the environment.

As we are interested in assessing the information accessible through possible measurements on the environment, we evaluate the classical mutual information (CMI) between the system and the environment. Measurements on the system are always performed in the pointer basis, which happens to be the computational one for this particular model. We aim at finding the environmental measurement basis maximising the CMI between the system and one ancilla-emitter pair. The measurement basis maximising the CMI between the system and two or more ancilla-emitter pairs may also be different, but here we want to maximise what an observer can infer from just one pair. We will also restrict ourselves to the case of projective measurements.

In fig. 5.9 we show the CMI between system and one ancilla-emitter pair for all possible one qubit measurement bases, calculated using the analytical solution of the model. On the horizontal and vertical axis there are two angles ϕ and ξ that uniquely define a single qubit basis defined as $|0'\rangle = \cos(\phi/2)|0\rangle + e^{i\xi}\sin(\phi/2)|1\rangle$ and $|1'\rangle = \sin(\phi/2)|0\rangle - e^{i\xi}\cos(\phi/2)|1\rangle$.

In fig. 5.10 we show the same quantity by using the experimental states reconstructed using tomography. Both figures show that the classical mutual information is maximised by measuring the environmental qubits in the $\{|+\rangle, |-\rangle\}$ basis.

Finally, by imposing that all ancilla-emitter pair are measured in the same $\{|+\rangle, |-\rangle\}$ basis, we compute the CMI between the system and an environmental fraction as a

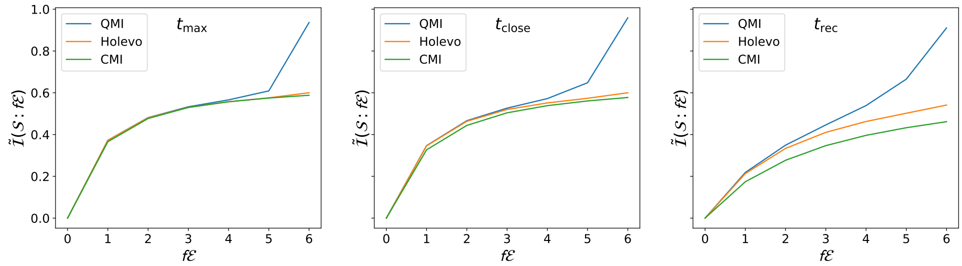

FIGURE 5.11: **Comparison between quantum mutual information, classical mutual information and Holevo bound for the three tomographically reconstructed states.** While the three quantities have the same values for t_{max}, there are discrepancies for the other physical times, in particular, CMI is consistently lower than the Holevo bound, which is in turn consistently lower than the QMI. The leftmost figure corresponds to $t = t_{\text{max}}$, the central to $t = t_{\text{close}}$ and the one on the right is for $t = t_{\text{rec}}$. Values are $t_{\text{max}} = \ln 2$, $t_{\text{close}} = \ln \frac{2}{1.3}$ and $t_{\text{rec}} = \ln 6$.

function of the environmental size. We show in fig. 5.11 a comparison between the QMI, the Holevo χ and the maximised CMI. The Holevo χ is computed by projecting the system in the computational basis, so that it acts as an upper bound of the CMI. We can see that, when $t = t_{\text{max}}$ and $t = t_{\text{close}}$, the CMI can be used as a signature of objectivity. It is also interesting to notice that while the Holevo χ and the maximised CMI are almost the same at $t = t_{\text{max}}$ and $t = t_{\text{close}}$, they are instead numerically different at $t = t_{\text{rec}}$, meaning that when the state is far from being objective, it is not possible to saturate the bound of the Holevo χ through local projective measurements alone.

5.5 Conclusions

In this chapter we have witnessed objectivity in the framework of quantum Darwinism, for a stochastic collision model, using a quantum computer as the experimental platform; which paves the way for future applications of quantum computers to foundational problems such as the definition of objectivity and the quantum-to-classical transition.

Our results show that, with the appropriate simulation techniques, current NISQ devices are capable of reproducing states with objective features. The quantum computer is subject to uncontrolled decoherence due to its own surrounding environment (with an irreversible loss of quantum information) that, along with the crosstalk between qubits hinders the emergence of objectivity. Nonetheless it is reasonable to assume, given the rapid technological advance of the field, that it will soon be possible to produce with high fidelity states that cannot be currently modeled with classical resources alone. However, it is important to point out that the results presented here require to perform the full tomographic reconstruction of the global state. Regardless of the level of technological advancements, full tomography is an expensive task that scales exponentially with the size of the system, and represent the biggest bottleneck in terms of experimental realization of large objective states. This motivates the search for appropriate and efficient witnesses of objectivity, an interesting future direction in the field of quantum objectivity.

Outlook

In this work we have discussed several aspects concerning the objective features of quantum states. We started by introducing the main frameworks used in the context of quantum objectivity, namely quantum Darwinism and spectrum broadcast structure. These frameworks are now well established, but many open questions still remain in the context of quantum objectivity. Indeed, much of the research undertaken in this context makes use of assumptions that effectively correspond to considering ideal scenarios, and several effects that could potentially hinder the emergence of objectivity are often overlooked.

We believe that one of the most promising directions in the field of quantum objectivity is to study cases where non-ideal scenarios are taken into account, or where some of the assumptions that are usually made in this context are relaxed. This would allow to appreciate subtleties that do not arise in simpler cases. As a matter of fact, we have seen that the distinction between redundancy and consensus emerges when nonlocal or asymmetric information encodings are taken into account.

Studying the conditions for objectivity to emerge is considered as a promising strategy to tackle the quantum-to-classical transition, usually intended as the transition from a purely quantum system, to a fully classical one. In this sense, the quantum-to-classical transition can be seen as dynamical process. Measures of quantum objectivity however are only concerned with the properties of a given state, with little concern over the underlying process through which that state was generated. This allows to consider quantum objectivity and the quantum-to-classical transition as two separate, if connected, research topics, and opens the possibility for novel research directions. In particular, this would allow to explore the distinction between a measurement process and one that generates objective states, since it is possible for a system -initially in a pure state- to become objective while no information about the initial state is encoded into the environment.

On the other hand, studying which dynamics generate objective states is a more popular but still relevant research area. In particular, not much is known regarding the connections between properties of the open system dynamics and the objectivity of the resulting states. This further justifies the need to explore the phenomenology of the processes though which systems become objective. Our characterisation of the objective features emerging form stochastic collision models, that allowed us to show the connection -under appropriate assumptions- between entanglement production and objectivity, goes precisely in this direction.

Characterising the phenomenology of quantum objectivity would also benefit from experimental investigation of objective states, with our work on simulating objective states on superconducting quantum processors giving promising results towards the usefulness of such platforms for these tasks. Regardless, experimental witnesses of objectivity still face many challenges, whose solutions constitute interesting future research directions.

Acknowledgements

Il primo ringraziamento di questa tesi va a Massimo Palma, senz'altro per il ruolo svolto in quanto supervisor di dottorato, ma anche per per lo spaccio di caffè filtro arabica e per le importanti lezioni sul commissario Maigret e i programmi radio della BBC. Un ringraziamento va ai membri del gruppo quantum di Unipa (presenti e passati): Francesco Ciccarello, Salvatore Lorenzo, Angelo Carollo, Umberto de Giovannini, Claudio Pellitteri, Federico Roccati, Luca Leonforte e Marcel Pinto.

Delle persone che condividevano con me i corridoi del dipartimento di fisica, un ringraziamento speciale va a Dario Cilluffo, Luca Innocenti e Alessia Castellini. A Dario, probabilmente la singola persona con cui mi sono lamentata in assoluto di più durante il mio dottorato, per avermi sempre saputo ascoltare e offrire il suo supporto e consiglio, ma sopratutto per non avermi mai detto che mi stavo lamentando troppo. A Luca per essere arrivato nel luogo giusto al momento giusto, per essersi rivelato uno splendido collaboratore e un ottimo amico. Ad Alessia per essere stata, seppur inconsapevolmetne, una figura di riferimento che mi è stata di grande ispirazione. Vederti spledere nei miei momenti più bui è stato come avere un faro nella tempesta.

I also wish to thank all the people at QteQ (and friends, you're included too Luke) for their amazing hospitality during my (alas short) stay there. I had a great time with you all and I can't wait to keep working and slacking off with you.

Un ringraziamento a tutti i miei amici, sia quelli di lunga data ma anche a chi era solo di passaggio, che mi hanno saputo dare il loro supporto durante i momenti difficili, e con cui ho condiviso i momenti felici. Billo per sopportare il mio amore per l'hyperpop, Cisca per non essersi mai arresa con me, Elena per tutto il tempo passato ad aspettarmi sotto casa, Louka per avermi ricorato che ci sono cose belle nel mondo, Marta per gli occhi dei pesci, Laura per le imprecazioni contro la vita e il mondo. Ma anche Giulia Lag, Martina, Sueli, Davide, Pietri, Giulia Cici, Francesca. Scrivere una frase per ognuno di voi era troppo faticoso, ma ci tenevo a citare anche voi.

Bibliography

[1] Heinz-Peter Breuer and Francesco Petruccione. *The Theory of Open Quantum Systems.* Oxford University Press, Oxford, 2007.

[2] Angel Rivas and Susana F Huelga. *Open quantum systems*, volume 10. Springer, 2012.

[3] Maximilian Schlosshauer. Decoherence, the measurement problem, and interpretations of quantum mechanics. *Reviews of Modern Physics*, 76(4):1267–1305, February 2005.

[4] Wojciech Hubert Zurek. Decoherence, einselection, and the quantum origins of the classical. *Reviews of Modern Physics*, 75(3):715–775, May 2003.

[5] Harold Ollivier, David Poulin, and Wojciech H. Zurek. Objective Properties from Subjective Quantum States: Environment as a Witness. *Physical Review Letters*, 93(22):220401, November 2004.

[6] Mario A. Ciampini, Giorgia Pinna, Paolo Mataloni, and Mauro Paternostro. Experimental signature of quantum Darwinism in photonic cluster states. *Physical Review A*, 98(2):020101, August 2018.

[7] Ming-Cheng Chen, Han-Sen Zhong, Yuan Li, Dian Wu, Xi-Lin Wang, Li Li, Nai-Le Liu, Chao-Yang Lu, and Jian-Wei Pan. Emergence of classical objectivity of quantum Darwinism in a photonic quantum simulator. *Science Bulletin*, 64(9):580–585, May 2019.

[8] T. K. Unden, D. Louzon, M. Zwolak, W.H. Zurek, and F. Jelezko. Revealing the Emergence of Classicality Using Nitrogen-Vacancy Centers. *Physical Review Letters*, 123(14):140402, October 2019.

[9] Diana A. Chisholm, Guillermo García-Pérez, Matteo A. C. Rossi, Sabrina Maniscalco, and G. Massimo Palma. Witnessing objectivity on a quantum computer. *Quantum Science and Technology*, 7(1):015022, December 2021.

[10] Michael A Nielsen and Isaac Chuang. Quantum computation and quantum information, 2002.

[11] John Preskill. Quantum shannon theory. *arXiv preprint arXiv:1604.07450*, 2016.

[12] Crispin W Gardiner et al. *Handbook of stochastic methods*, volume 3.

[13] Sonja Daffer, Krzysztof Wódkiewicz, James D Cresser, and John K McIver. Depolarizing channel as a completely positive map with memory. *Physical Review A*, 70(1):010304, 2004.

[14] Heinz-Peter Breuer and Bassano Vacchini. Quantum semi-markov processes. *Physical review letters*, 101(14):140402, 2008.

[15] Dariusz Chruściński, Andrzej Kossakowski, and Saverio Pascazio. Long-time memory in non-markovian evolutions. *Physical Review A*, 81(3):032101, 2010.

[16] Ángel Rivas, Susana F Huelga, and Martin B Plenio. Quantum non-markovianity: characterization, quantification and detection. *Reports on Progress in Physics*, 77(9):094001, 2014.

[17] Mary Beth Ruskai. Beyond strong subadditivity? improved bounds on the contraction of generalized relative entropy. *Reviews in Mathematical Physics*, 6(05a):1147–1161, 1994.

[18] Heinz-Peter Breuer, Elsi-Mari Laine, and Jyrki Piilo. Measure for the degree of non-markovian behavior of quantum processes in open systems. *Phys. Rev. Lett.*, 103:210401, Nov 2009.

[19] Jayaseetha Rau. Relaxation phenomena in spin and harmonic oscillator systems. *Physical Review*, 129(4):1880, 1963.

[20] M. Ziman, P. Štelmachovič, V. Bužek, M. Hillery, V. Scarani, and N. Gisin. Diluting quantum information: An analysis of information transfer in system-reservoir interactions. *Phys. Rev. A*, 65:042105, Mar 2002.

[21] Francesco Ciccarello. Collision models in quantum optics. *Quantum Measurements and Quantum Metrology*, 4(1):53–63, 2017.

[22] Francesco Ciccarello, Salvatore Lorenzo, Vittorio Giovannetti, and G. Massimo Palma. Quantum collision models: Open system dynamics from repeated interactions. *Physics Reports*, 954:1–70, 2022. Quantum collision models: Open system dynamics from repeated interactions.

[23] Dario Cilluffo, Angelo Carollo, Salvatore Lorenzo, Jonathan A. Gross, G. Massimo Palma, and Francesco Ciccarello. Collisional picture of quantum optics with giant emitters. *Phys. Rev. Research*, 2:043070, Oct 2020.

[24] S. Lorenzo, R. McCloskey, F. Ciccarello, M. Paternostro, and G. M. Palma. Landauer's principle in multipartite open quantum system dynamics. *Phys. Rev. Lett.*, 115:120403, Sep 2015.

[25] Gabriele De Chiara, Gabriel Landi, Adam Hewgill, Brendan Reid, Alessandro Ferraro, Augusto J Roncaglia, and Mauro Antezza. Reconciliation of quantum local master equations with thermodynamics. *New Journal of Physics*, 20(11):113024, nov 2018.

[26] Salvatore Lorenzo, Francesco Ciccarello, and G. Massimo Palma. Class of exact memory-kernel master equations. *Phys. Rev. A*, 93:052111, May 2016.

[27] F. Ciccarello, G. M. Palma, and V. Giovannetti. Collision-model-based approach to non-markovian quantum dynamics. *Phys. Rev. A*, 87:040103, Apr 2013.

[28] V. Giovannetti and G. M. Palma. Master equations for correlated quantum channels. *Phys. Rev. Lett.*, 108:040401, Jan 2012.

[29] Arne L. Grimsmo. Time-delayed quantum feedback control. *Phys. Rev. Lett.*, 115:060402, Aug 2015.

[30] Steve Campbell, Francesco Ciccarello, G. Massimo Palma, and Bassano Vacchini. System-environment correlations and markovian embedding of quantum non-markovian dynamics. *Phys. Rev. A*, 98:012142, Jul 2018.

[31] V. Vedral. The role of relative entropy in quantum information theory. *Rev. Mod. Phys.*, 74:197–234, Mar 2002.

[32] Alexander Semenovich Holevo. Bounds for the quantity of information transmitted by a quantum communication channel. *Problemy Peredachi Informatsii*, 9(3):3–11, 1973.

[33] Harold Ollivier and Wojciech H. Zurek. Quantum Discord: A Measure of the Quantumness of Correlations. *Physical Review Letters*, 88(1):017901, December 2001.

[34] Leah Henderson and Vlatko Vedral. Classical, quantum and total correlations. *Journal of physics A: mathematical and general*, 34(35):6899, 2001.

[35] Marco Piani, Paweł Horodecki, and Ryszard Horodecki. No-local-broadcasting theorem for multipartite quantum correlations. *Phys. Rev. Lett.*, 100:090502, Mar 2008.

[36] Harold Ollivier, David Poulin, and Wojciech H. Zurek. Environment as a witness: Selective proliferation of information and emergence of objectivity in a quantum universe. *Phys. Rev. A*, 72:042113, Oct 2005.

[37] Wojciech H Zurek. From quantum to classical. *Phys Today*, 37.

[38] Johannes Kofler and Časlav Brukner. Classical world arising out of quantum physics under the restriction of coarse-grained measurements. *Physical Review Letters*, 99(18):180403, 2007.

[39] Eugene P Wigner. The problem of measurement. *American Journal of Physics*, 31(1):6–15, 1963.

[40] Arthur Fine. Insolubility of the quantum measurement problem. *Physical Review D*, 2(12):2783, 1970.

[41] Maximilian Schlosshauer. Quantum decoherence. *Physics Reports*, 831:1–57, 2019.

[42] Robin Blume-Kohout and Wojciech H. Zurek. Quantum Darwinism: Entanglement, branches, and the emergent classicality of redundantly stored quantum information. *Physical Review A*, 73(6):062310, June 2006.

[43] Wojciech Hubert Zurek. Quantum Darwinism. *Nature Physics*, 5(3):181–188, March 2009.

[44] R. Horodecki, J. K. Korbicz, and P. Horodecki. Quantum origins of objectivity. *Physical Review A*, 91(3):032122, March 2015.

[45] Michel Brune, E Hagley, J Dreyer, X Maitre, Abdelhamid Maali, Ch Wunderlich, JM Raimond, and S Haroche. Observing the progressive decoherence of the "meter" in a quantum measurement. *Physical Review Letters*, 77(24):4887, 1996.

[46] Wojciech H Zurek. Pointer basis of quantum apparatus: Into what mixture does the wave packet collapse? *Physical review D*, 24(6):1516, 1981.

[47] DGBJ Dieks. Communication by epr devices. *Physics Letters A*, 92(6):271–272, 1982.

[48] William K Wootters and Wojciech H Zurek. A single quantum cannot be cloned. *Nature*, 299(5886):802–803, 1982.

[49] Alexia Auffèves and Philippe Grangier. Contexts, systems and modalities: a new ontology for quantum mechanics. *Foundations of Physics*, 46(2):121–137, 2016.

[50] Michael Zwolak, HT Quan, and Wojciech H Zurek. Redundant imprinting of information in nonideal environments: Objective reality via a noisy channel. *Physical Review A*, 81(6):062110, 2010.

[51] Nadia Milazzo, Salvatore Lorenzo, Mauro Paternostro, and G. Massimo Palma. Role of information backflow in the emergence of quantum Darwinism. *Physical Review A*, 100(1):012101, July 2019.

[52] Nicolás Mirkin and Diego A. Wisniacki. Many-Body Localization and the Emergence of Quantum Darwinism. *Entropy*, 23(11):1377, November 2021.

[53] Robin Blume-Kohout and Wojciech H. Zurek. A Simple Example of "Quantum Darwinism": Redundant Information Storage in Many-Spin Environments. *Foundations of Physics*, 35(11):1857–1876, November 2005.

[54] P. Mironowicz, J.K. Korbicz, and P. Horodecki. Monitoring of the Process of System Information Broadcasting in Time. *Physical Review Letters*, 118(15):150501, April 2017.

[55] Thao P. Le and Alexandra Olaya-Castro. Strong Quantum Darwinism and Strong Independence are Equivalent to Spectrum Broadcast Structure. *Physical Review Letters*, 122(1):010403, January 2019.

[56] JK Korbicz, Paweł Horodecki, and Ryszard Horodecki. Objectivity in a noisy photonic environment through quantum state information broadcasting. *Physical review letters*, 112(12):120402, 2014.

[57] Thao P. Le, Piotr Mironowicz, and Paweł Horodecki. Blurred quantum Darwinism across quantum reference frames. *Physical Review A*, 102(6):062420, December 2020.

[58] Thao P. Le and Alexandra Olaya-Castro. Objectivity (or lack thereof): Comparison between predictions of quantum Darwinism and spectrum broadcast structure. *Physical Review A*, 98(3):032103, September 2018.

[59] Thao P. Le and Alexandra Olaya-Castro. Witnessing non-objectivity in the framework of strong quantum Darwinism. *Quantum Science and Technology*, 5(4):045012, August 2020.

[60] Guillermo García-Pérez, Diana A. Chisholm, Matteo A. C. Rossi, G. Massimo Palma, and Sabrina Maniscalco. Decoherence without entanglement and quantum Darwinism. *Physical Review Research*, 2(1):012061, March 2020.

[61] Diana A Chisholm, Guillermo García-Pérez, Matteo A C Rossi, G Massimo Palma, and Sabrina Maniscalco. Stochastic collision model approach to transport phenomena in quantum networks. *New Journal of Physics*, 23(3):033031, mar 2021.

[62] Bassano Vacchini. General structure of quantum collisional models. *International Journal of Quantum Information*, 12(02):1461011, 2014.

[63] Goran Lindblad. On the generators of quantum dynamical semigroups. *Communications in Mathematical Physics*, 48(2):119–130, 1976.

[64] Vittorio Gorini, Andrzej Kossakowski, and Ennackal Chandy George Sudarshan. Completely positive dynamical semigroups of n-level systems. *Journal of Mathematical Physics*, 17(5):821–825, 1976.

[65] Ruari McCloskey and Mauro Paternostro. Non-markovianity and system-environment correlations in a microscopic collision model. *Phys. Rev. A*, 89:052120, May 2014.

[66] Fernando Galve, Roberta Zambrini, and Sabrina Maniscalco. Non-markovianity hinders quantum darwinism. *Scientific reports*, 6(1):19607, 2016.

[67] Graeme Pleasance and Barry M Garraway. Application of quantum darwinism to a structured environment. *Physical Review A*, 96(6):062105, 2017.

[68] Aniello Lampo, Jan Tuziemski, Maciej Lewenstein, and Jarosław K Korbicz. Objectivity in the non-markovian spin-boson model. *Physical Review A*, 96(1):012120, 2017.

[69] SM Oliveira, AL de Paula Jr, and RC Drumond. Quantum darwinism and non-markovianity in a model of quantum harmonic oscillators. *Physical Review A*, 100(5):052110, 2019.

[70] Stella Seah, Stefan Nimmrichter, and Valerio Scarani. Nonequilibrium dynamics with finite-time repeated interactions. *Phys. Rev. E*, 99:042103, Apr 2019.

[71] Eoin O'Connor, Bassano Vacchini, and Steve Campbell. Stochastic collisional quantum thermometry. *Entropy*, 23(12), 2021.

[72] Jonathan A Gross, Carlton M Caves, Gerard J Milburn, and Joshua Combes. Qubit models of weak continuous measurements: markovian conditional and open-system dynamics. *Quantum Science and Technology*, 3(2):024005, feb 2018.

[73] Frank Verstraete, Michael M. Wolf, and J. Ignacio Cirac. Quantum computation and quantum-state engineering driven by dissipation. *Nature Physics*, 5(9):633–636, Sep 2009.

[74] Patrick Rebentrost, Masoud Mohseni, Ivan Kassal, Seth Lloyd, and Alán Aspuru-Guzik. Environment-assisted quantum transport. *New Journal of Physics*, 11(3):033003, mar 2009.

[75] Filippo Caruso, Alex W Chin, Animesh Datta, Susana F Huelga, and Martin B Plenio. Highly efficient energy excitation transfer in light-harvesting complexes: The fundamental role of noise-assisted transport. *The Journal of Chemical Physics*, 131(10):09B612, 2009.

[76] A W Chin, A Datta, F Caruso, S F Huelga, and M B Plenio. Noise-assisted energy transfer in quantum networks and light-harvesting complexes. *New Journal of Physics*, 12(6):065002, jun 2010.

[77] Chikako Uchiyama, William J. Munro, and Kae Nemoto. Environmental engineering for quantum energy transport. *npj Quantum Information*, 4(1):33, Jul 2018.

[78] Jianshu Cao, Richard J. Cogdell, David F. Coker, Hong-Guang Duan, Jürgen Hauer, Ulrich Kleinekathöfer, Thomas L. C. Jansen, Tomáš Mančal,

R. J. Dwayne Miller, Jennifer P. Ogilvie, Valentyn I. Prokhorenko, Thomas Renger, Howe-Siang Tan, Roel Tempelaar, Michael Thorwart, Erling Thyrhaug, Sebastian Westenhoff, and Donatas Zigmantas. Quantum biology revisited. *Science Advances*, 6(14):eaaz4888, 2020.

[79] R. E. Fenna and B. W. Matthews. Chlorophyll arrangement in a bacteriochlorophyll protein from chlorobium limicola. *Nature*, 258(5536):573–577, Dec 1975.

[80] R.E. Fenna, L.F.Ten Eyck, and B.W. Matthews. Atomic coordinates for the chlorophyll core of a bacteriochlorophyll a-protein from green photosynthetic bacteria. *Biochemical and Biophysical Research Communications*, 75(3):751–756, 1977.

[81] Shinji Saito, Masahiro Higashi, and Graham R. Fleming. Site-dependent fluctuations optimize electronic energy transfer in the fenna–matthews–olson protein. *The Journal of Physical Chemistry B*, 123(46):9762–9772, Nov 2019.

[82] Nikos Yannaros. Weibull renewal processes. *Annals of the Institute of Statistical Mathematics*, 46(4):641–648, Dec 1994.

[83] Bassano Vacchini. Quantum renewal processes. *Scientific reports*, 10(1):1–13, 2020.

[84] Salvatore Lorenzo, Francesco Ciccarello, G Massimo Palma, and Bassano Vacchini. Quantum non-markovian piecewise dynamics from collision models. *Open Systems & Information Dynamics*, 24(04):1740011, 2017.

[85] Katarzyna Siudzińska and Dariusz Chruściński. Memory kernel approach to generalized pauli channels: Markovian, semi-markov, and beyond. *Physical Review A*, 96(2):022129, 2017.

[86] Oliver Mülken and Alexander Blumen. Continuous-time quantum walks: Models for coherent transport on complex networks. *Physics Reports*, 502(2-3):37–87, 2011.

[87] Gregory S Engel, Tessa R Calhoun, Elizabeth L Read, Tae-Kyu Ahn, Tomáš Mančal, Yuan-Chung Cheng, Robert E Blankenship, and Graham R Fleming. Evidence for wavelike energy transfer through quantum coherence in photosynthetic systems. *Nature*, 446(7137):782–786, 2007.

[88] Stephan Hoyer, Mohan Sarovar, and K Birgitta Whaley. Limits of quantum speedup in photosynthetic light harvesting. *New Journal of Physics*, 12(6):065041, 2010.

[89] Saverio Pascazio. All you ever wanted to know about the quantum zeno effect in 70 minutes. *Open Systems & Information Dynamics*, 21(01n02):1440007, 2014.

[90] AI Shushin. The effect of measurements, randomly distributed in time, on quantum systems: stochastic quantum zeno effect. *Journal of Physics A: Mathematical and Theoretical*, 44(5):055303, 2011.

[91] Stefano Gherardini, Shamik Gupta, Francesco Saverio Cataliotti, Augusto Smerzi, Filippo Caruso, and Stefano Ruffo. Stochastic quantum zeno by large deviation theory. *New Journal of Physics*, 18(1):013048, 2016.

[92] Sergey Belan and Vladimir Parfenyev. Optimality and universality in quantum zeno dynamics. *New Journal of Physics*, 22(7):073065, 2020.

[93] Seogjoo J Jang and Benedetta Mennucci. Delocalized excitons in natural light-harvesting complexes. *Reviews of Modern Physics*, 90(3):035003, 2018.

[94] Filippo Caruso, Alex W Chin, Animesh Datta, Susana F Huelga, and Martin B Plenio. Entanglement and entangling power of the dynamics in light-harvesting complexes. *Physical Review A*, 81(6):062346, 2010.

[95] Martin B Plenio and Susana F Huelga. Dephasing-assisted transport: quantum networks and biomolecules. *New Journal of Physics*, 10(11):113019, 2008.

[96] Marcel Schmidt am Busch, Frank Muh, Mohamed El-Amine Madjet, and Thomas Renger. The eighth bacteriochlorophyll completes the excitation energy funnel in the fmo protein. *The journal of physical chemistry letters*, 2(2):93–98, 2011.

[97] Dale E Tronrud, Jianzhong Wen, Leslie Gay, and Robert E Blankenship. The structural basis for the difference in absorbance spectra for the fmo antenna protein from various green sulfur bacteria. *Photosynthesis research*, 100(2):79–87, 2009.

[98] Jeremy Moix, Jianlan Wu, Pengfei Huo, David Coker, and Jianshu Cao. Efficient energy transfer in light-harvesting systems, iii: The influence of the eighth bacteriochlorophyll on the dynamics and efficiency in fmo. *The Journal of Physical Chemistry Letters*, 2(24):3045–3052, 2011.

[99] Jianlan Wu, Fan Liu, Jian Ma, Robert J Silbey, and Jianshu Cao. Efficient energy transfer in light-harvesting systems: Quantum-classical comparison, flux network, and robustness analysis. *The Journal of chemical physics*, 137(17):174111, 2012.

[100] David M Wilkins and Nikesh S Dattani. Why quantum coherence is not important in the fenna–matthews–olsen complex. *Journal of chemical theory and computation*, 11(7):3411–3419, 2015.

[101] David E Golberg. Genetic algorithms in search, optimization, and machine learning. *Addion wesley*, 1989(102):36, 1989.

[102] Mauro Faccin, Piotr Migdał, Tomi H Johnson, Ville Bergholm, and Jacob D Biamonte. Community detection in quantum complex networks. *Physical Review X*, 4(4):041012, 2014.

[103] Diana A. Chisholm, Luca Innocenti, and G. Massimo Palma. Nonlocality breaks the relations between measures of quantum objectivity. *arXiv preprint arXiv:2211.09150*, 2022.

[104] Diana A. Chisholm, Luca Innocenti, and G. Massimo Palma. *Manuscript in preparation*, 2022.

[105] Eoghan Ryan, Mauro Paternostro, and Steve Campbell. Quantum darwinism in a structured spin environment. *Physics Letters A*, 416:127675, 2021.

[106] Gian Luca Giorgi, Fernando Galve, and Roberta Zambrini. Quantum Darwinism and non-Markovian dissipative dynamics from quantum phases of the spin-1/2 XX model. *Physical Review A*, 92(2):022105, August 2015.

[107] Thao P. Le, Andreas Winter, and Gerardo Adesso. Thermality versus Objectivity: Can They Peacefully Coexist? *Entropy*, 23(11):1506, November 2021.

[108] J. K. Korbicz. Roads to objectivity: Quantum Darwinism, Spectrum Broadcast Structures, and Strong quantum Darwinism – a review. *Quantum*, 5:571, November 2021.

[109] Howard M. Wiseman. Quantum discord is Bohr's notion of non-mechanical disturbance introduced to counter the Einstein–Podolsky–Rosen argument. *Annals of Physics*, 338:361–374, November 2013.

[110] Scott N. Walck and David W. Lyons. Only n-Qubit Greenberger-Horne-Zeilinger States Are Undetermined by Their Reduced Density Matrices. *Physical Review Letters*, 100(5):050501, February 2008.

[111] Scott N. Walck and David W. Lyons. Only n-qubit Greenberger-Horne-Zeilinger states contain n-partite information. *Physical Review A*, 79(3):032326, March 2009.

[112] W. Dür, G. Vidal, and J. I. Cirac. Three qubits can be entangled in two inequivalent ways. *Phys. Rev. A*, 62:062314, Nov 2000.

[113] Salvatore Lorenzo, Mauro Paternostro, and G. Massimo Palma. Anti-zeno-based dynamical control of the unfolding of quantum darwinism. *Physical Review Research*, 2(1):013164, February 2020.

[114] Nina Megier, Andrea Smirne, Steve Campbell, and Bassano Vacchini. Correlations, Information Backflow, and Objectivity in a Class of Pure Dephasing Models. *Entropy*, 24(2):304, February 2022.

[115] Akram Touil, Bin Yan, Davide Girolami, Sebastian Deffner, and Wojciech Hubert Zurek. Eavesdropping on the Decohering Environment: Quantum Darwinism, Amplification, and the Origin of Objective Classical Reality. *Physical Review Letters*, 128(1):010401, January 2022.

[116] Katarzyna Roszak and Jarosław K. Korbicz. Entanglement and objectivity in pure dephasing models. *Physical Review A*, 100(6):062127, December 2019.

[117] Katarzyna Roszak and Jarosław K. Korbicz. Glimpse of objectivity in bipartite systems for nonentangling pure dephasing evolutions. *Physical Review A*, 101(5):052120, May 2020.

[118] Barış Çakmak, Özgür E Müstecaplıoğlu, Mauro Paternostro, Bassano Vacchini, and Steve Campbell. Quantum darwinism in a composite system: Objectivity versus classicality. *Entropy*, 23(8):995, 2021.

[119] Michael Zwolak and Wojciech H Zurek. Redundancy of einselected information in quantum darwinism: The irrelevance of irrelevant environment bits. *Physical Review A*, 95(3):030101, 2017.

[120] Richard P Feynman. Simulating physics with computers. In *Feynman and computation*, pages 133–153. CRC Press, 2018.

[121] Seth Lloyd. Universal quantum simulators. *Science*, 273(5278):1073–1078, 1996.

[122] Alberto Peruzzo, Jarrod McClean, Peter Shadbolt, Man-Hong Yung, Xiao-Qi Zhou, Peter J Love, Alán Aspuru-Guzik, and Jeremy L O'brien. A variational eigenvalue solver on a photonic quantum processor. *Nature communications*, 5(1):1–7, 2014.

[123] Abhinav Kandala, Antonio Mezzacapo, Kristan Temme, Maika Takita, Markus Brink, Jerry M Chow, and Jay M Gambetta. Hardware-efficient variational quantum eigensolver for small molecules and quantum magnets. *Nature*, 549(7671):242–246, 2017.

[124] Amira Abbas, David Sutter, Christa Zoufal, Aurélien Lucchi, Alessio Figalli, and Stefan Woerner. The power of quantum neural networks. *Nature Computational Science*, 1(6):403–409, 2021.

[125] Jaroslav Řeháček, Zdeněk Hradil, E Knill, and AI Lvovsky. Diluted maximum-likelihood algorithm for quantum tomography. *Physical Review A*, 75(4):042108, 2007.